HAWAII INSTITUTE OF GEOPHYSICS
UNIVERSITY OF HAWAII

A STUDY OF THE DEGREE TO WHICH SATELLITE-DERIVED GRAVITATIONAL DATA CAN BE RELATED TO THE ANOMALOUS SURFACE GRAVITY FIELD AND OTHER ANOMALOUS GEOPHYSICAL PARAMETERS

by

George P. Woollard

Mohammad Asadullah Khan

Simo Laurila

Final Report

on

National Aeronautics and Space Administration Grant No. NGR 12-001-045

January, 1969

PREFACE

In preparing this report the sections on the mathematical presentation on methods of frequency analysis as well as the frequency analysis and its geophysical interpretation are the work of Khan. The geophysical analysis is the work of Woollard. Laurila collaborated with both the other two authors in preparing the final report.

CONTENTS

LIST OF ILLUSTRATIONS

LIST OF TABLES

INTRODUCTION

Spherical harmonic representations of the anomalous external gravity field of the Earth as derived from satellite orbital perturbations by various investigators (Kaula, 1966; Kohnlein, 1966; Strange, 1966; Khan and Woollard, 1968) all give a consistent global pattern of large-scale mass anomalies. That a similar pattern of mass anomaly distribution is obtained using a spherical harmonic representation of the available surface gravity data expressed as free air anomalies, (Uotila, 1962; Kaula, 1966; Strange, 1966) is convincing evidence that the satellite-derived anomalous gravity field is related to the real earth and is not a product of mathematical analysis having dubious physical significance. The fact that the half-width values of the individual anomalies portrayed range from around 7^{o} to 20^{o} (corresponding to depths of origin ranging from about 700 km to 2000 km) strongly suggests that the gravity terms expressed are of deep-seated origin. An alternate explanation is that the gravity field sensed at satellite height, which represents the upward continuation and integration of the surface gravity field over an area whose effective size is a function of satellite height, embraces sufficient area that the average values of actual surface observations for this size area are not critically affected by existing deficiencies in data and that the anomaly pattern defined is a fortuitous product of integration over the area represented and spherical harmonic analysis. For example, if a 10^{o} x 10^{o} square includes two 3^{o} wide 20 mgal anomaly features extending across it separated by a 4^{o} area with zero anomaly, the average value is +12 mgal for the 10^{o} x 10^{o} square. A satellite at a height of 400 km would not sense the actual pattern but only this mean value. When we consider also that a 6th degree spherical harmonic representation corresponds to a surface area of approximately 30^{o} x 30^{o} size and a 15th degree representation to an area of approximately 12^{o} x 12^{o} size, this is not an unreasonable explanation for the high degree of agreement between satellite and surface data.

The fact that neither satellite gravity data nor averaged surface gravity data show any correlation in anomaly values with the distribution of the continents and ocean basins representing major inequalities in surface mass distribution can be attributed to the phenomenon of

isostasy. This results in regional variations in surface mass associated with surface relief being compensated by associated changes in subsurface mass distribution (principally changes in crustal composition and thickness) so that equal mass is obtained above some level of the order of 113 km on the basis of gravity studies, but probably nearer 150 km on the basis of seismological studies. Most areas that are out of isostatic equilibrium are of small areal extent (1^{o} to 3^{o} in width) although some areas do have dimensions of 10^{o} or more (Eastern Canada, Peninsula India, Western Europe, the North Atlantic Ocean, Eastern Central Atlantic Ocean, Eastern Central Pacific Ocean, Gulf of Alaska).

As shown by Strange (1966) areas of positive satellite-derived gravity in general correlate with areas of Tertiary to Recent vulcanism and orogeny (island arcs, the mid-Atlantic Ridge, Andes and Rocky Mts.). Areas of negative satellite-derived gravity appear to correlate with areas of abyssal depth in the oceans and areas of recent deglaciation (Eastern Canada). However, there are inconsistencies in that neither the Alps nor the Himalaya Mts. of Tertiary age appear to have significant expression. Also not all abyssal plains in the oceans have gravity expression nor does Fenno-Scandinavia which was the center of the European ice caps in Pleistocene time. The explanation for these inconsistencies appears to lie in fortuitous zero average values where there are adjacent anomaly areas of opposite sign. This would certainly explain the absence of any pronounced satellite anomaly for the Himalaya Mts. and the Alps. Where there are broad areas having one sign anomalies as the North Atlantic Ocean (see Fig. 1), 10^{o} x 10^{o} averages give a very similar pattern to that derived from satellite as shown by Figure 2.

Part of these inconsistencies can also be related to the reference figure used for the Earth. Surface gravity data is referred to the International Ellipsoid with a polar flattening of 1/297. Most satellite-derived data have been referred to an ellipsoid with f = 1/298.25. O'Keefe (1965) and Khan (1968a,b) have advocated that neither of these reference ellipsoid be used if a true picture of mass inhomogeneities is to be defined, but rather a figure for a hydrostatically flattened earth with f = 1/299.75. As the equatorial and polar radii are also different for the different reference figures, there are corresponding changes in theoretical

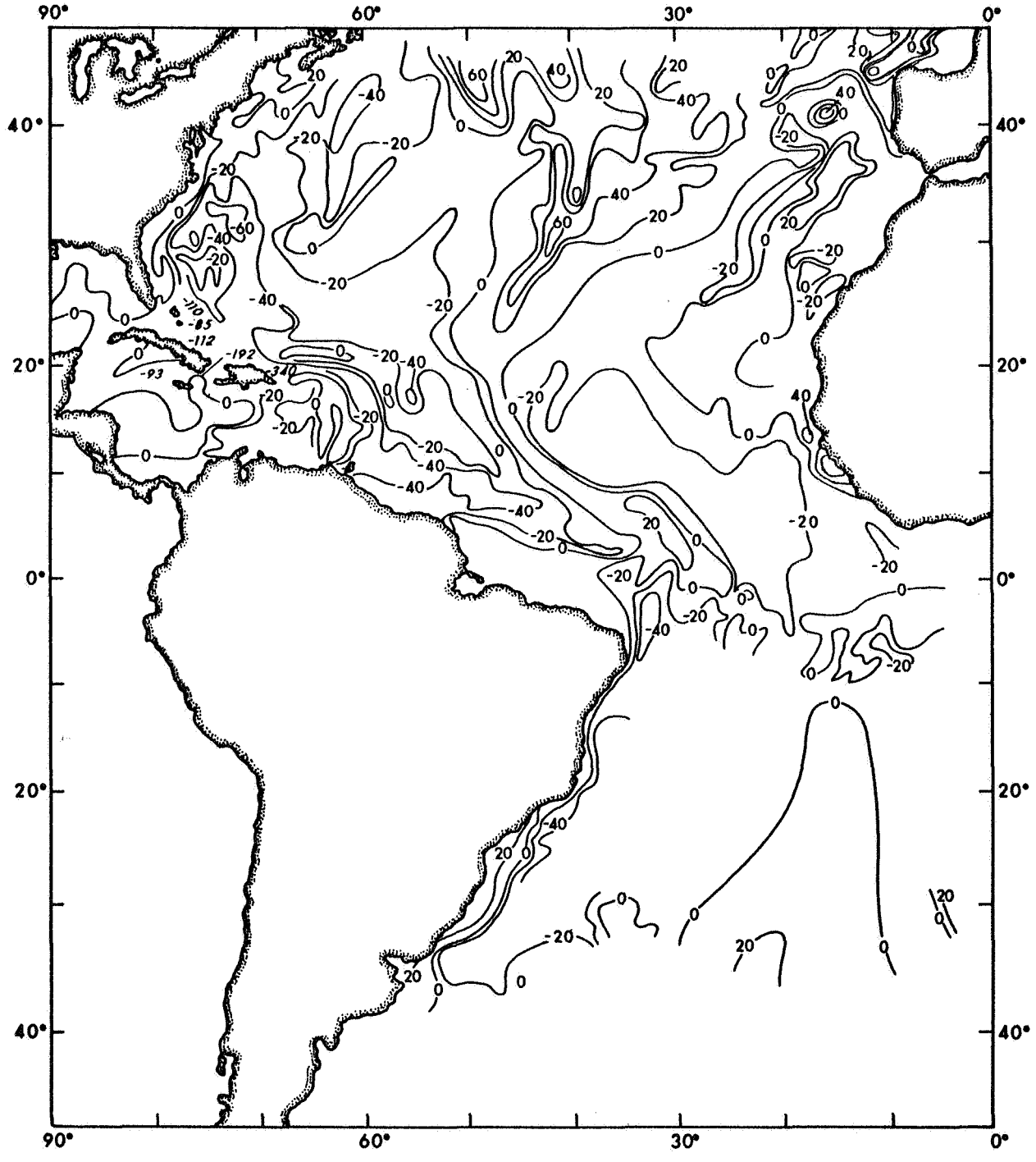

Fig. 1. Free air gravity anomaly map of the Atlantic Ocean area. Contour interval: 20 mgal.

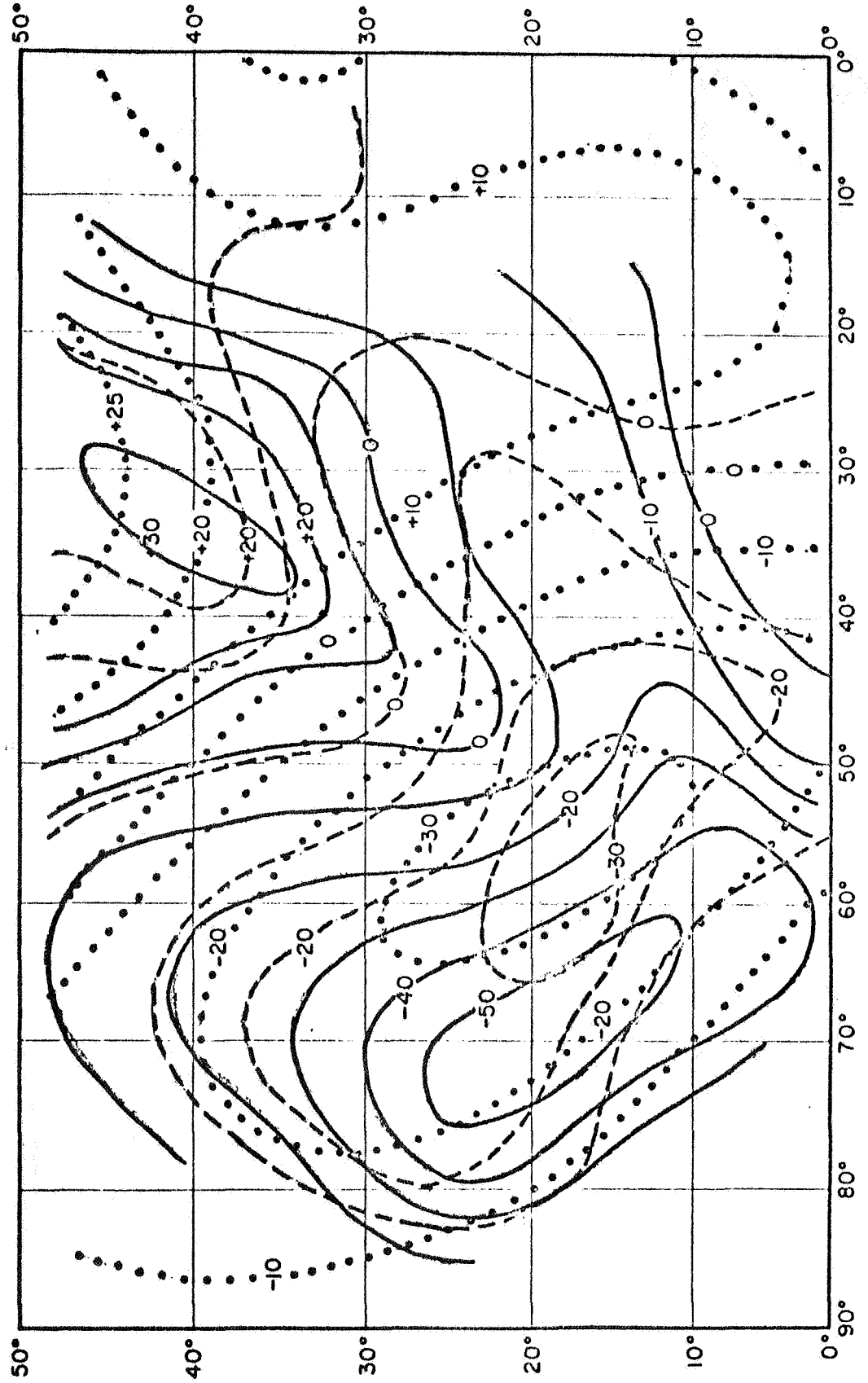

Fig. 2. Comparison of 10° x 10° free air anomaly values and the satellite-determined gravity field in the North Atlantic area.

gravity at the Equator and the poles as well as with latitude. As the effect of these changes results in over 10 mgal change in gravity between the Equator and the poles, it is clear that areas of small anomalous gravity of the order of 10 mgal defined by either surface or satellite data will be markedly dependent on the reference figure used, and that the relative amplitudes of larger anomalous changes as their areal extent will be modified significantly using different reference figures. At this stage, however, there is no general concensus as to what reference figure is preferable and the problem is complicated by the fact that the recalculation of all surface data relative to a new reference figure with an attendant change in the vertical gradient of gravity in evaluating the effect of elevation would be a truly monumental task in itself.

Pending resolution of the above and the determination of higher coefficients beyond degree 15 in the spherical harmonic representation of gravity, it appears best to examine methods of analysis that might help to resolve whether the areas of anomalous gravity now defined by an 8th degree spherical harmonic representation are really related to mass anomalies at depth or are a product of integration at satellite height of near-surface mass anomalies. In connection with the last, it is known that marked changes in gravity field are associated with apparent changes in the composition of both the upper mantle and crust, and that there are marked departures also associated with observable surface features such as the circum-Pacific belt of tectonic orogeny, vulcanism and seismicity which over much of its extent correlates in position with positive anomalous gravity defined by satellite data. This is well brought out in Figure 3, Figure 4 and Figure 5. Figure 3 is a spherical harmonic representation of the anomalous gravity field based on the coefficients derived by Gaposhkin (1966) using a reference ellipsoid with $f = 1/298.25$. This map is similar to that prepared by Strange (1966) which was also based on Gaposhkin's coefficients. Figure 4 is a tectonic map of the Pacific Ocean Basin prepared by Woollard (unpublished) and Figure 5 shows the distribution of seismic epicenters as defined by the U. S. Coast and Geodetic Survey.

Although the width of the circum-Pacific tectonic belt and associated seismicity is fragmented and narrower than that of the satellite-defined

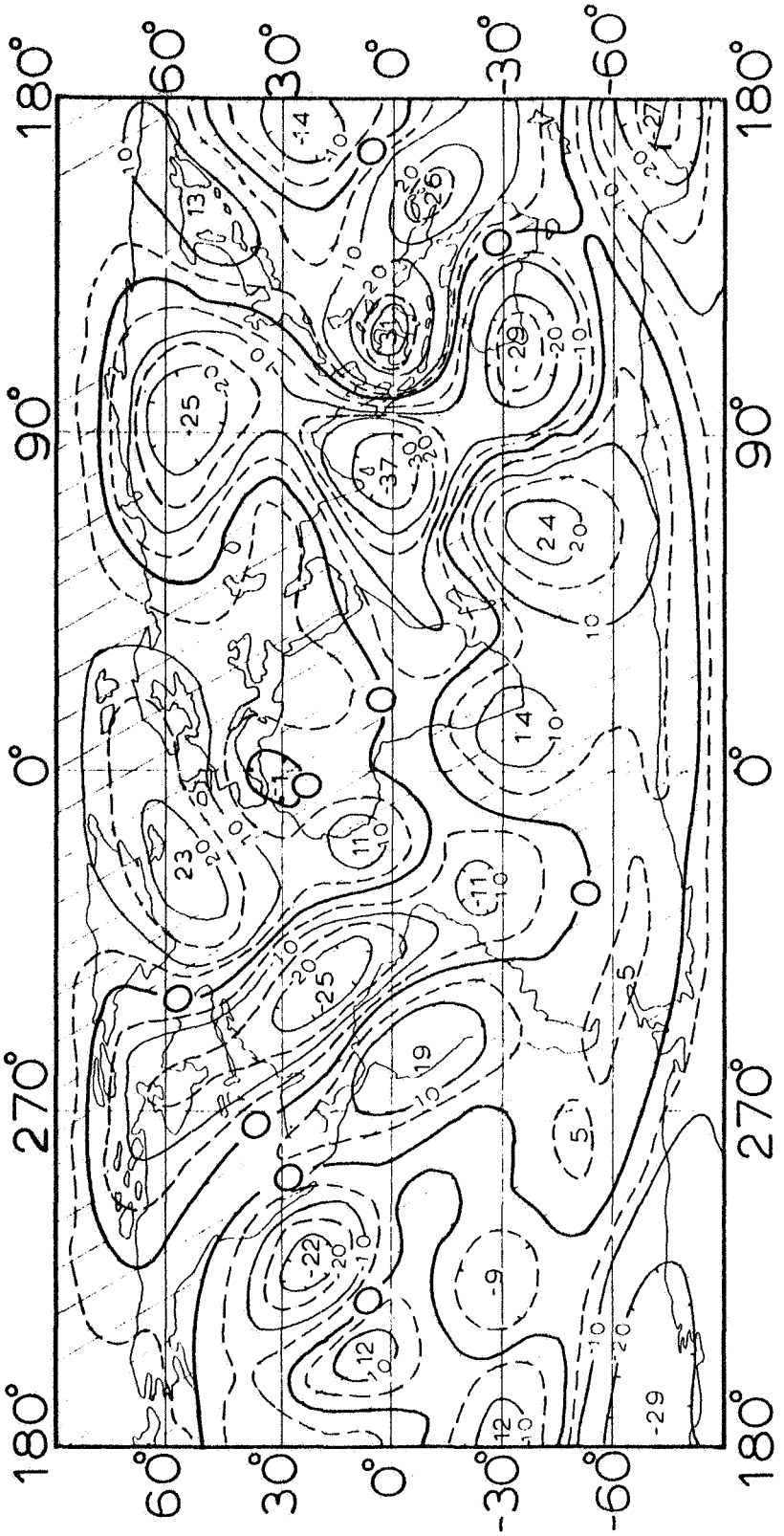

Fig. 3. Satellite-defined anomalous gravity field to 8th degree, with respect to a flattening of 1/298.25 based on Kozai's (1964) zonal and Gaposhkin's (1966) tesseral harmonic coefficients.

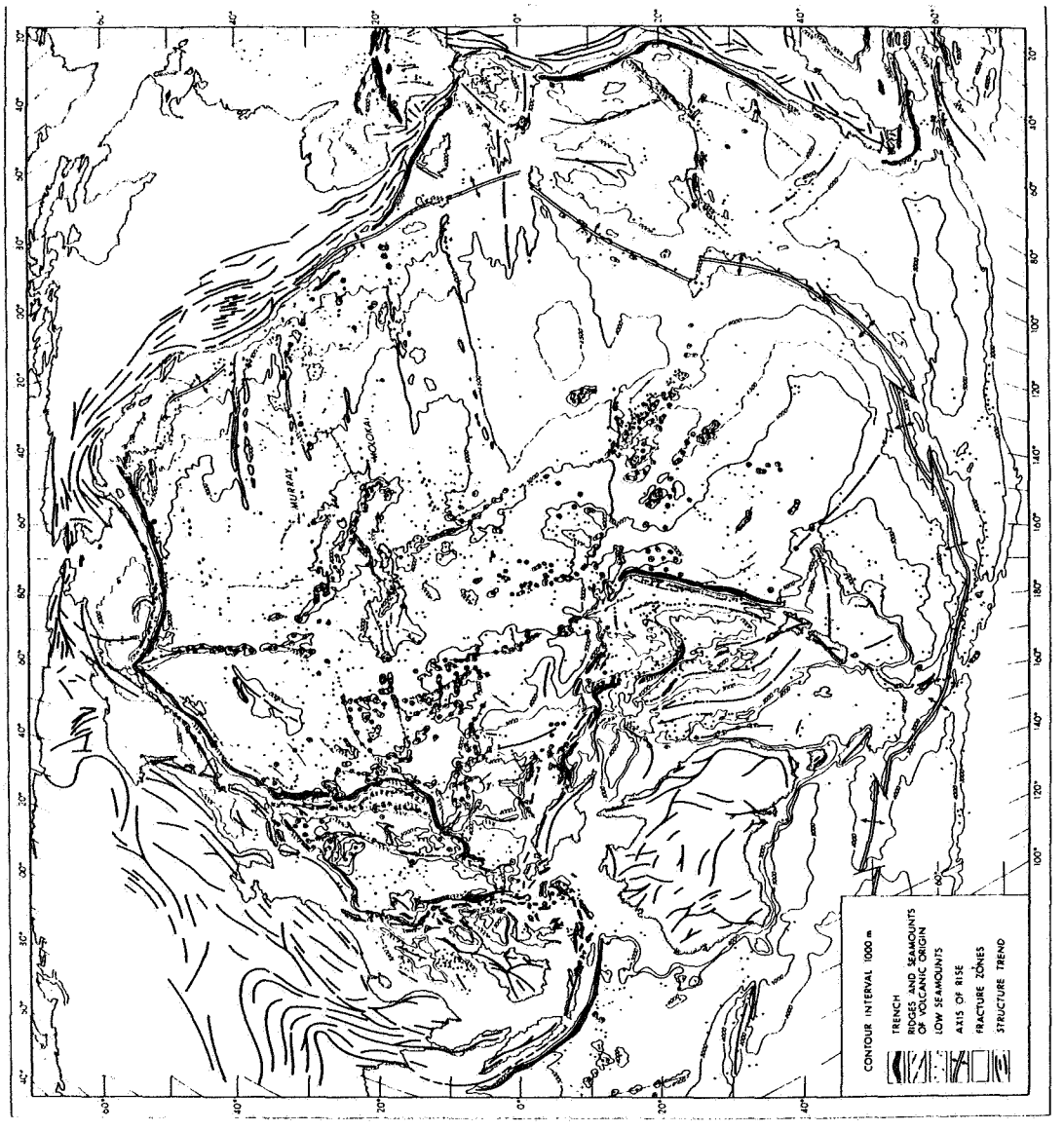

Fig. 4. Tectonic map of the Pacific Ocean Basin.

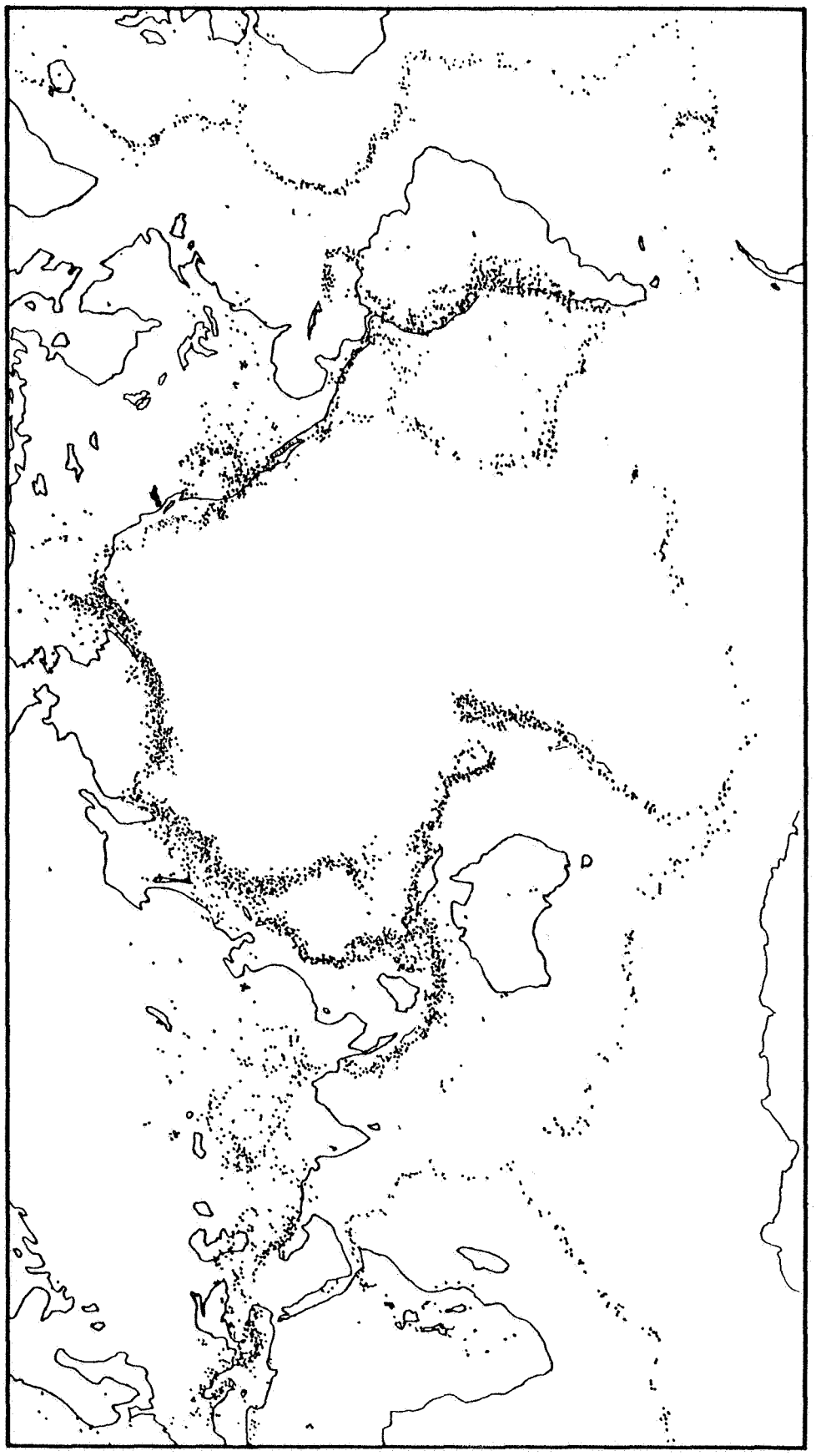

Fig. 5. World pattern of seismicity.

disturbed gravity field, this is to be expected since there is both an areal integration and a spreading of the gravitational field from each point source with distance. The important point is that the center of the disturbed gravitational field corresponds closely with that of tectonic disturbance. In terms of current thought among geologists this tectonic belt is a zone of crustal convergence with the oceanic crustal plate underthrusting the adjacent continental block as a result of crustal spreading away from loci of upwelling mantle material in the oceans forming new crustal material. This tectonic explanation at least appears to be well substantiated by seismic refraction crustal studies using explosive charges in the Aleutian Islands, the Kurile Islands, the Phillipine Islands, the Solomon Islands, the Peru-Chile Trench and the Middle America Trench as well as by age relationships defined by apparent periodic reversals in the Earth's magnetic field. See Figure 6 based on Heirtzler (1968). The available gravity data, admittedly sparse in some of these areas, also appear to substantiate this tectonic picture. Runcorn (1967) has suggested that the basic tectonic pattern and gravity pattern are both a result of convection cells with positive gravity being associated with the areas of convergence at the surface and negative gravity being associated with the areas of divergence and crustal spreading. Our interpretation of Figure 3 on this basis is shown in Figure 7. This explanation, however, only partially fits the tectonic pattern of crustal spreading shown in Figure 6, and there are as many points of exception as there are agreement.

Although various other explanations have been advanced to explain the satellite-derived gravity field, none can be said to be proved at this time. The facts that appear to be critical to any explanation and which must be recognized are: (1) The field represented is an integrated one as shown by the data of Figure 2 for the North Atlantic Ocean; (2) the depth of origin of the mass anomaly will be no greater than that defined by the anomaly half-width. As is evident from Figure 3 the pattern is a series of highs and lows and there is no reason to suspect that the true base line departs significantly from zero anomaly. If profiles based on Figure 3 are drawn for each 30^{o} of latitude as shown in Figure 8, and a smooth regional base line is approximated, it is

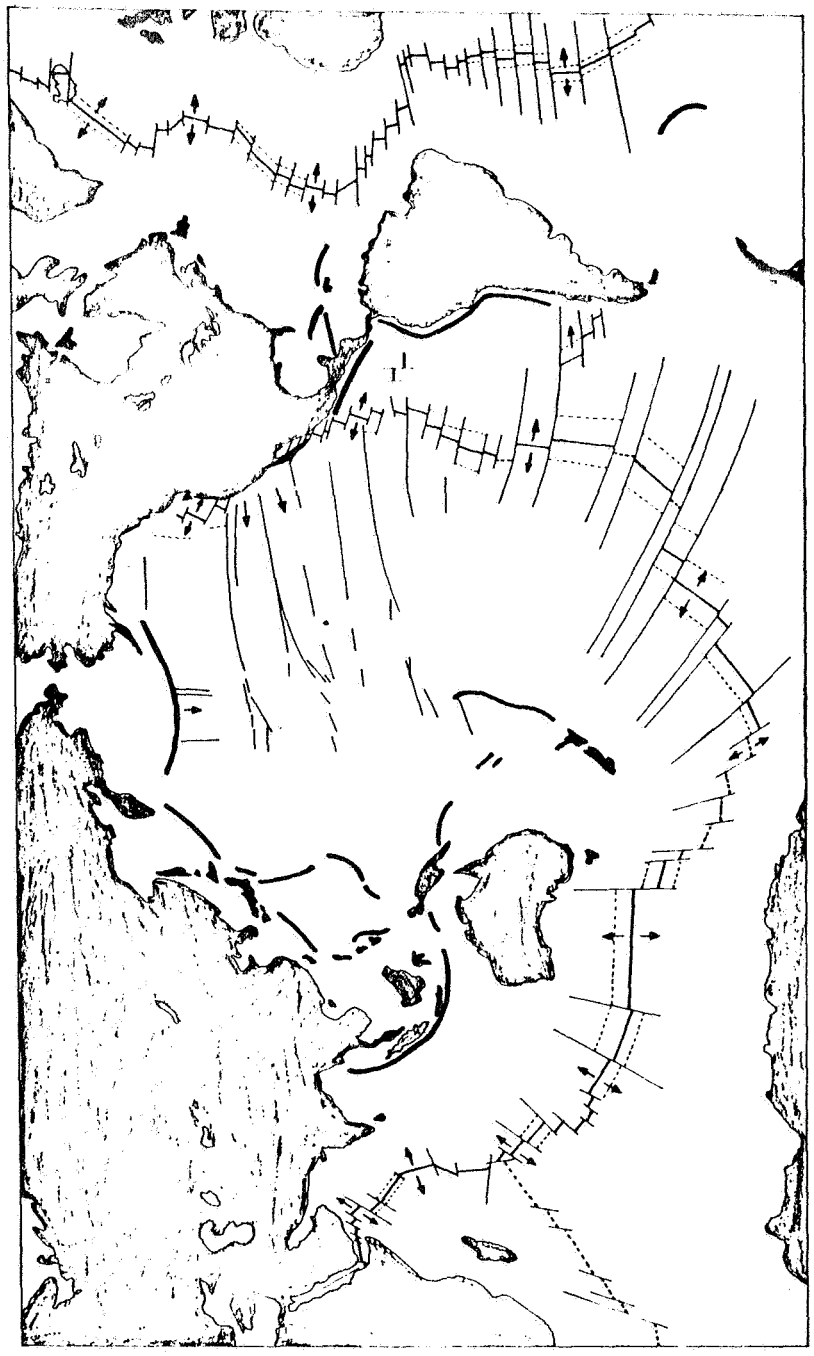

Fig. 6. Tectonic pattern of crustal spreading (after Heirtzler, 1968).

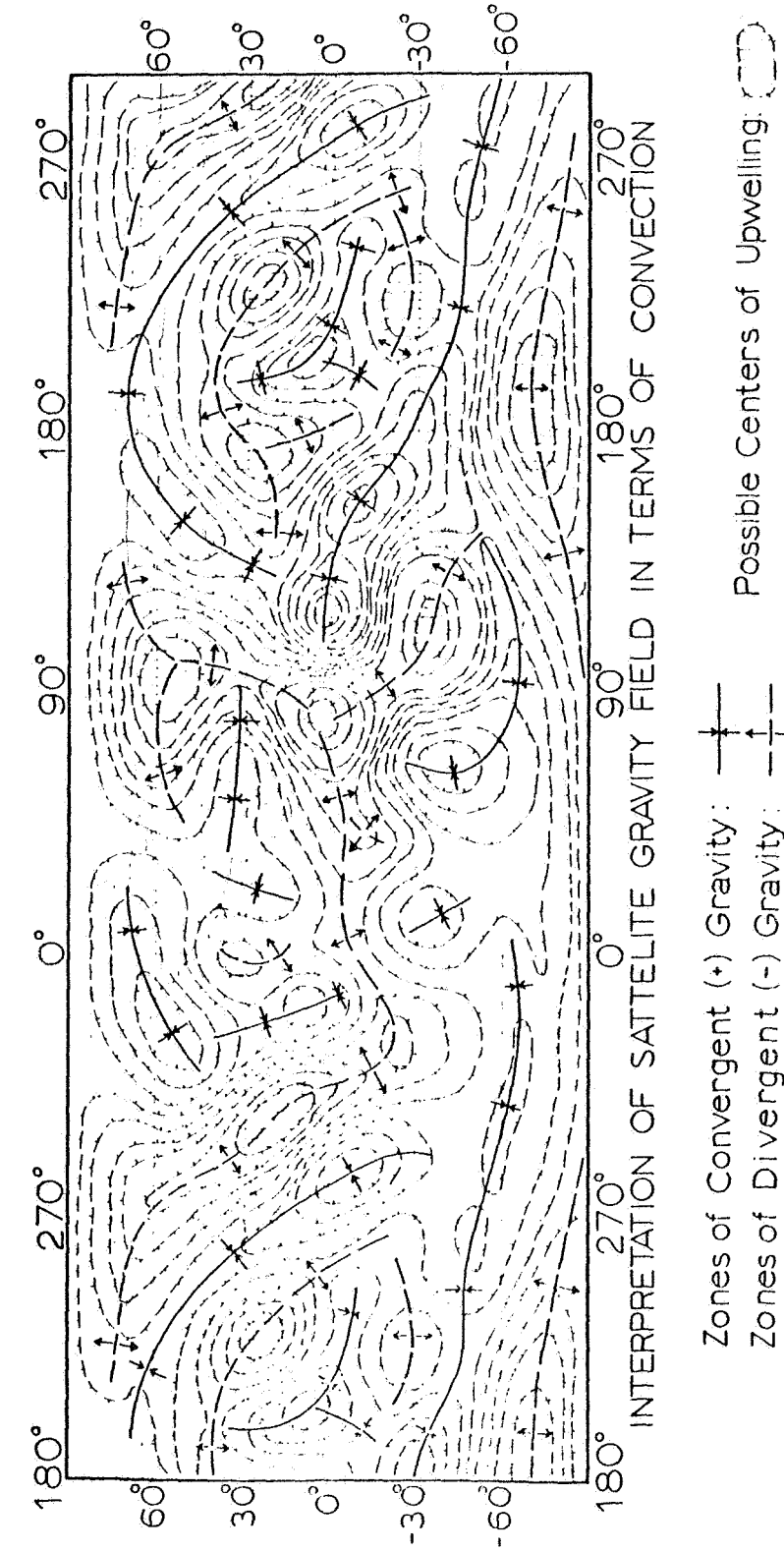

Fig. 7. Interpretation of satellite-determined gravity field in terms of convection currents.

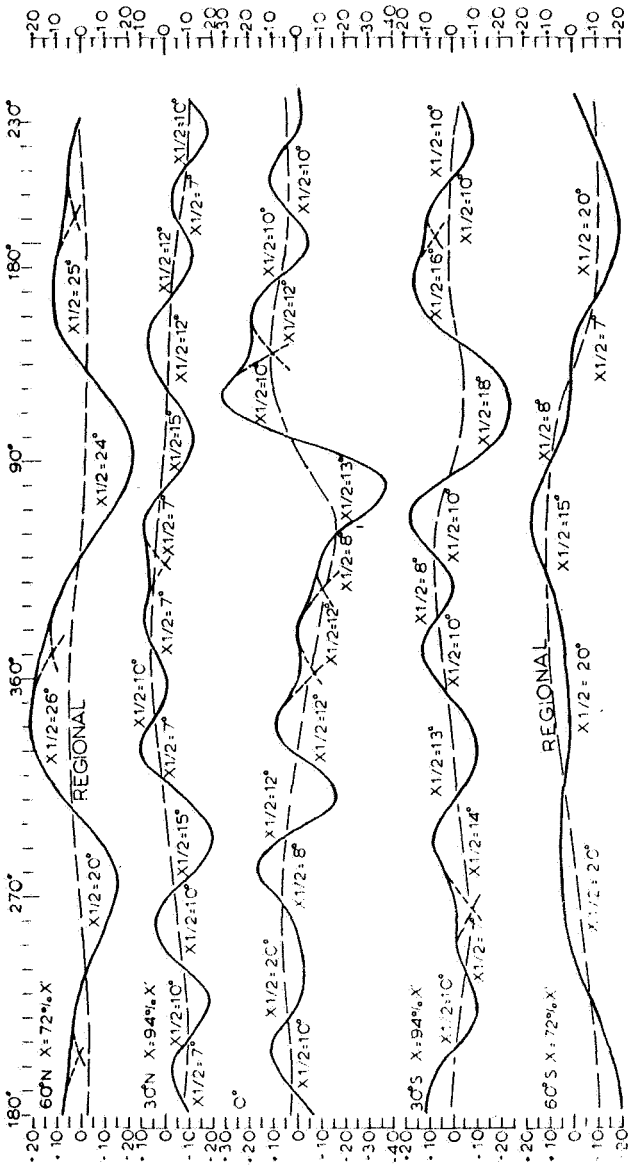

Fig. 8. Satellite-determined anomalies, gravity profiles, and half-width anomaly values.

evident that the regional line does suggest a triaxial figure for the Earth as well as inequalities in mass that could be associated with the Earth's core. However, the superimposed anomalies have a much shallower depth of origin. The half-width values (half the width of the anomaly at half amplitude above the base line) which are directly related to the depth of anomalous mass if from a single source body vary from 7^{o} to 26^{o}. If allowance is made for the convergence in meridian, since Figure 3 is on a Mercator projection, the modifying terms are approximately 72% at 60^{o} latitude, and 94% at 30^{o} latitude. As few of the anomaly areas are circular and some are elongate in an East-West direction, the half widths portrayed on the profile in excess of 20^{o} (uncorrected) are for the most part incorrect. This is especially true for the 60^{o}N and 60^{o}S profiles. A half-width value of about 15^{o} is actually about the largest value indicated.

To a first approximation the shape of the disturbing masses suggested can be visualized as spheres (the circular anomaly areas) and horizontal cylinders (the elongate anomaly areas). On this basis, the depth to the center for the circular anomalies is 1.35 times the half-width value. For the elongate anomalies the depth to the center equals the half-width value. The maximum depth defined is 20^{o}, and if allowance is made for satellite height (approximately the equivalent of 4^{o}), the maximum depth to the center of mass disturbance from the Earth's surface is 16^{o}. Without knowing anything about the density contrast involved, the depth to top of the disturbing mass can only be surmised. However, it would not be unreasonable to relate the deep anomalous masses if they are real to the 1000 km seismic discontinuity. Although current thought attributes this discontinuity entirely to a change in rigidity and incompressibility, it could equally as well be caused entirely or partially by an increase in density. The minimum depth to the center of origin indicated is about 7^{o}, or 3^{o} below the surface which suggests the anomalous mass could be related to the base of the low-velocity layer in the upper mantle. As many of the anomalous areas shown in Figure 3 appear to be associated pairs of opposite sign, it is conceivable as with a magnetic dipole pattern to visualize the causative mechanism as occurring beneath the point of inflection between the two with mass being subtracted on one side and deposited on the other. This

implies horizontal currents rafting lighter components along on a preferential basis over heavier components in association with deep convection and either magmatic differentiation or phase transformations induced by temperature. As a working hypothesis this concept is worthy of study especially if it can be related to crustal spreading.

The above discussion has been based on the assumption of a deep source. However, since detailed gravity sections across the mid-Atlantic Ridge show a series of positive and negative anomalies of about 1^{o} to 2^{o} width which average positive on a 10^{o} x 10^{o} basis, and this pattern correlates with a thinning of the crust and replacement of the basal layer having a velocity of 6.5 to 6.8 km per second as shown in Figure 9, the surface and near surface mass distribution could explain the anomaly pattern equally as well as a mass distribution whose center lies at a depth of 20^{o}.

As there are more surface gravity data for the Solomon Islands region than for any other portion of the circum-Pacific tectonic belt as well as refraction seismic studies of the crust and upper mantle in the area, it is a logical area for testing analytical procedures in studying the significance of the satellite-derived gravity field, both in terms of its relation to the local anomaly pattern and the associated regional anomaly pattern that should reflect a deep-seated mass origin if one is present.

Our purpose here is not to try to prove any preconceived idea, but rather to examine with an open mind all the data bearing on what appears to be the most obvious correlation between a surface feature of the Earth and the satellite-derived gravity field. If this apparent correlation can be shown to be fortuitous, it goes without saying that there are mass anomalies at depth about which there is little or nothing known at present. If the surface gravity and crustal data show the satellite-derived gravity field could have a near-surface origin, at least it is known that there are two possible explanations that are valid.

The only other area where a similar analysis can be made is the North Atlantic Region. Although Figure 1 suggests a broad pattern of long-wavelength anomalies over this area, this is fortuitous and results from using widely spaced submarine gravity observations.

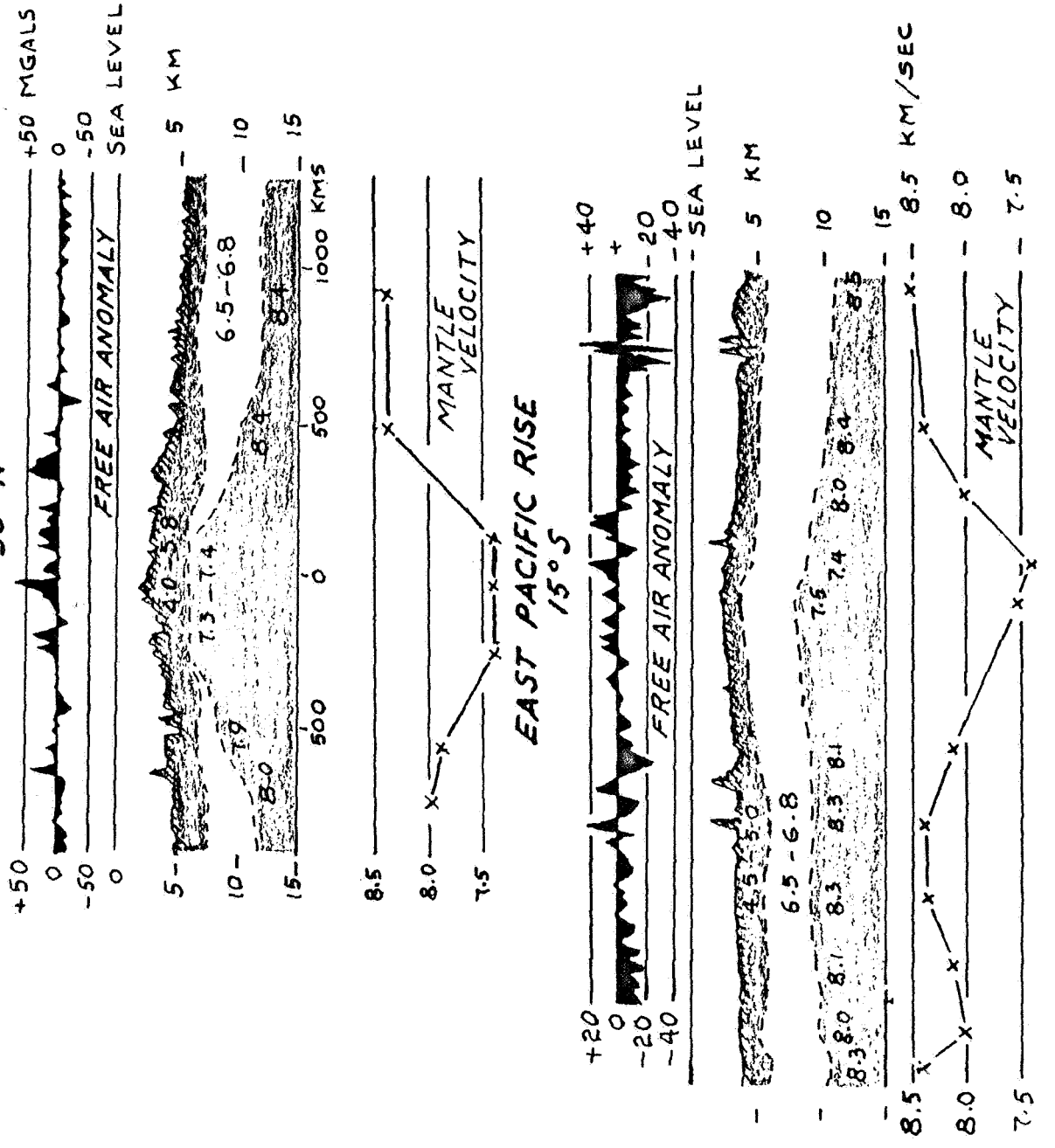

Fig. 9. Relationships between the crustal thickness and mantle velocity over the mid-Atlantic Ridge and the East Pacific Rise.

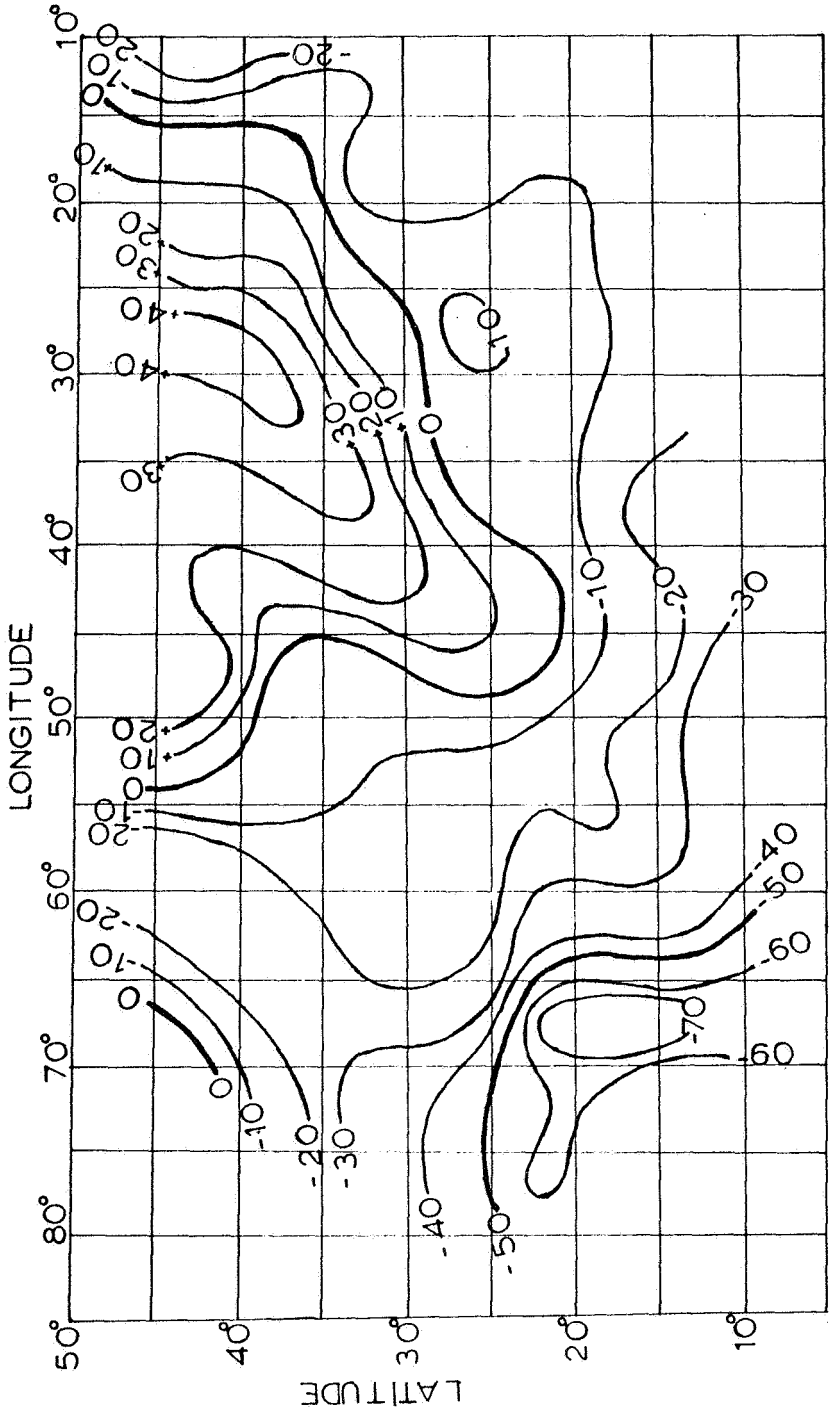

Fig. 10. Mean free air anomaly map of North Atlantic area, based on 5° x 5° average values.

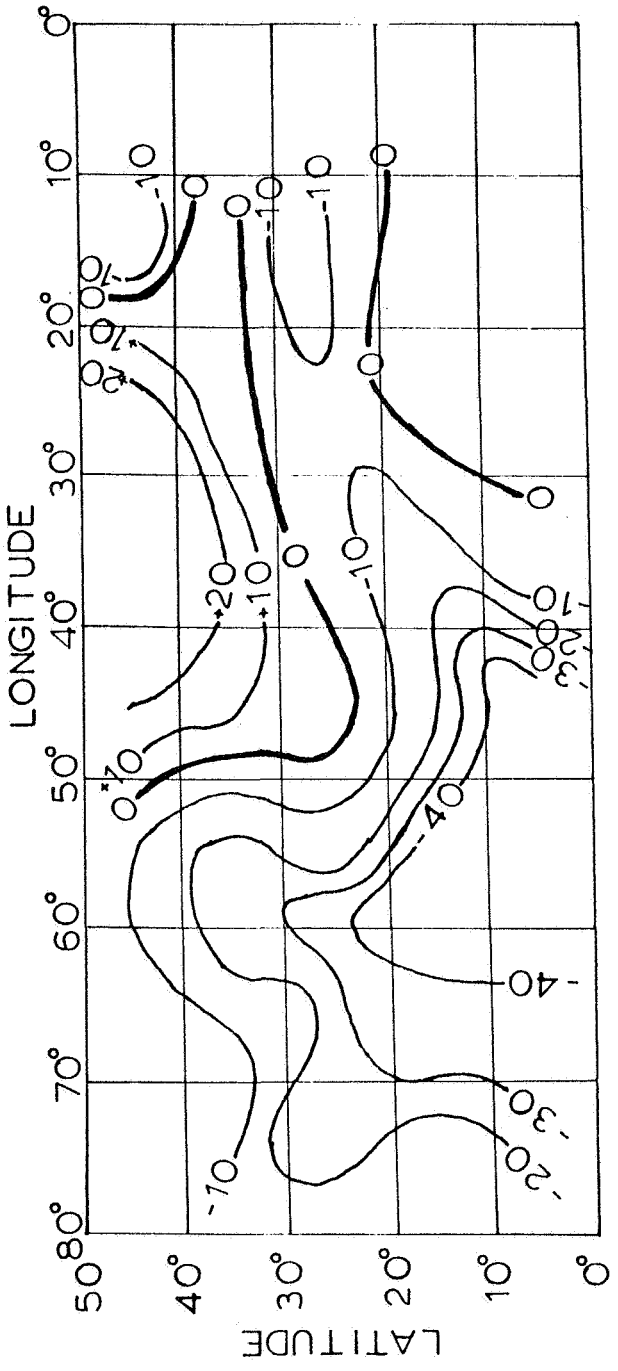

Fig. 11. Mean free air anomaly map of North Atlantic area, based on 10° x 10° average values.

Details of the actual field show numerous short-wavelength anomalies as brought out in Figure 9. Also as shown in Figure 9, a similar pattern of anomalies is found over the East Pacific Rise. Although both the mid-Atlantic Ridge and the East Pacific Rise are loci of crustal spreading, the two areas are characterized by somewhat different crustal structure which apparently results in differences in gravity expression.

That the smoothing effect of integration at satellite height is real, is indicated by the progressive change in anomaly pattern obtained in averaging the data of Figure 1. Figure 10 shows a map of $5^{o} \times 5^{o}$ average values and Figure 11 a map of $10^{o} \times 10^{o}$ average values. It is the $10^{o} \times 10^{o}$ averages for this area that give a pattern which agrees closely with the satellite derived anomalous gravity field as was shown in Figure 2.

Talwani et al. (1961) have shown that the positive anomaly values associated with the mid-Atlantic Ridge is mostly of topographic origin and the Bouguer anomaly which removes the topographic effect gives a pronounced minimum that either calls for a very thick crust (not defined seismically) or the introduction of lower than normal density material in the upper mantle immediately beneath the Ridge. Worzel (1965) in commenting on the gravity field over this area and the crustal models that would satisfy it states "the anomaly cannot be attributed to a very much deeper (>25 to 35 km) mass distribution." At least in this area there seems to be little doubt that the positive anomaly is related to uncompensated topography associated with the Ridge.

The Solomon Islands represent both a different type geological association (zone of convergence rather than a zone of divergence) and the anomaly pattern is not connected with any single geologic feature. For both reasons it is a significant area for study in connection with both the surface gravity field and the satellite-derived anomalous gravity field.

In carrying out the present study no attempt has been made to construct crustal models that would fit the gravity data as this has already been done by Rose et al. (1968). Instead we have made an attempt to establish statistically from a frequency analysis whether the satellite field is related to a deep or shallow source and reviewed these results in terms of the surface gravity field and what is known of the crustal

structure in the Solomon Island region as defined by seismic refraction data.

METHOD OF FREQUENCY ANALYSIS

The techniques of frequency analysis for one-dimensional data are widely discussed in the literature (see, for example, Lighthill, 1964; Hardy and Rogosinski, 1962; Tolstov, 1962; Byerly, 1959; Miller, 1956). Discussions of the two-dimensional frequency analysis are less commonly found and almost invariably the mathematical equations presented (Wangsness, 1963; Tolstov, 1962; Byerly, 1959) have to be adapted to be applicable to geophysical problems. Below we summarize the two-dimensional Fourier theory and derive the appropriate formulas for the spectral analysis of gravity data.

Fourier Series in Two Variables

Let $g_i(x,y)$, $i = 1, 2,...i$ be a system of continuous functions that do not vanish identically and are defined on a rectangle R in the x,y plane. The functions $g_i(x,y)$, $i = 1, 2,...i$ are said to be orthogonal if

$$\int_R\int g_i(x,y)g_j(x,y)\ dx\ dy = 0 \text{ for all } i\neq j \tag{1}$$

They are said to be normalized if

$$\int_R\int g_i^{\,2}(x,y)\ dx\ dy = 1 \tag{2}$$

The quantity $\sqrt{\int_R\int g_i^{\,2}(x,y)\ dx\ dy}$ is called the norm of the function $g_i(x,y)$ and is denoted by $||\ g_i(x,y)\ ||$ so that

$$||\ g_i(x,y)\ ||^2 = \int_R\int g_i^{\,2}(x,y)\ dx\ dy \tag{2a}$$

Let $f(x,y)$ be an absolutely integrable function defined on the rectangle R. Its Fourier series representation then becomes

$$f(x,y) = \sum_{i=0}^{\infty} a_i \, g_i(x,y) \tag{3}$$

where

$$a_i = \frac{\iint f(x,y) g_i(x,y) \, dx \, dy}{||g_i(x,y)||^2} \tag{4}$$

The system of functions $g_i(x,y)$ is said to be <u>complete</u> if for any square integrable function $f(x,y)$, we have the relation

$$\iint f^2(x,y) \, dx \, dy = \sum_{i=0}^{\infty} a_i^2 \, ||g_i(x,y)||^2 \tag{5}$$

For incomplete systems the equality sign is replaced by the inequality $\geq$, in which case the relation is known as Bessel's inequality.

Consider two square integrable functions $f(x,y)$ and $F(x,y)$. Their Fourier series representations are

$$f(x,y) = \sum_{i=0}^{\infty} a_i g_i(x,y)$$

$$F(x,y) = \sum_{i=0}^{\infty} A_i g_i(x,y)$$

With the help of equation (5) we get

$$\int_R \int \left(f(x,y) + F(x,y)\right)^2 dx \, dy = \sum_{i=0}^{\infty} (a_i + A_i)^2 ||g_i(x,y)||^2 \tag{6}$$

and

$$\int_R \int \left(f(x,y) - F(x,y)\right)^2 \, dx \, dy = \sum_{i=0}^{\infty} (a_i - A_i)^2 ||g_i(x,y)||^2 \quad (7)$$

which finally yields

$$\int_R \int f(x,y) \, F(x,y) \, dx \, dy = \sum_{i=0}^{\infty} a_i A_i ||g_i(x,y)||^2 \quad (8)$$

Equation (8) is known as Parseval's Theorem and is of basic importance in our further work.

Now define the rectangle R by $0 \leq x \leq 2\ell$, $0 \leq y \leq 2k$ and for the system of functions $g_i(x,y)$, $i = 1, 2, \ldots i$, choose the trigonometric functions

$$1, \cos \frac{\pi n x}{\ell}, \sin \frac{\pi n x}{\ell}$$

$$1, \cos \frac{\pi m y}{k}, \sin \frac{\pi m y}{k} \quad (9)$$

$$\cos \frac{\pi n x}{\ell} \cos \frac{\pi m y}{\ell}, \sin \frac{\pi n x}{\ell} \cos \frac{\pi m y}{\ell}, \cos \frac{\pi n x}{\ell} \sin \frac{\pi m y}{\ell},$$

$$\sin \frac{\pi n x}{\ell} \sin \frac{\pi m y}{\ell}$$

These functions form the basic trigonometric system in two variables. Each of them is of period 2ℓ in x and $2k$ in y. Further, they form an orthogonal system. This can be readily verified with the help of the orthogonality condition stated in Equation (1). For example,

$$\int_R \int 1 \cdot \begin{matrix} \cos \\ \sin \end{matrix} \left(\frac{\pi n x}{\ell}\right) dx \, dy = \int_R \int 1 \cdot \begin{matrix} \cos \\ \sin \end{matrix} \left(\frac{\pi m y}{k}\right) dx \, dy = 0 \quad (10)$$

and similarly

$$\int_R \int \begin{bmatrix} \cos \\ \sin \end{bmatrix} \left(\frac{\pi n x}{\ell}\right) \begin{bmatrix} \cos \\ \sin \end{bmatrix} \left(\frac{\pi i x}{\ell}\right) dx\, dy = 0$$

and (10a)

$$\int_R \int \begin{bmatrix} \cos \\ \sin \end{bmatrix} \left(\frac{\pi n x}{\ell}\right) \begin{bmatrix} \cos \\ \sin \end{bmatrix} \left(\frac{\pi m y}{k}\right) \begin{bmatrix} \cos \\ \sin \end{bmatrix} \left(\frac{\pi i x}{\ell}\right) \begin{bmatrix} \cos \\ \sin \end{bmatrix} \left(\frac{\pi j y}{k}\right)$$

$$dx\, dy = 0$$

for all $n \neq i$, $m \neq j$, and so on for the other possible pairs.

For the special case when $n = i$, $m = j$, equation (10a) becomes

$$\int_R \int \begin{bmatrix} \cos \\ \sin \end{bmatrix} \left(\frac{\pi n x}{\ell}\right) \begin{bmatrix} \cos \\ \sin \end{bmatrix} \left(\frac{\pi m y}{k}\right)^2 dx\, dy = k\ell$$

$$= \left\| \begin{bmatrix} \cos \\ \sin \end{bmatrix} \left(\frac{\pi n x}{\ell}\right) \begin{bmatrix} \cos \\ \sin \end{bmatrix} \left(\frac{\pi m y}{k}\right) \right\|^2 \qquad (10b)$$

Also

$$\int_R \int \begin{bmatrix} \cos \\ \sin \end{bmatrix} \left(\frac{\pi n x}{\ell}\right)^2 dx\, dy = 2\ell k = \left\| \begin{bmatrix} \cos \\ \sin \end{bmatrix} \left(\frac{\pi n x}{\ell}\right) \right\|^2$$

and similarly (11)

$$\int_R \int \begin{bmatrix} \cos \\ \sin \end{bmatrix} \left(\frac{\pi m y}{k}\right)^2 dx\, dy = 2\ell k = \left\| \begin{bmatrix} \cos \\ \sin \end{bmatrix} \left(\frac{\pi m y}{k}\right) \right\|^2$$

Note that in Equations (10a) and (10b) above, the horizontal as well as diagonal pairing is permissible.

It is instructive to investigate the geometric structure of some

of the two-dimensional trigonometric functions in some of their normal modes. Consider the following system of functions:

$$\cos \frac{\pi nx}{\ell} \cos \frac{\pi my}{k} \tag{12a}$$

$$\sin \frac{\pi nx}{\ell} \cos \frac{\pi my}{k} \tag{12b}$$

$$\cos \frac{\pi nx}{\ell} \sin \frac{\pi my}{k} \tag{12c}$$

$$\sin \frac{\pi nx}{\ell} \sin \frac{\pi my}{k} \tag{12d}$$

The functions (12a) are plotted in Figure 12a for a few selected values of n and m which are shown on each figure. Note that the nodal lines are straight lines parallel to the edges of the rectangular area under consideration. The number of nodal lines in any direction in an interval equal to half the period of the function in that direction, is equal to the index associated with that direction. The harmonic function divides the ℓ x k rectangular area into m x n rectangles with alternating signs.

Now consider the system (12b). These functions are plotted in Figure 12b for selected values of n and m. In this case, the number of nodal lines normal to the x-axis in the interval $0 \leq x \leq \ell$, is one less than the index associated with x-axis, while those normal to the y-axis, in the interval $0 \leq y \leq k$, are equal to the index associated with y-axis.

Figure 12c shows the plots of (12c). It is obvious that there are n nodal lines perpendicular to the x-axis in the interval ℓ and m - 1 nodal lines perpendicular to the y-axis in the interval k.

In Figure 12d are plotted the functions given at (12d). This harmonic has n - 1 nodal lines normal to the x-axis in the interval 0 to ℓ and m - 1 nodal lines normal to the y-axis in the interval o to k.

It is interesting to compare the geometric structure of the above harmonics with that of the surface spherical harmonics.

If the function f(x,y) is now expanded in terms of system of functions given in (9), the coefficients of expansion are given by Equation (4) as:

$$a_{nm} = \frac{\lambda_{nm}}{\ell k} \iint f(x,y) \cos \frac{\pi n x}{\ell} \cos \frac{\pi m y}{k} \, dx \, dy$$

$$b_{nm} = \frac{\lambda_{nm}}{\ell k} \iint f(x,y) \sin \frac{\pi n x}{\ell} \cos \frac{\pi m y}{k} \, dx \, dy$$

$$c_{nm} = \frac{\lambda_{nm}}{\ell k} \iint f(x,y) \cos \frac{\pi n x}{\ell} \sin \frac{\pi m y}{k} \, dx \, dy \qquad (13)$$

and

$$d_{nm} = \frac{\lambda_{nm}}{\ell k} \iint f(x,y) \sin \frac{\pi n x}{\ell} \sin \frac{\pi m y}{k} \, dx \, dy$$

where

$$n = 0, 1, 2, \ldots$$

$$m = 0, 1, 2, \ldots$$

and

$$\lambda_{nm} = \begin{cases} \frac{1}{4} \text{ for } n = m = 0 \\ \frac{1}{2} \text{ for } n > 0, \; m = 0, \text{ or } n = 0, \; m > 0 \\ 1 \text{ for } n > 0, \; m > 0 \end{cases} \qquad (13a)$$

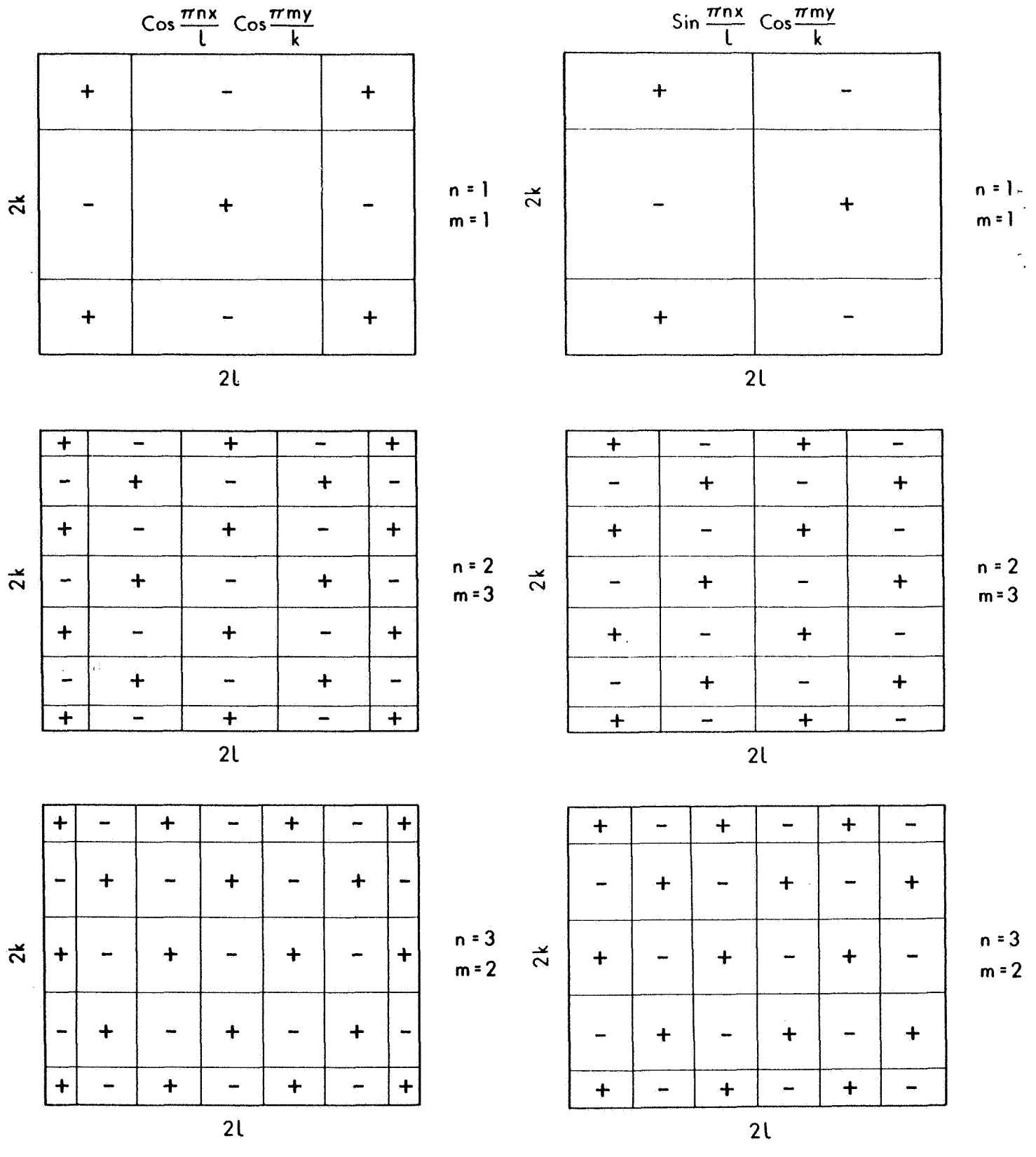

Fig. 12. Geometric structure of the (a) harmonic $\cos \frac{\pi nx}{\ell} \cos \frac{\pi my}{k}$; (b) harmonic

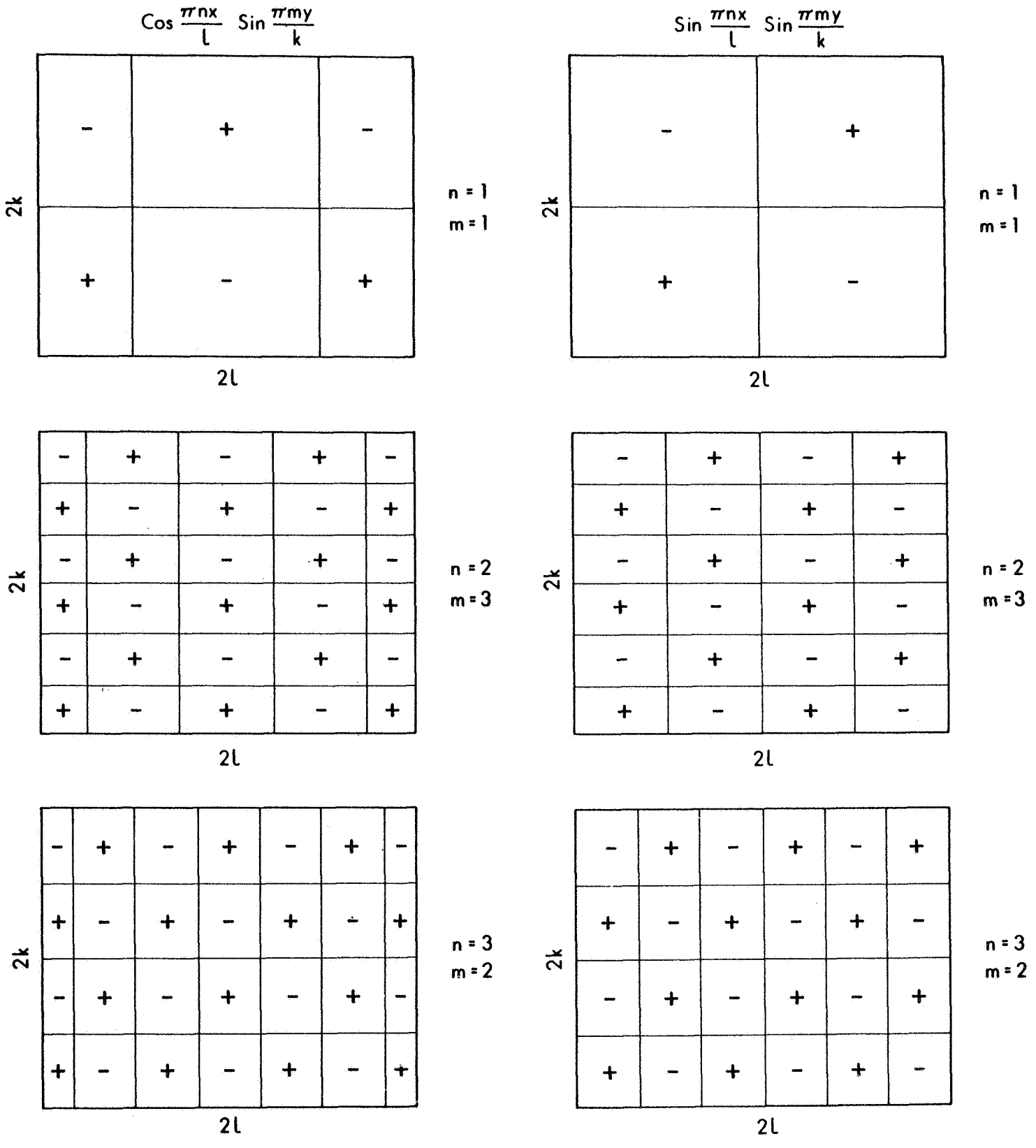

$\sin \frac{\pi nx}{\ell} \cos \frac{\pi my}{k}$; (c) harmonic $\cos \frac{\pi nx}{\ell} \sin \frac{\pi my}{k}$; (d) harmonic $\sin \frac{\pi nx}{\ell} \sin \frac{\pi my}{k}$.

The Fourier representation of the function f(x,y) then becomes

$$f(x,y) = \sum_{n=0}^{\infty} \sum_{m=0}^{\infty} \lambda_{nm} \left[a_{nm} \cos \frac{\pi nx}{\ell} \cos \frac{\pi my}{k} + b_{nm} \sin \frac{\pi nx}{\ell} \cos \frac{\pi my}{k} + c_{nm} \cos \frac{\pi nx}{\ell} \sin \frac{\pi my}{k} + d_{nm} \sin \frac{\pi nx}{\ell} \sin \frac{\pi my}{k} \right] \tag{14}$$

If the linear sum in Equation (14) gives a complete representation of the function f(x,y), Equation (5) will hold. If two different functions, f(x,y) and F(x,y), can be represented 'completely' by (14), Equation (8) will hold. These relations provide convenient tests of whether or not the Fourier series representation of the function in question is 'complete.'

The Fourier series for f(x,y) can be written, more compactly, in the complex form

$$f(x,y) = \sum_{n=-\infty}^{\infty} \sum_{m=-\infty}^{\infty} E_{nm} e^{i\pi(n\omega_1 x + n\omega_2 y)}$$

$$(n = 0, \pm 1, \pm 2, \ldots; \; m = 0, \pm 1, \pm 2, \ldots) \tag{15}$$

where

$$\omega_1 = \frac{2\pi}{2\ell}$$

$$\omega_2 = \frac{2\pi}{2k}$$

and the coefficients are given by

$$E_{nm} = \frac{1}{4\ell k} \int_R \int f(x,y)\ e^{-i\pi(n\omega_1 x + m\omega_2 y)}\ dx\ dy \qquad (16)$$

$$(n = 0, \pm 1, \pm 2, \ldots;\ m = 0, \pm 1, \pm 2, \ldots)$$

The quantity E_{nm} is closely related to the Fourier transform of the function $f(x,y)$. In fact, it is equal to the Fourier transform in the discrete case with which we will be concerned in the actual analysis. We denote it by $F(n,m)$ just to follow the usually accepted notation. $F(n,m)$ is called the complex spectrum of $f(x,y)$. Its absolute value or modulus is called the amplitude spectrum while its argument is called the phase spectrum. Obviously, the Fourier transform $F(n,m)$ is a harmonic function and is the representation of the function $f(x,y)$ in the frequency domain.

Crosscovariance

Let $f_1(x,y)$ and $f_2(x,y)$ be two functions which have the same fundamental angular frequencies ω_1 and ω_2 in the x- and y-directions respectively. Further, let τ_1 and τ_2 denote small displacements along x and y axes respectively. Then the integral

$$\frac{1}{4\ell k} \int_R \int f_1(x,y)\ f_2(x + \tau_1,\ y + \tau_2)\ dx\ dy \qquad (17)$$

is called the crosscovariance function of $f_1(x,y)$ and $f_2(x,y)$. Denote it by $C_{12}(\tau)$ so that

$$C_{12}(\tau) = \frac{1}{4\ell k} \int_R \int f_1(x,y)\ f_2(x + \tau_1,\ y + \tau_2)\ dx\ dy \qquad (18)$$

where

$$\tau = \sqrt{\tau_1^2 + \tau_2^2}$$

Now if we put $\tau_1 = \tau_2 = 0$, Equation (18) becomes

$$C(0) = \frac{1}{4\ell k} \int_R \int f_1(x,y)\ f_2(x,y)\ dx\ dy = \langle f_1(x,y)\ f_2(x,y) \rangle \quad (19)$$

The quantity C(0) is called the crossvariance function of the functions $f_1(x,y)$ and $f_2(x,y)$. The right-hand side of this equation is the mean power of the product of $f_1(x,y)$ $f_2(x,y)$. The subscripts of C have been dropped because the order of subscripts merely indicates the function to which the displacement τ should be given. However, when the displacement is zero, the subscripts no longer remain meaningful.

Consider the Fourier expansion of the functions $f_1(x,y)$ and $f_2(x,y)$ (Equation 14):

$$\begin{matrix} f_1(x,y) \\ f_2(x,y) \end{matrix} = \sum_{n=0}^{\infty} \sum_{m=0}^{\infty} \lambda_{nm} \left(\begin{matrix} a_{nm} \\ A_{nm} \end{matrix} \cos n\omega_1 x \cos m\omega_2 y + \begin{matrix} b_{nm} \\ B_{nm} \end{matrix} \right.$$

$$\sin n\omega_1 x \cos m\omega_2 y + \begin{matrix} c_{nm} \\ C_{nm} \end{matrix} \cos n\omega_1 x \sin m\omega_2 y \quad (20)$$

$$\left. + \begin{matrix} d_{nm} \\ D_{nm} \end{matrix} \sin n\omega_1 x \sin m\omega_2 y \right)$$

The application of Parseval's Theorem (Equation 8) gives

$$\int_R \int f_1(x,y)\ f_2(x,y)\ dx\ dy = \sum\sum \lambda_{nm}^2 a_{nm} A_{nm} \left|\left|\cos n\omega_1 x \cos m\omega_2 y\right|\right|^2 + b_{nm} B_{nm} \left|\left|\sin n\omega_1 x \cos m\omega_2 y\right|\right|^2 + c_{nm} C_{nm} \left|\left|\cos n\omega_1 x \sin m\omega_2 y\right|\right|^2 + d_{nm} D_{nm} \left|\left|\sin n\omega_1 x \sin m\omega_2 y\right|\right|^2 \tag{21}$$

or

$$\langle f_1(x,y)\ f_2(x,y) \rangle = \sum\sum \frac{\lambda_{nm}}{4} (a_{nm} A_{nm} + b_{nm} B_{nm} + c_{nm} C_{nm} + d_{nm} D_{nm}) \tag{22}$$

Now consider a quantity D_n such that

$$D_n = \sum_m \frac{\lambda_{nm}}{4} (a_{nm} A_{nm} + b_{nm} B_{nm} + c_{nm} C_{nm} + d_{nm} D_{nm}) \tag{23}$$

and

$$C(0) = \sum_n D_n = \langle f_1(x,y)\ f_2(x,y) \rangle \tag{24}$$

The quantity D_n is called the degree crossvariance of the functions $f_1(x,y)$ and $f_2(x,y)$. The choice of summation index (m or n) in Equation (23) gives information on the concentration of a certain frequency normal to the axis with which the summation symbol is associated. Equation (24) shows that D_n is the crosspower spectrum of the functions $f_1(x,y)$ and $f_2(x,y)$.

Covariance

Suppose that in Equation (8) we put $f_1(x,y) = f_2(x,y) = f(x,y)$ so that

$$C(\tau) = \langle f(x,y)\ f(x + \tau_1,\ y + \tau_2) \rangle \tag{25}$$

The funcion $C(\tau)$ is called the covariance function of $f(x,y)$. If $\tau_1 = \tau_2 = 0$, we get

$$C(0) = \langle f^2(x,y) \rangle \tag{26}$$

The quantity $C(0)$ is the variance of the function $f(x,y)$ and, by analogy with Equation (22), is obviously given by

$$C(0) = \sum\sum \frac{\lambda_{nm}}{4} (a_{nm}^2 + b_{nm}^2 + c_{nm}^2 + d_{nm}^2) \tag{27}$$

Now consider again a quantity D_n so that

$$D_n = \sum_m \frac{\lambda_{nm}}{4} (a_{nm}^2 + b_{nm}^2 + c_{nm}^2 + d_{nm}^2) \tag{28}$$

and

$$C(0) = \sum_n D_n = \langle f^2(x,y) \rangle \tag{29}$$

Equation (29) states that D_n is the power spectrum of the function $f(x,y)$. D_n is called the degree variance of the function $f(x,y)$.

As stated before, the choice of the summation index (n or m) is made depending upon the direction along which the frequency concentration is sought to be studied. As in the case of crosspower spectrum, the

information contained in the degree variance reflects the frequency concentration normal to the axis with which the summation variable is associated.

The spectral analysis in terms of degree variance and degree crossvariance can also be used to study the correlation of two functions as a function of frequency. Let $\rho_n(f_1, f_2)$ denote the correlation coefficient (Kaula, 1967a) between the nth terms of the series representation of the two functions $f_1(x,y)$ and $f_2(x,y)$, then

$$\rho_n(f_1, f_2) = \frac{D_n(f_1, f_2)}{[D_n(f_1)\ D_n(f_2)]^{1/2}} \tag{30}$$

The quantity ρ_n is said to be the degree correlation coefficient of the two functions.

The formulas for spectral analysis techniques associated with one-dimensional series are widely available in literature and can be found in any standard text on time series analysis (for example, see Lee, 1964). The spectral representation of two-dimensional data on a sphere is discussed by Schoenberg (1942), Jones (1963), Heiskanen and Moritz (1966) and Kaula (1967b).

The frequency representation of two-dimensional data on a plane is discussed by Mesko (1965), Darby and Davies (1967), as well as several other authors, though from a different point of view. The discussions on the spectral analysis of two-dimensional data on a plane given in this report, are not commonly available in literature but can be obtained as an extension of the theory for one-dimensional data.

The above formulas are derived for periodic functions. It is possible to derive analogous formulas for random functions, since a random function can be obtained from a periodic function by letting its period approach infinity.

The above method of frequency analysis was used to analyse and compare the surface and the satellite-derived versions of the anomalous gravity field as well as the bathymetry of the Solomon Islands Area. In the course of discussion of the results of this analysis, a few other interpretation techniques will be considered which are believed to be of general applicability in a study of the nature considered here.

COMMENTS ON GRAVITY ANOMALIES AND THEIR GEOLOGIC SIGNIFICANCE

Of the various types of gravity anomalies that have been devised, the free air anomaly is most free from bias due to assumptions. The only bias present results from uncertainties in the reference ellipsoid and vertical gradient of gravity. The computation is based on the following expression:

$FA = g_o - (g\phi - k\Delta h)$, where g_o = observed gravity on the Potsdam datum and g_ϕ = theoretical sea level gravity for the latitude of the observation site as defined by the International Gravity Formula.

$g = 978.030\ (1 + 0.005302\ \sin^2\phi - 0.000007\ \sin^2 2\phi)$

k = vertical gradient gravity (.3086 mgal/meter)

Δh = elevation relative to sea level

The Bouguer anomaly allows for the mass attraction of the topography above sea level on land and the mass deficiency of the water column down to the sea floor in the oceans. The expression for the Bouguer anomaly can be written: $BA = FA - \Delta g_B$ where FA is the free air anomaly, and on land $\Delta g_B = 2\pi G\ \sigma_c\ \Delta h$ where σ_c = the mean density of the crust above the depth of isostatic compensation.

Whether one ascribes to the Pratt concept of isostasy whereby the mean density of the crust above the depth of compensation varies inversely with change in surface elevation; or the Airy concept of isostasy whereby surface elevation is a function of variations in thickness of a hydrostatically supported crust, it is clear that the mass distribution within the crust has nothing to do with surface elevation. Under either concept the mean density of the crust is the only density value having any significance in determining the surface elevation. The Bouguer anomaly reduction, therefore, to have significance in relating gravity to abnormalitiesin the subsurface mass distribution should be based on a best estimate of crustal density rather than that of the geologic column above sea level or some arbitrary value, such as 2.67 gm/cm^3, which was adopted 40 years ago when essentially nothing was known about the earth's crust. If one were to choose a most probable value today as that derived by Woollard (1966, 1968), it would be about 2.92 gm/cm^3

with a density contract between the crust and mantle of about 0.39 gm/cm^3.

In the oceans

$$BA = FA + \Delta g_{B'}$$

where

$$\Delta g_{B'} = 2\pi\gamma\ (\sigma_c - \sigma_w)\ \Delta h'$$

and

σ_c = density of the crust

σ_w = density of sea water

$\Delta h'$ = depth of water

The above expression treats the water column as a geologic correction in that allowance is made for the mass deficiency of the water. Although a value of 2.67 gm/cm^3 has been commonly used for σ_c, in recent years where gravity has been used for studying crustal abnormalities and relating gravity to seismic data, σ_c has been taken as 2.84, 2.87 and 2.90 gm/cm^3. These values were adopted by different investigators in their attempts to reconcile the gravity data with the seismic observations.

The most convincing evidence that σ_c should be about 2.9 gm/cm^3 is that presented by Woollard (1962) in which he showed that a linear relation can be obtained between surface elevation and the depth of the mantle if the water column is condensed to equivalent rock material

having a density (2.745 gm/cm^3) equivalent to the crystalline rock complex on the continents underlying the surficial sediments. This plot (Fig. 13) which incorporates both continental elevations and mantle depths as well as equivalent rock elevations and mantle depths in the oceans has a slope of 7.5. That is for each 1 km change in surface elevation there is 7.5 km change in mantle depth. The zero elevation intercept value is about 33 km. The resulting equation, $M = 33 + 7.5\ \Delta h$, gives results that agree with the hydrostatic buoyancy equation

$$R = \frac{H_c \sigma_c}{\sigma m}$$

when

$$\sigma_c = 2.92$$

and

$$\sigma_m = 3.31 \text{ gm/cm}^3.$$

The related gravitational expression is

$$\Delta R = \frac{\Delta g}{2\pi G \Delta \sigma}$$

where

$$\Delta \sigma = 0.39 \text{ gm/cm}^2$$

and Δg is based on a crustal density of 2.92 gm/cm^3. These relations give results that agree to within ±6 km with seismic data 65% of the time, and indicate that the Airy concept of isostasy is operative most

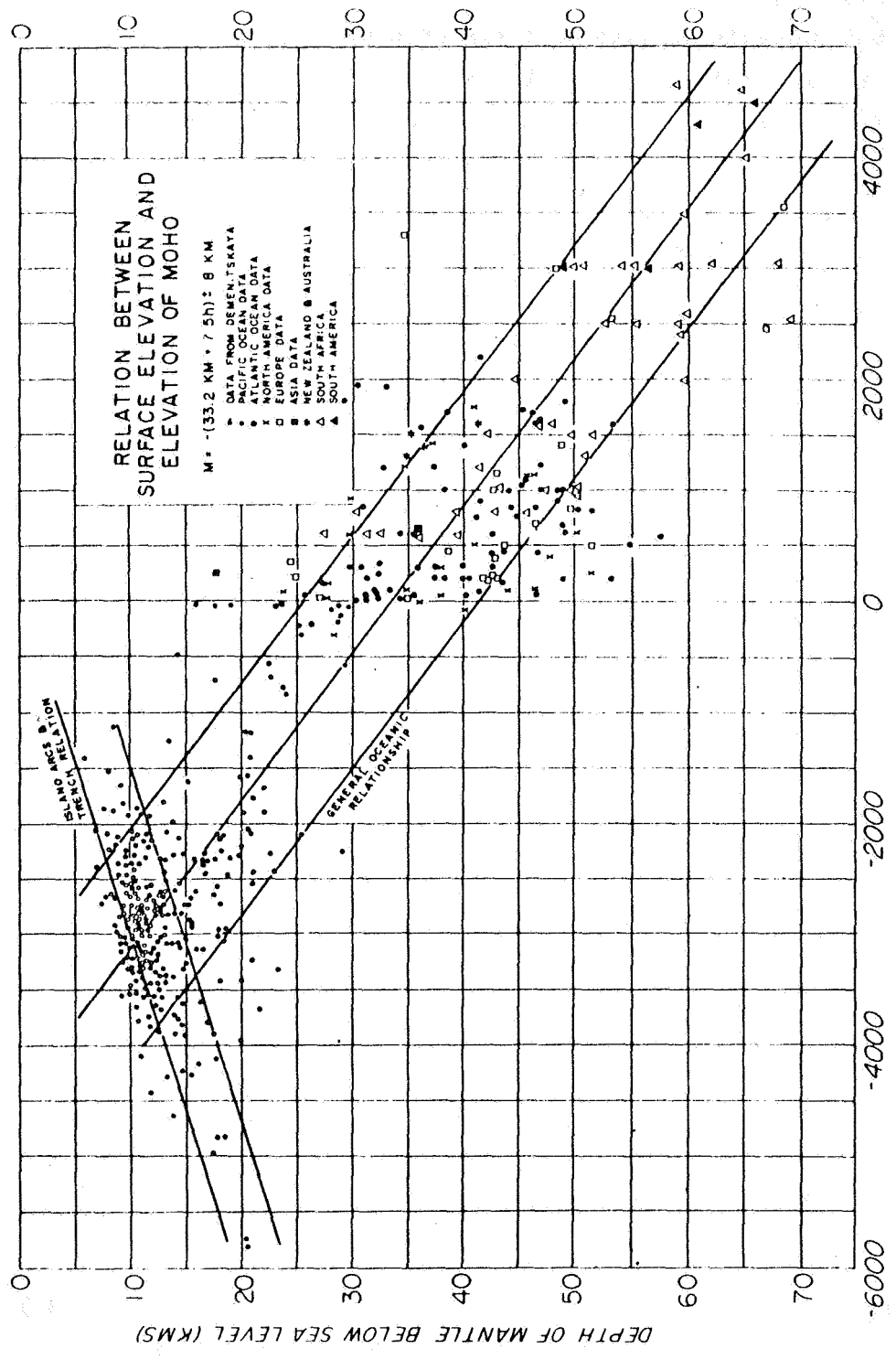

Fig. 13. Relation between surface elevation and elevation of Moho (after Woollard, 1962).

of the time. The departures exceeding 6 km, and in places exceeding 15 km, can be related to variations in $\Delta\sigma$ and tectonic displacement of the crust (lack of isostatic equilibrium). Both situations have gravity expression, but opposite in sign in terms of crustal thickness. Areas with a subnormal crustal density (subnormal seismic velocity) usually have a subnormal crustal thickness for the surface elevation and negative free air gravity anomalies. There are also areas of crustal uplift and as shown by Woollard (1968) are also areas where there is usually a subnormal mantle velocity.

Areas with an abnormal crustal density as defined by abnormal seismic velocity values usually have an abnormal crustal thickness for the surface elevation and positive free air gravity anomalies. These are also areas of crustal subsidence and as shown by Woollard are usually areas where there is an abnormal mantle velocity.

In studying these areas, Woollard (1962) showed that the Bouguer anomaly could be related to the actual crustal parameters (density and thickness) if there are no departure from hydrostatic equilibrium by introducing a correction term that takes into consideration the difference in $\Delta\sigma$ from the normal value. The basic expression for such cases are as shown below.

Under normal relations with a fixed density contrast between the crust and mantle a floating crust of thickness H and density $\bar{\sigma}_s$ will displace its own mass of mantle material with density σ_m, and the root increment (ΔR) for any change in elevation (Δh) will be related to the increase in crustal mass (ΔM_c) so that

$$\Delta R = \frac{\Delta M_c}{\sigma_m} = \frac{\Delta H \bar{\sigma}_s}{\sigma_m} = \frac{(\Delta R + \Delta h)\bar{\sigma}_s}{\sigma_m} \tag{31}$$

or

$$\Delta R\left(1 - \frac{\bar{\sigma}_s}{\sigma_m}\right) = \frac{\Delta h \bar{\sigma}_s}{\sigma_m} \tag{32}$$

and

$$\Delta R \frac{(\sigma_m - \bar{\sigma}_s)}{\sigma_m} = \frac{\Delta h \bar{\sigma}_s}{\sigma_m} \tag{33}$$

or

$$\Delta R(\sigma_m - \bar{\sigma}_s) = \Delta h \bar{\sigma}_s \tag{34}$$

and

$$\Delta R = \frac{\Delta h \bar{\sigma}_s}{(\sigma_m - \bar{\sigma}_s)} \tag{35}$$

For any other crustal density ($\bar{\sigma}_c = \bar{\sigma}_s + \Delta\sigma_c$);

$$\Delta M_c = (H_s + \Delta H)\ (\bar{\sigma}_s + \Delta\sigma c) - H_s \bar{\sigma}_s \tag{36}$$

or

$$\Delta M_c = \Delta\sigma_c H_s + \bar{\sigma}_c \Delta H \tag{37}$$

and

$$\Delta h = \Delta H - \frac{1}{\sigma_m} (\Delta\sigma_c H_s + \bar{\sigma}_c \Delta H) \tag{38}$$

or

$$\Delta h = \Delta H \frac{(\sigma_m - \bar{\sigma}_c)}{\sigma_m} - \frac{\Delta\sigma_c}{\sigma_m} H_s \tag{39}$$

and

$$\Delta R = \frac{\bar{\sigma}_c}{\sigma_m} \Delta H + \frac{\Delta\sigma}{\sigma_m} H_s \tag{40}$$

or

$$\Delta R(\sigma_m - \bar{\sigma}_c) = \Delta h\bar{\sigma}_c + H_s\Delta\sigma_c \tag{41}$$

or

$$\Delta R = \frac{\Delta\sigma_c H_s}{(\sigma_m - \bar{\sigma}_c)} + \frac{\sigma_c \Delta h}{(\sigma_m - \bar{\sigma}_c)} \tag{42}$$

ΔR in this case has two terms; one

$$\frac{(\sigma_c \cdot \Delta h)}{\sigma_m - \bar{\sigma}_c}$$

corresponds to that for the normal situation with the actual crustal density ($\bar{\sigma}_c$) instead of the standard density ($\bar{\sigma}_s$), and the other

$$\frac{(\Delta\sigma H_s)}{\sigma_m - \bar{\sigma}_c}$$

is a correction term for the difference in density ($\Delta\sigma$) for the actual crust and the standard crust. In terms of the Bouguer anomaly which is based on $2\pi G\Delta h\bar{\sigma}_s$ for normal conditions, there are two terms $\Delta g_1 = 2\pi G\Delta h\bar{\sigma}_c$ and $\Delta g_2 = 2\pi G H_s \Delta\sigma_c$. Whereas with the normal Bouguer anomaly ($2\pi G\Delta h\bar{\sigma}_s$);

$$\Delta R = \frac{2\pi G\Delta h\bar{\sigma}_s}{2\pi G(\sigma_m - \bar{\sigma}_s)} \tag{43}$$

with a crust of abnormal density

$$\Delta R = \frac{\Delta g_1 + \Delta g_2}{2\pi G(\sigma_m - \bar{\sigma}_c)} \tag{44}$$

As will be shown, a crustal density difference ($\Delta\sigma$) of .06 gm/cm^3 can result in a gravity difference of 80 mgal in gravitational compensation because of the resulting difference in crustal thickness under equilibrium conditions.

As the free air anomaly incorporates the gravity effect resulting from changes in crustal composition, it shows about the same degree of bias from this cause as would be revealed by isostatic anomalies which only measure the departure in Bouguer anomaly from that deduced for a standard model of the crust whose thickness or mean density is directly related to surface elevation. $IA = BA + \Delta g_i$ where Δg_i = the isostatic compensation required for the surface elevation. That the free air anomalies should show a bias under equilibrium conditions with changes in crustal composition can be related to the Earth curvature effect which becomes important beyond a distance of about 166 km from an observation site and the fact that g varies inversely as the square of the distance from the observation site to any mass anomaly, and that only the vertical component of gravity (g_z) = g cos θ is measured. As the compensation mass (ΔR) lies at a depth related to the base of the sea level crustal column which is of the order of 32 km, the compensation effect is near zero immediately beneath the observation site, and only about 75% achieved when the crustal block has a radius of 166 km. By contrast, over 90% of the surficial mass effect is realized within a radius of 10 km. To achieve a similar degree of compensation requires a crustal block with a radius of about 4^o. This applies where there is no anomalous mass between sea level and the depth of the base of the sea level column. With an anomalous crustal density, this intervening crustal section between sea level and 32 km below sea level constitutes an additional contributing mass distribution whose gravity effect is approximated by the term $\Delta g = 2\pi G H_s \Delta\sigma$.

That the above gives realistic results can be shown by example.

Assumed standard crust:

$$H_s = 32 \text{ km}, \ \sigma_s = 2.92 \text{ gm/cm}^3, \ \sigma_m = 3.31 \text{ gm/cm}^3$$

Anomalous crust:

$$H_c = 37.7 \text{ km}, \ \bar{\sigma}_c = 2.86 \text{ gm/cm}^3, \ \Delta h = 1.36 \text{ km},$$

$$\Delta\sigma_c = 2.92 - 2.86 = -.06 \text{ gm/cm}^3$$

Mass solution:

$$\Delta R = \frac{\Delta\sigma_c H_s}{(\sigma_m - \bar{\sigma}_c)} + \frac{\bar{\sigma}_c \Delta h}{(\sigma_m - \bar{\sigma}_c)}$$

$$\Delta R = \frac{-.06 \times 32}{(3.31 - 2.86)} + \frac{2.86 \times 1.36}{(3.31 - 2.86)} = 4.35 \text{ km}$$

Gravity solution:

$$\Delta R = \frac{\Delta g_1 + \Delta g_2}{2\pi G(\sigma_m - \sigma_c)}$$

$$\Delta g_1 = 41.85 \times \Delta h \times \bar{\sigma}_c = 41.85 \times 1.36 \times 2.86 = 162.9$$

$$\Delta g_2 = 41.85 \times H_s \times \Delta\sigma_c = 41.85 \times 32 \times -.06 = 80.3$$

$$\Delta R = \frac{162.9 - 80.3}{41.85 \times 0.45} = 4.35 \text{ km}$$

Proof: For a standard column the mantle displaced under equilibrium conditions:

$$R_s = \frac{H_s \sigma_s}{\sigma_m} = \frac{32 \times 2.92}{3.31} = 28.22 \text{ km}$$

For the column with anomalous density of -.06 gm/cm^3

$$R_c = \frac{37.7 \times 2.86}{3.31} = 32.57 \text{ km}$$

$$\Delta R = R_c - R_s = 32.57 - 28.22 = 4.35 \text{ km}$$

Although the above example is based on a flat earth (no curvature), it shows conclusively that the crustal composition is a significant factor since the calculated compensation effect under equilibrium conditions (82 mgal) is only about one-half that of the surficial mass above sea level (162 mgal) rather than equal to it.

For a normal crust having the same elevation (Δh = 1.36 km) the Bouguer anomaly would be BA = 41.85 x 1.36 x 2.92 = 166 mgal and $\Delta R = \frac{166}{41.85 \times .39} = \frac{166}{16.32} = 10.17$ km. As the actual root increment for the anomalous crust considered relative to the standard column is 4.35 km, the difference in compensation root for the change in crustal density of -0.06 gm/cm^3 is -5.82 km.

If the relations had been reversed, i.e., there had been an increase in crustal density of 0.6 km so that $\bar{\sigma}_c$ = 2.98 gm/cm^3 with the same surface elevation of 1.36 km, H_c would have been 51.42 km, and the displaced mantle (R) = $\frac{51.42 \times 2.98}{3.31}$ = 46.30 km. As R for the standard sea level column assumed is 28.32 km, the root increment (ΔR) would be 46.30 - 28.23 = 18.07 km and the abnormal root increment 18.07 - 10.17 = 7.9 km.

This is verified by the gravity solution for ΔR

$$\Delta R = \frac{\Delta g_1 + \Delta g_2}{2\pi G(\sigma_m - \bar{\sigma}_c)}$$

$$\Delta g_1 = 41.85 \times \Delta h \times \bar{\sigma}_c = 41.85 \times 1.36 \times 2.98 = 169.5 \text{ mgal}$$

$$\Delta g_2 = 41.85 \times H_s \times \Delta\sigma_c = 41.85 \times 32 \times .06 = 80.3$$

$$\Delta R = \frac{169.5 + 80.3}{41.85 \times .33} = \frac{249.8}{13.8} = 18.1 \text{ km}$$

In this case the compensation effect is 249.8 mgal rather than 169.5 mgal as based on the mass distribution above sea level, and as before the contribution from the abnormal crustal density was 80 mgal.

These examples are cited to bring out the importance of crustal parameters in defining the surface gravity field, and to show also the potential error that can result from using a fixed density for the crust and mantle in interpreting Bouguer anomalies where there are no seismic subsurface crustal data. Although it is not possible to relate the free air and isostatic anomaly directly to abnormality in crustal density because the size of the area involved also contributes to anomalous gravity, it is instructive to review some of the crustal relations noted in areas of anomalous isostatic values where it appears the anomalous gravity is due to variations in crustal density rather than an actual departure in isostatic equilibrium.

The crustal reference standard used in the above tabulation is based on the relation established by Woollard (1962) and shown in Figure 13 which relates crustal thickness to surface elevation. These data define $H = 33.2 + 7.5\ \Delta h + \Delta h$ where Δh is in kilometers. A plot of the departure (δH) of the observed crustal thickness values from the derived normal values based on the surface elevation (Fig. 14) shows that except for the data from the Basin and Range area of Utah, Nevada and California, a relation is obtained that can be written $\delta H = .35$ IA + 0 km, where IA is the isostatic anomaly. In the Basin and Range area the expression $\delta H = .35$ IA - 13.7 km appears to be applicable.

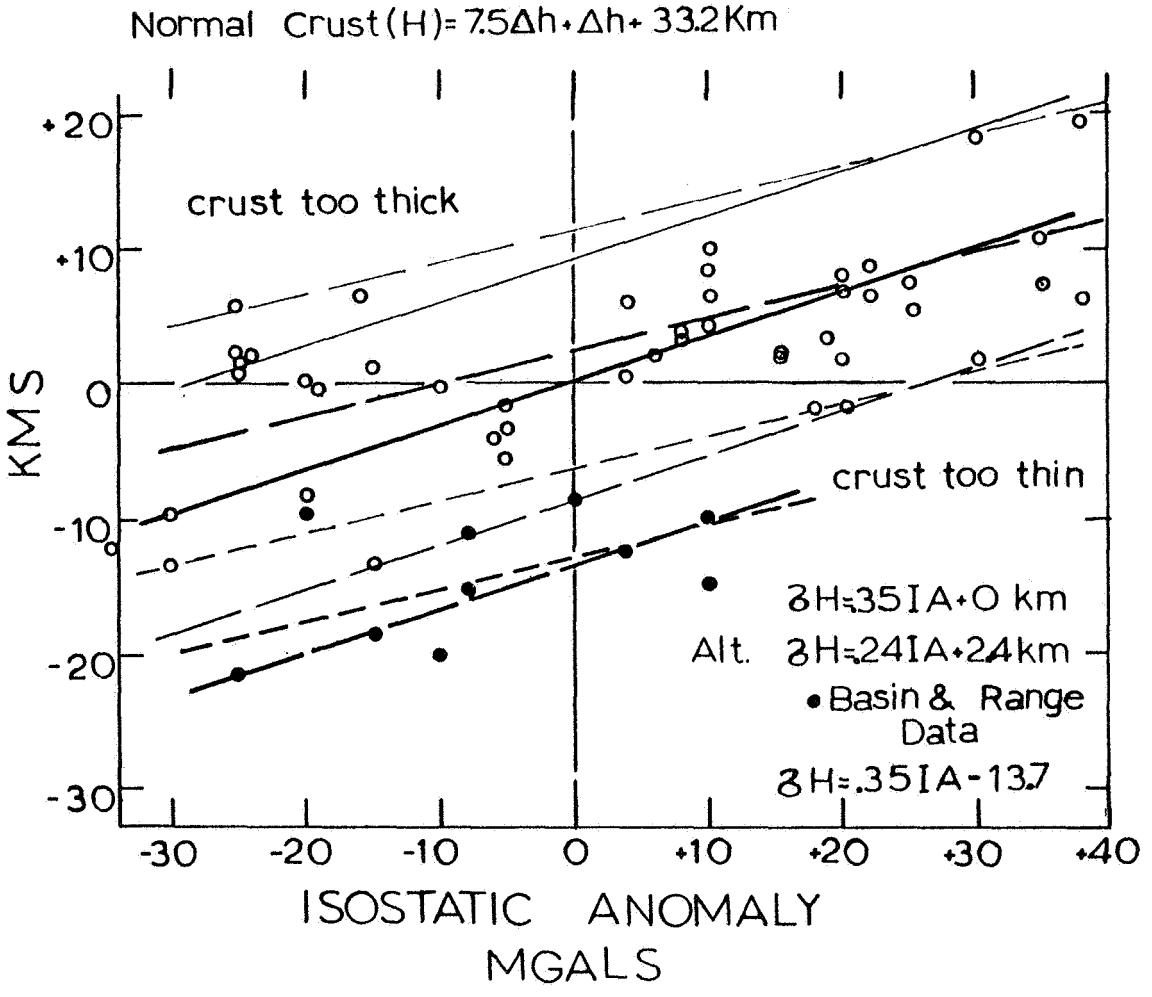

Fig. 14. Plot of departure (δH) of observed crustal thickness from derived normal values based on surface elevation.

As there are few areas for which there are isostatic anomaly values, a first approximation of these values can be deduced from the free air anomaly values. A general relationship that is probably more reliable is defined by a plot of free air anomalies as a function of isostatic anomalies. Figure 15 shows such a plot for about 1000 sites having a general distribution in the United States and where there is no obvious dependence of the free air anomaly values on topographic relief. The relation defined is FA = 1.15 IA + 6 mgal or IA = 0.87 FA - 5 mgal. In connection with Figure 15 it is to be noted that the range in isostatic and free air anomalies that fall within ±10 mgal of the average relation defined is from about -60 to +60 mgal with 80% of the values concentrated between -40 and +40 mgal. Although local geology contributes to this wide spread in values, it is almost identical with that represented in the regional data shown in Table 1 for locations where there are seismic crustal measurements. These data show a change of 70 mgal associated with an anomalous change of 22 km in crustal thickness.

The displacement of the Basin and Range data from the rest of North America (-13.7 km in mean values of crustal thickness for the same isostatic anomaly values) introduces a factor in crustal relations to gravity that is not yet understood. The relations suggest that some factor in the upper mantle has contributed about +47 mgal to the gravity field. The only distinguishing seismic characteristic other than a markedly sub-normal crustal thickness for the surface elevation is a markedly sub-normal seismic mantle velocity (7.6 to 7.9 km/sec rather than 8.0 to 8.4 km/sec as observed elsewhere). As shown by Woollard (1968) there is a direct relationship between the mean seismic velocity of the crust and the thickness of the crust to the seismic mantle velocity. The higher the mantle velocity, the higher the mean crustal velocity and the thicker the crust for a given elevation. Just as there is a relation between isostatic anomaly values and crustal thickness there is a relation between isostatic anomaly values and seismic crustal velocity and mantle velocity. As in general, density is directly related to seismic velocity, the anomalous mass could lie either in the crust or mantle or both. Woollard (1968) has suggested on the basis of the development of a thick high-velocity basal crustal layer where there is a high mantle velocity and the absence of this layer where the mantle

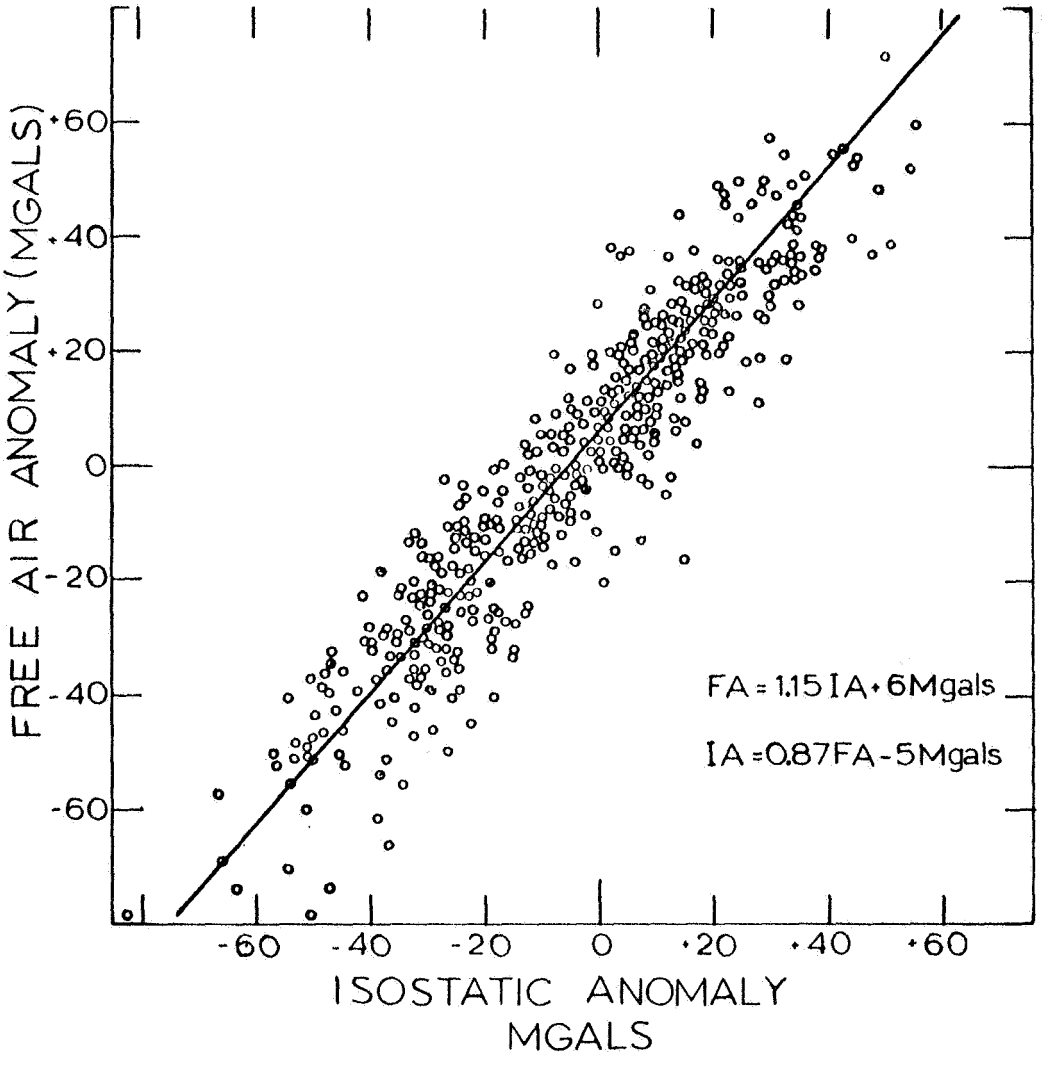

Fig. 15. Relation of free air anomalies to isostatic anomalies in the United States based on 1000 sites.

velocity is low, that there is a transfer of mass between the crust and mantle which tends to maintain isostatic equilibrium. This appears to be supported by the deduced density contrast between the crust and mantle based on density equivalents of seismic velocities observed for different rock types under high confining pressures. For example, with a mantle velocity of8.4 km/sec the deduced density contrast is 0.52 gm/cm^3 whereas at 8.0 km/sec the density contrast is 0.41 gm/cm^3. The corresponding crustal velocity values are 6.65 km/sec and 6.48 km/sec, and the corresponding depths of the mantle below sea level are 50 km and 37 km. One mineralogic transformation in the mantle that would give these relations is a change from fayalite (iron-rich olivine) to fosterite (magnesium-rich olivine). Another would be a change from iron garnet to a magnesium garnet. If the iron in either case could migrate from the mantle to the crust, it would raise the velocity of the mantle and also cause its density to be lowered. Serpentinization of the olivine by the addition of water would also lower the density of the mantle but the attendant drop in velocity and expansion in volume would give opposite relations from those observed; i.e., there would be crustal uplift rather than subsidence as observed where the crust is thick and the mantle velocity is high. Serpentinization would account for the Basin and Range relations where there is a thin crust that is incompatible with the high surface elevation and a low mantle velocity if it were not for the +47 mgal offset in isostatic anomaly values for this area. A possible explanation is that the mantle has changed from an olivine phase (dunite) with a density of about 3.31 gm/cm^3 to possibly a garnet phase (eclogite) with a density of around 3.5 gm/cm^3.

Although it is not possible to completely resolve problems such as the above short of drilling to the mantle, our purpose in discussing them here is to show that there is good evidence for significant changes in mass associated with the crust and upper mantle having marked effects on gravity, and that it is not preposterous to think they might not exist on a more widespread scale in the oceans which are the areas of most interest from the standpoint of satellite gravity but about which very little is known as yet. Certainly in the case of the North Atlantic Ocean where the surface gravity field is known and there are

abundant seismic data, 10^{o} x 10^{o} free air anomaly averages of the surface data give a remarkably similar pattern of anomalous gravity to that defined by the satellite data. Here, as indicated by Worzel (1965), it appears the gravity anomalies can be explained by the seismic parameters of the crust and mantle without recourse to a deep-seated mass distribution.

FREQUENCY ANALYSIS OF THE GRAVITY FIELD OVER THE SOLOMON ISLANDS AREA

General Remarks

The Solomon Islands lie along the southwestern border of the Pacific Ocean. They form a chain of oceanic islands starting with the Island of Bougainville in the northwest and ending with San Cristoval in the southeast. Except for these two terminal islands, they occur in a double chain whose two wings are separated by a narrow strait called 'The Slot' which separates the islands of Choiseul, Santa Ysabel and Malaita from the Shortland Islands, New Georgia Group, Russel Islands, Guadalcanal and San Cristoval. As a group, they stand on a broad bathymetric high, generally known as the Solomon Islands Platform, which extends from New Ireland in the northwest (see Fig. 16) to the east of the chain.

Politically the Solomon Islands consist of: 1) the British protectorate and 2) the Australian protectorate. The British protectorate includes the larger islands of Guadalcanal, Choiseul, Malaita, Santa Ysabel, the Florida Group, San Cristoval, New Georgia Group and the smaller Shortland Islands, Treasury Islands, Russel Islands and the Santa Cruz group. The Australian protectorate is limited to the islands of Bougainville and the Buka Islands. The principal geological and structural features of the British Solomon Islands are described in considerable detail in 'The British Solomon Islands Geological Record', vol. II, 1959-1962, particularly by Coleman et al. (1962) and Coleman (1962). The geology of the Australian protectorate have been reported on by Blake and Miezitis (1966).

The Solomon Islands are an area of recent emergence from the sea that is characterized by faulting, intrusions and volcanism. The volcanoes are mainly andesitic and range in age from Pleistocene time to contemporary activity. The distribution of the volcanic centers, except for those on the island of Choiseul, lie roughly along an arc which is convex towards Australia.

The area is marked by high seismicity. Most of the earthquake shocks are shallow with foci less than 50 km. Intermediate to deep earthquake shocks are relatively infrequent. In contrast to normal island arcs the seismic zones at depth do not dip towards Australia but

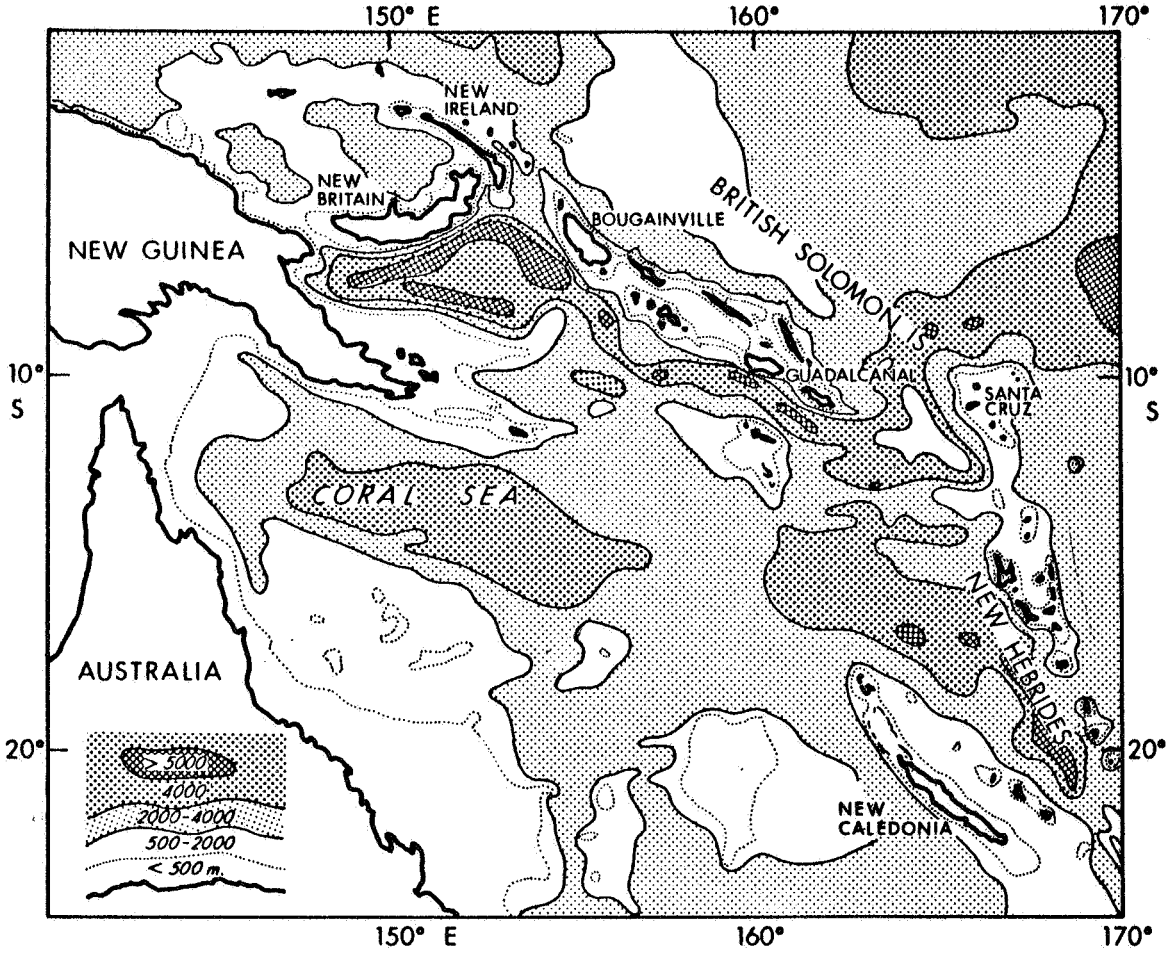

Fig. 16. Location and generalized bathymetry of the Solomon Islands area (after Coleman, 1962).

are either vertical or inclined towards the Pacific.

Grover (1968) thinks there is a pattern of deep focus earthquakes which migrate progressively towards the surface from both ends of the islands, and that when two such series happen to be in phase and converge at the same time in the central area, there is vulcanism. The concept of progressive migration of earthquakes along a fault system is not new, but the overall pattern proposed by Grover is new and if true may be peculiar to the Solomon Islands.

Surface Gravity Data

Most of the gravity observations used in this analysis were obtained as a part of an integrated program of geophysical and geological study of the Solomon Islands and adjacent sea area conducted by the University of Wisconsin (Grover, 1968; Laudon, 1968); and the University of Hawaii (Rose, et al. 1968). These data were supplemented by submarine pendulum gravity measurements carried out by the Lamont Geological Laboratory (Worzel, 1965). In using the observations from the three different sources, equal weights were given to all observations.

Free Air Anomaly Maps

Figure 17 shows the free air gravity map of Rose et al. (1968) for the oceanic areas. Figure 18 is the free air anomaly map of the land areas of the Solomon Islands region based on Laudon's data and prepared by Woollard (unpublished). These anomalies are computed with respect to the International Gravity Formula. The elevation data used for the reduction of land area gravity observations are discussed in the section on 'Elevation and Bathymetric Data.'

Bouguer Anomaly Maps

Figure 19 shows the Bouguer anomaly map of Rose et al. (1968) for the oceanic areas. These anomalies were computed by standard procedures, using a variable crustal density of 2.84 to 2.9 gm/cm for the Bouguer plate reduction. The reason for using variable crustal density rather than a fixed value stems from the fact that water pressure affects the

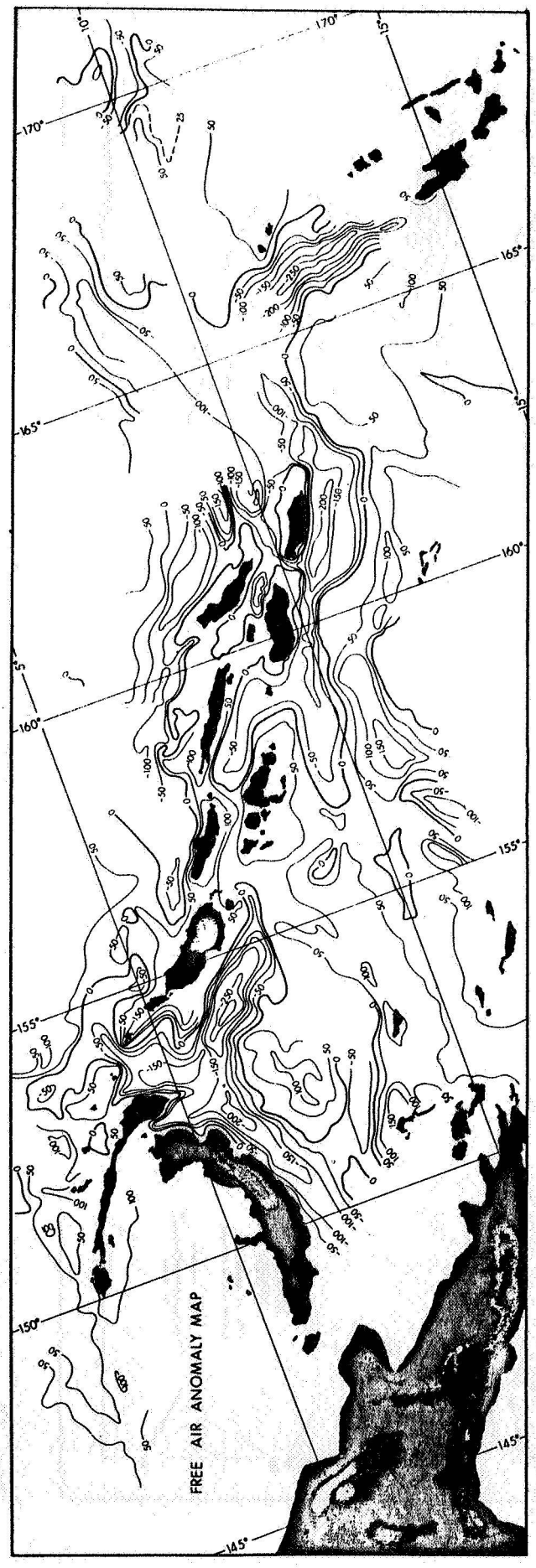

Fig. 17. Free air anomaly map of the Solomons (oceanic area); after Rose, Woollard, and Malahoff (1968).

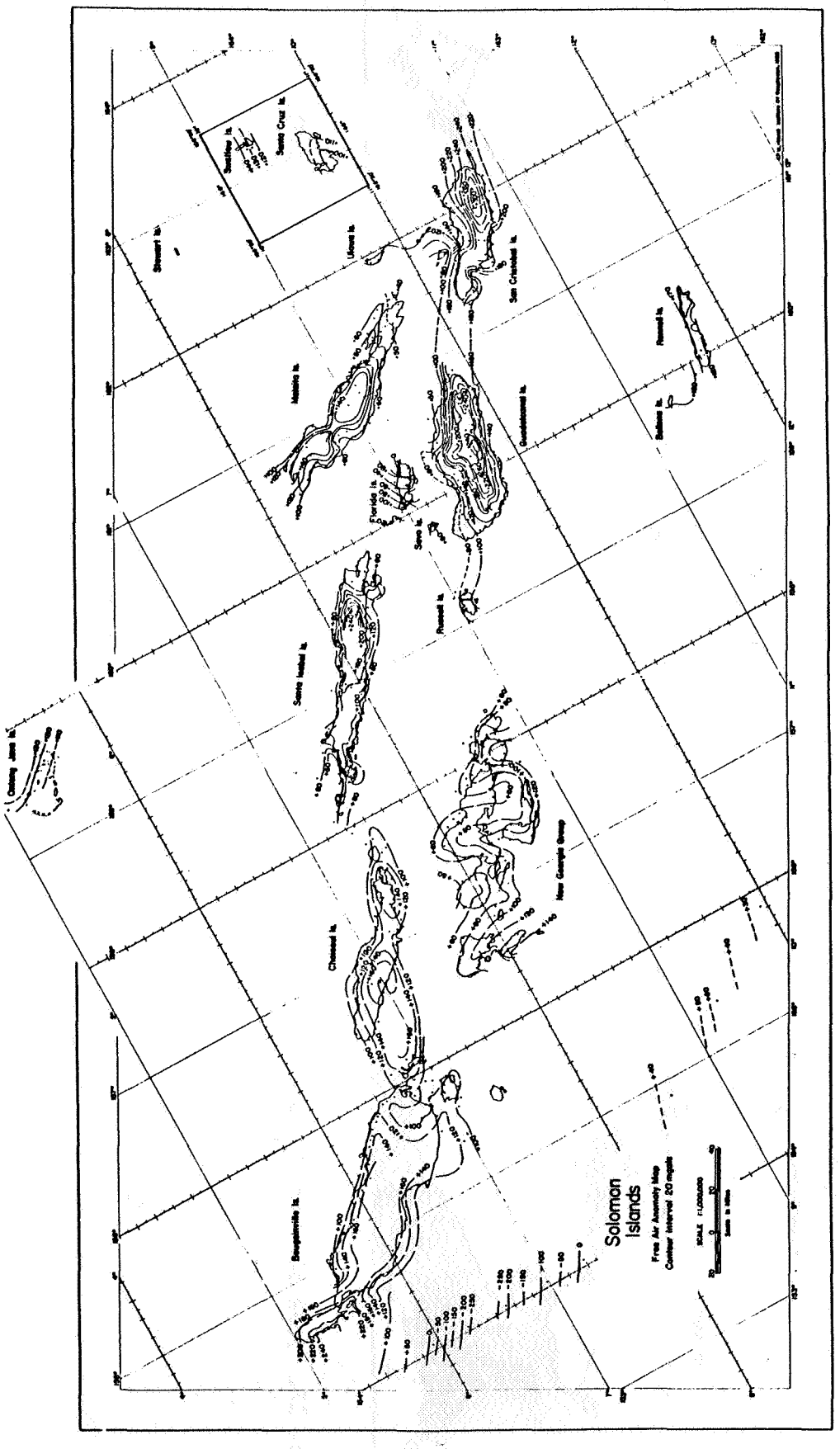

Fig. 18. Free air anomaly map of the Solomons (land area).

vesicle size and the resulting porosity of lavas emplaced in a marine environment (Moore, 1965), and hence, the density of the basalts associated with topography on the ocean floor increases with water depth. The use of a variable crustal density (Rose et al., 1968; Moore, 1965) would tend to minimize the effect of bathymetry on the Bouguer anomalies where there is topography by taking into account the appropriate density for each particular depth. However, as pointed out by Rose et al. (1968) using variable crustal density correction method rather than a fixed density of 2.87 gm/cm results in changes of 10 milligals or less in the Bouguer anomalies.

Figure 20 shows the Bouguer anomaly map of the land area (Woollard, unpublished). The density used in the Bouguer reduction was the accepted standard value of 2.67 gm/cm^3 for the crustal material between the observation station and sea level. If a more realistic density of 2.92 had been used the anomaly values would be increased by about 10 mgal per 1000 meters change in elevation.

1^o x 1^o Free Air and Bouguer Gravity Anomalies

The information given in Figures 17 to 20, supplemented by submarine gravity data (Worzel, 1965) was used to compute the 1^o x 1^o mean anomalies (by standard linear combination procedure) for the rectangular area between longitude 148^oE to 168^oE and latitude 5^oS to 12^oS. About 30% of the 1^o x 1^o squares do not have any data. Gravity anomalies for such squares were determined from the free air anomaly map and by linear interpolation from the surrounding anomalies.

The mean free air and Bouguer anomalies for 1^o x 1^o squares are given in Tables 2 and 3 respectively and the contoured 1^o x 1^o free air anomaly values are shown in Figure 21. The big change in Figure 21 over Figures 17 and 18 (the original free air anomaly maps) is the suppression in anomaly values. The largest 1^o x 1^o values is 125 mgal whereas original values exceeded 300 mgal.

Bathymetric and Elevation Data

The bathymetric map of Rose et al. (1968) is shown in Figure 22. This map is based upon the existing Admiralty charts, the echo-sounding

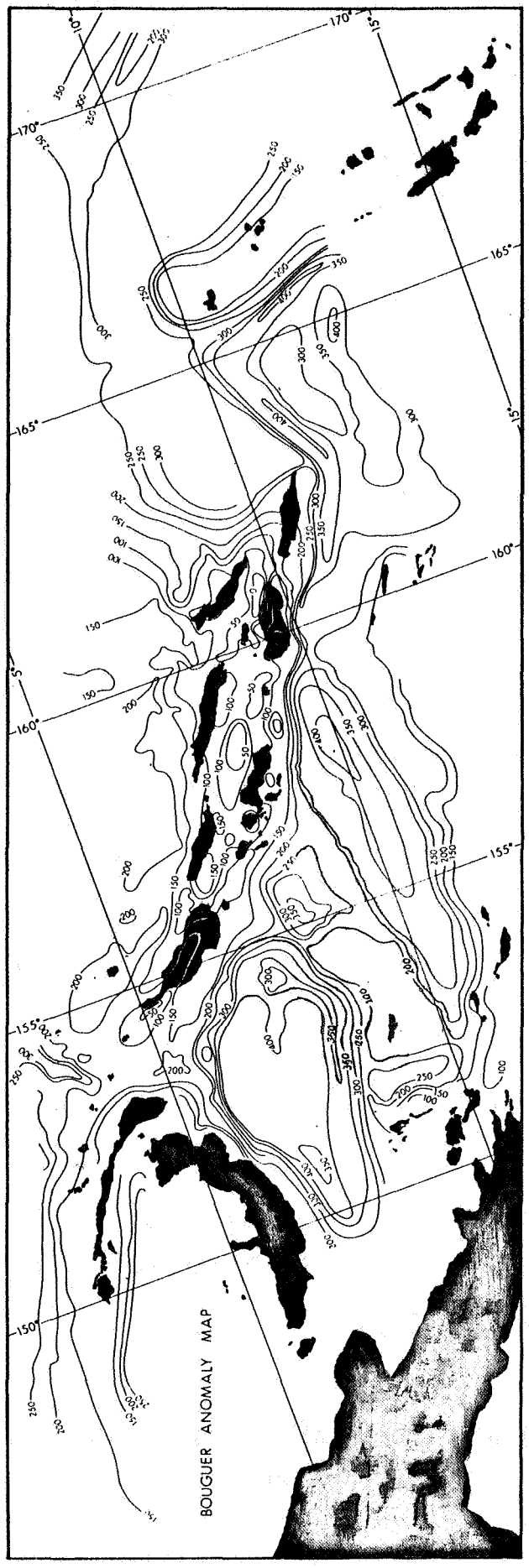

Fig. 19. Bouguer anomaly map of the Solomons (oceanic area); after Rose, Woollard, and Malahoff (1968).

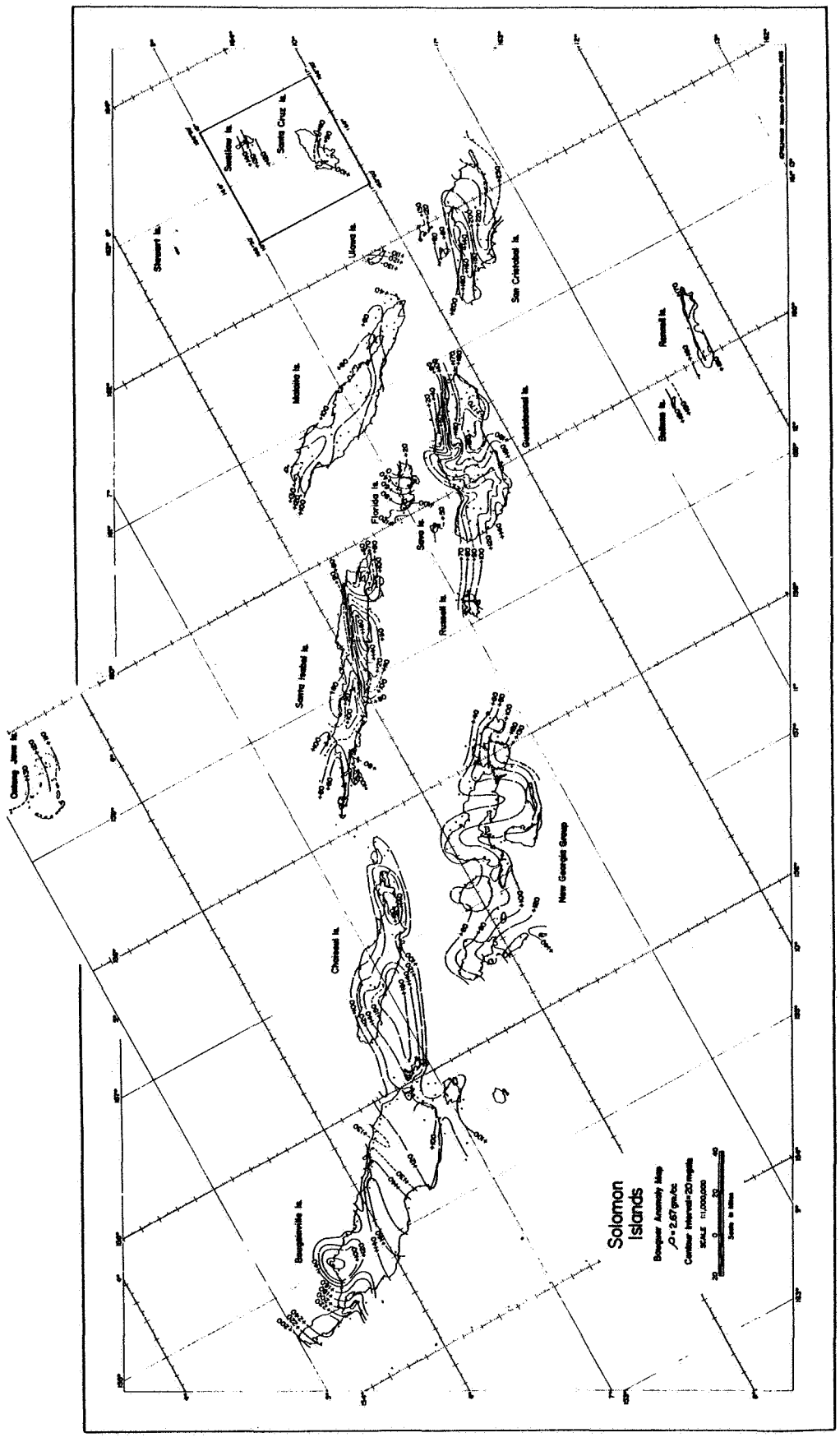

Fig. 20. Bouguer anomaly map of the Solomons (land area).

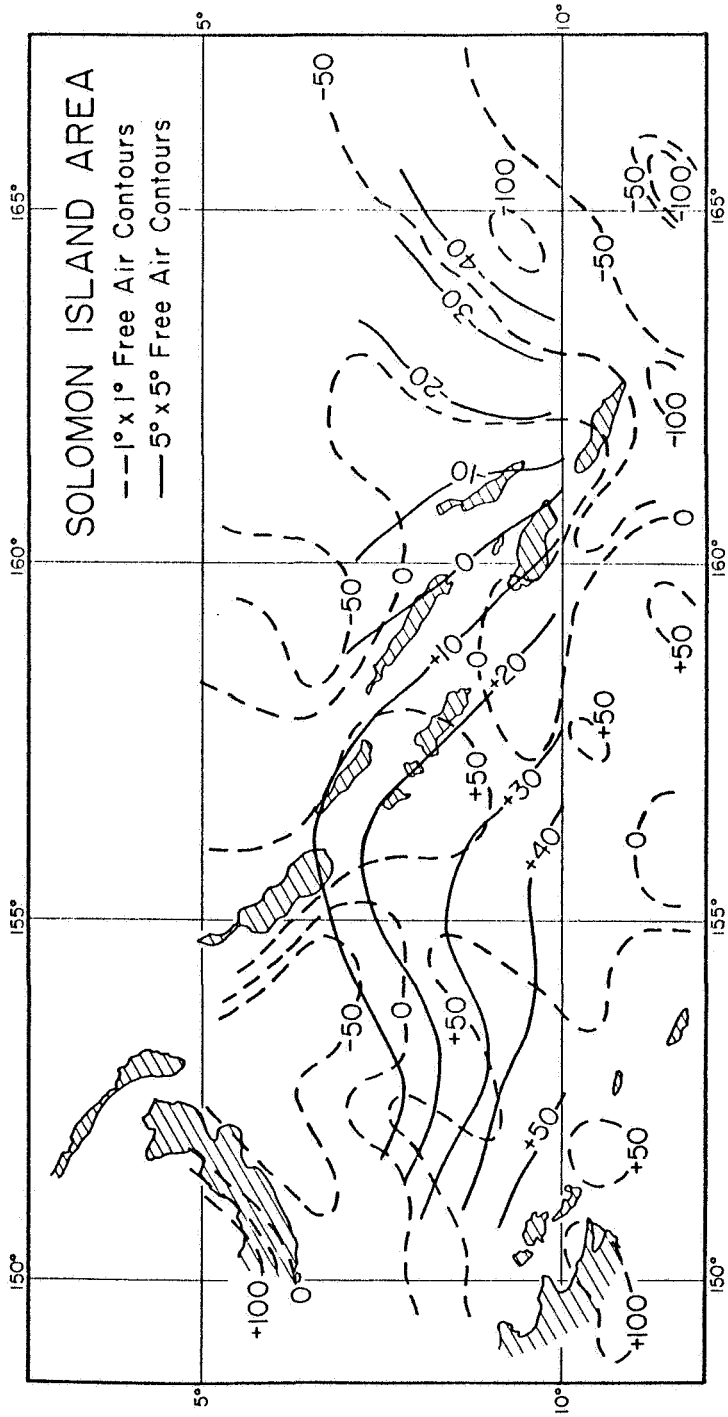

Fig. 21. 1° x 1° and 5° x 5° free air anomaly map of the Solomon Islands area.

data obtained on HMS Dampier in 1965, USS Wandank in 1964, Proa expedition in 1962 and the Monsoon expedition in 1960-61. The corrections applied to these data for changes in temperature with depth are discussed by Rose et al. (1968).

For the land areas the elevation were obtained in part by levelling and in part from barometric altimetry. Only a few gravity stations were located at points whose elevation had previously been determined by levelling. The elevations of all of the coastal stations were determined by hand levelling from the beach. Barometric altimetry was used for the balance of the stations, and these have an uncertainty of ±50 feet on average (±3 mgal in the Bouguer anomaly).

$1^{o} \times 1^{o}$ Mean Elevations and Bathymetry

Mean elevation and bathymetry values for $1^{o} \times 1^{o}$ squares for the rectangle bounded by longitude 148^{o}E to 168^{o}E and latitude 5^{o}S to 12^{o}S were determined from Figure 22, supplemented by elevations supplied by Laudon, and the western Pacific bathymetric map of the Scripps Institution of Oceanography (unpublished). These average values are given in Table 4. All the water depths are given as negative values.

Satellite-Determined Gravity Values

The satellite representation of the gravity field, to 8th degree of spherical harmonic expansion, was obtained from Kozai's (1964) zonal and Gaposhkin's (1966) tesseral harmonic coefficients. As indicated in the Introduction, such a representation corresponds to about a $22^{o} \times 22^{o}$ area. As the area of investigation is small, $1^{o} \times 1^{o}$ values were used in order to obtain a sufficient number of data points. This was justified since the gravity anomaly in terms of spherical harmonics is a continuous function of the space domain. Note, however, that the information content of the function is not compatible with this sampling interval. Also note that the function cannot be averaged over $1^{o} \times 1^{o}$ squares for any area whose size is less than or equal to $20^{o} \times 20^{o}$ as the information content of the function is already below

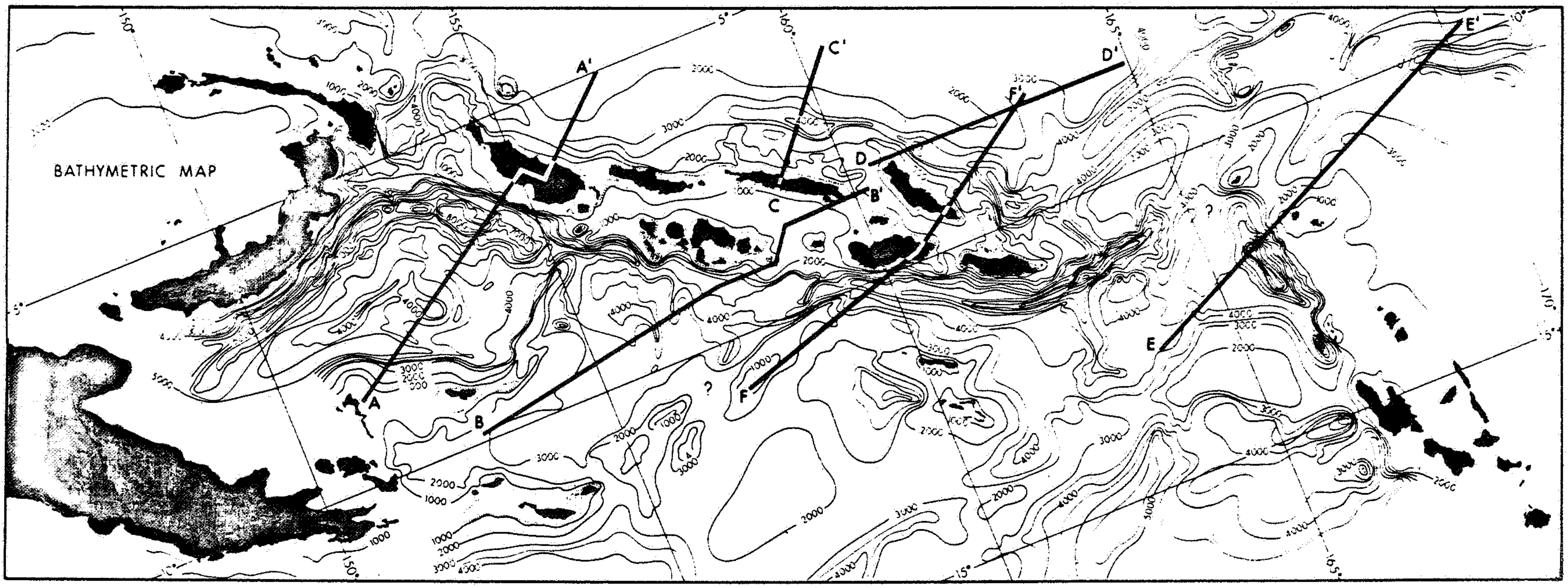

Fig. 22. Bathymetric map of the Solomons; after Rose, Woollard, and Malahoff (1968).

this level.

Tables 5A and 5B give the satellite-determined gravity values of 1^{o} intervals. The gravity anomalies in Table 5A are with respect to the International Reference Ellipsoid; those in Table 5B are with respect to the equilibrium figure of flattening 1/299.75 (Khan, 1968a,b; Jeffreys, 1963; Henriksen, 1960). Figure 21 shows a contoured map of the 1^{o} x 1^{o} free air anomaly values which is a smoothed version of the original map. Figure 21 also shows a contoured map of the 5^{o} x 5^{o} free air anomaly values. It is to be noted that the last approximates closely in pattern that is defined by the satellite-derived anomalous gravity field in showing a center of positive closure over the area lying south of the Solomon Islands.

Analysis of Data

The decomposition of the gravity anomaly Δg into its harmonic components was made by the linear sum represented by Equation ~~(44)~~ (14) as applied to a discrete case, i.e.,

$$\Delta g = \sum_{n=0}^{N} \sum_{m=0}^{M} \lambda_{nm} (a_{nm} \cos n\omega_1 x \cos n\omega_2 y + b_{nm} \sin n\omega_1 x \cos m\omega_2 y + c_{nm} \cos n\omega_1 x \sin m\omega_2 y + d_{nm} \sin n\omega_1 x \sin m\omega_2 y) \qquad (45)$$

where

$$\begin{matrix} a_{nm} \\ b_{nm} \\ c_{nm} \\ d_{nm} \end{matrix} = \frac{1}{\ell k} \sum_{i=0}^{L} \sum_{j=0}^{K} \Delta g_{ij} \begin{matrix} \cos \\ \sin \\ \cos \\ \sin \end{matrix} (n\omega_1 x) \begin{matrix} \cos \\ \cos \\ \sin \\ \sin \end{matrix} (m\omega_2 y)\, dx\, dy \quad (45a)$$

$$N = \frac{L - 1}{2}$$

$$M = \frac{K - 1}{2}$$

$$\omega_1 = \frac{\pi}{\ell}$$

$$\omega_2 = \frac{\pi}{k}$$

and

L x K = total number of data points in the rectangle

In Equation (45), the summation is carried to N and M only because the analysis is not meaningful beyond the Nyquist frequency.

Tables 6, 7 and 8 list the free air anomaly coefficients, Bouguer anomaly coefficients and satellite gravity coefficients, respectively. These coefficients are listed for anomalies both with respect to the International Reference Ellipsoid and the equilibrium figure. The topography (mainly bathymetry) coefficients are given in Table 9. It should be remembered that the index n applies to the x-axis which is east-west and the index m to the y-axis which is north-south.

The 'closeness' of the fit to a certain function can be tested by recomputing the function from the Fourier coefficients and studying the residuals, i.e., $g^i_{ij} - g^o_{ij}$ where g^i = input and g^o = output. These residuals are shown in Tables 10, 11, 12, and 13 for the free air and Bouguer anomalies, satellite gravity and the bathymetry, respectively. The residuals of the free air and Bouguer anomalies are computed with respect to the International Reference Ellipsoid only. It is easier to see the 'closeness' of fit by considering the variance of the input and the residual data where the variance of a function Δg, defined on a rectangle $R(0 \leq x \leq 2\ell,\ 0 \leq x \leq 2k)$, is given by

$$\mathrm{Var}(\Delta g) = \frac{1}{4\ell k} \iint \Delta g^2 \, dx \, dy \tag{46}$$

The variance is given in Table 14. It is readily seen that the Fourier fit does approximate the functions to a fairly close degree.

Another way of examining the 'closeness' of fit to the function is to test whether the linear sum representation of Δg given by Equation (45) is complete. This will indeed be true if the Parseval Theorem holds, i.e., if

$$\frac{1}{4\ell k} \iint \Delta g^2 \, dx \, dy - \sum_n D_n(\Delta g) \approx 0 \tag{46a}$$

Table 14 compares the results obtained from Equation (46) and the second term of Equation (46a). It is obvious that the frequency representation of the various functions is 'complete' in the mathematical sense.

Table 15 shows the spectrum of topography (mainly bathymetry) over the Solomon Islands area. Table 16 shows the spectra of the satellite-determined and the surface gravity field representations for the same area. Table 17 gives the cross-spectra of free air anomalies versus satellite gravity, free air anomalies versus bathymetry, satellite gravity versus bathymetry and Bouguer anomalies versus bathymetry. Table 18 lists the degree correlation coefficients for the various functions. Part 'A' of each of the Tables 16 and 17 is computed from

anomalies which were referred to the International Reference Ellipsoid. Part 'B' of each of these tables gives the corresponding quantities when the equilibrium figure (Henriksen, 1960; O'Keefe and Kaula, 1963; Jeffreys, 1963; Khan, 1968a,b) is adopted as the reference.

Discussion of Results

Comparison of Satellite and Surface Gravity

The comparison of the satellite-determined and surface gravity fields for local areas like the Solomon Islands using gravimetric data averaged over areas of the size of $1^o \times 1^o$ squares and satellite gravity data obtained from an 8th degree spherical harmonic representation could be rather elusive. One method of obtaining information of some general character is to study the spectra of the two representations of the gravity field. It is noteworthy that the problem of comparing the surface andthe satellite-determined versions of the gravity field is unique in character in that its objective is to compare two representations of the same function obtained by two different measurement techniques. If the two techniques are equally effective, they should give identical representation of the function. Of course, unless the actual representation of the function is known from an independent source, the more established of the above two techniques of measurement will have to be regarded as a standard of comparison for the relatively newer one.

The spectrum of the satellite-determined gravity field has relatively large concentrations of energy in the zero order harmonic. This harmonic is indicative of the mean value of the function over the area. The energy concentration in the next higher harmonic, i.e., the first order term, is about two orders of magnitude less. For the second order term, the energy decay is again about an order of magnitude relative to the first order term. For higher frequencies the energy is very small. In fact, for $n \geq 2$, the spectrum effectively diminishes to zero.

The degree correlation function $\rho_n(\Delta g_f, \Delta g_s)$ for the east-west axis, obtained from free air and satellite gravity field spectra (Table

18) is quite irregular and does not fall off 'steadily' as we approach higher frequencies. The reason probably is that $D_n(\Delta g_s)$ is almost zero for $n \geq 2$. Hence, it may not be really meaningful to correlate it with $D_n(\Delta g_f)$ which is about 10^3 times larger in the same band of frequencies. In spite of these limiting factors, however, the degree correlation function $\rho_m(\Delta g_f, \Delta g_s)$ along the north-south axis seems to be more regular, but the frequency range along this axis is not sufficiently wide to justify our confidence in its regularity.

The cross-degree variance function $C_n(\Delta g_f, \Delta g_s)$ given in Table 17 appears to give a more meaningful pattern. Its values for n = 0 and 1 are considerably larger than those for higher frequencies. The behavior of the function is similar along the north-south axis where its value for n = 0 is two orders of magnitude greater than that for higher frequencies.

Another parameter which could be examined to obtain, hopefully, some useful information involves the simple ratio of the two spectra being investigated. Let us call it the 'spectral ratio function' defined by:

$$R_n(\Delta g_f, \Delta g_s) = \frac{D_n(\Delta g_s)}{D_n(\Delta g_f)} \tag{47}$$

This function is given in Table 19, column 1. It can be seen that for n = 0, R_n is almost 10^3 times larger than that for $n \geq 1$. This would indicate that while the satellite-determined gravity field contains some information on components with wavelengths of the order of the size of the area under investigation, it does not have any significant information on higher frequencies ($n \geq 1$).

Normally, it would be expected that the ratio of the zero order terms should indicate that part of the mean value of the function which the satellite is able to see. However, this ratio is more than one in this case and great caution should be taken in interpreting it. It probably means that the data used in this analysis are not representing the long-wavelength component (of the order of the size of the area under investigation) to the same degree as the satellite data. This is

probably due to the fact that the gravity anomaly values, which were estimated for a considerable percentage of the data points by simple interpolation of the surrounding data, do not give a genuine representation of the actual gravity in the area. However, it alternately could mean that part of the long-wavelength component in the satellite representation of the gravity field orginates from the integrated effect of a number of short-wavelength surface features which cannot be resolved in the satellite data. However, such speculations should be reserved until the results of analysis involving a more complete gravity survey of the surrounding area become available.

The situation is about the same along the north-south axis where $R_0(\Delta g_f, \Delta g_s)$ is 10^3 times as large as R_m for $m \geq 1$. However, note that R_m for $m = 0$ is about an order of magnitude smaller than R_n (the spectral ratio function for the x axis) for $n = 0$.

The use of the equilibrium figure as the reference figure to compute the anomalous gravity field does not change the results to any significant degree. The principal change is that in the satellite gravity spectrum in which the concentration of energy in the zero order term ($n = 0$) is increased about twofold. The spectrum of the free air anomalies however does not change accordingly. This is unexpected. The reason may be due to the different wavelengths of the two functions [Legendre polynomial of the second degree and the Sin^2 (latitude)] which appear in the satellite gravity formula and the International Gravity Formula. This point has not been investigated, however, at this stage.

Topography and Gravity

As the free air anomalies usually are only slightly dependent on regional elevation but are always dependent on local topographic relief, a low correlation between free air anomaly and regional elevation is evidence for the isostatic compensation of topography. The Bouguer anomalies on the other hand are usually related to regional elevation, but show no dependence on local topographic relief. These relations indicate regional changes in elevation are compensated and the Bouguer anomaly is usually a direct measure of the compensation below at depth. The only exceptions as discussed earlier are where the density contrast between the crust and mantle depart significantly

from a constant value. In general, therefore, a low correlation between free air anomaly values and elevation with a simultaneous high correlation between elevation and Bouguer gravity anomaly indicates that topographic features are compensated.

The degree correlation function (Table 18) between elevation and the free air and Bouguer anomalies in the Solomon Islands region has several interesting features. For n = 0, the value of $\rho_n(\Delta g_f, T)$ is less than zero and $\rho_n(\Delta g_B, T)$ is nearly one. This shows that the compensation does occur on a regional scale. However, the fact that there is a negative value of $\rho_n(\Delta g_f, T)$ for n = 0 could mean that on the regional scale the topography is over-compensated or that there is a significant change in the density contrast between the crust and mantle. This point is discussed later in some detail. For n = 1, both $\rho_n(\Delta g_f, T)$ and $\rho_n(\Delta g_B, T)$ are significantly large. Part of the correlation between the free air gravity and the topography can be attributed to the fact that the gravitational attraction is a function of distance with the consequence that at a point on the physical surface of the earth, the attraction of the compensating material will always be smaller than that of the topographic feature even if the feature is perfectly compensated at depth as discussed earlier. At a point on the physical surface of the earth the total gravitational effect of the topographic feature will be attained in a relatively short distance, while at the same distance the effect of the compensating mass may be only 50% complete (Woollard, 1962). However, this effect is important only for higher frequencies when the wavelength of the features being considered is of the order of 2^o or smaller (in this case, it will correspond to frequencies for which $n \geq 4$). However, both $\rho_n(\Delta g_f, T)$ and $\rho_n(\Delta g_B, T)$ are significantly large even for frequencies for which the above-noted factor is not likely to make any appreciable difference. For example, $\rho_n(\Delta g_f, T) = 0.73$ for n = 2 and = 0.85 for n = 3. This would suggest that almost 50% to 60% gravity effect of the topography is not compensated at these wavelengths. Thus, while topography is compensated to some extent at more or less all wavelengths, the degree of compensation is generally less for higher frequencies. The cross-spectrum of the topography and Bouguer anomaly (Table 17) also leads to the same conclusions. The same conclusion is also arrived at later in the

discussion following a slightly different line of argument. The degree correlation function for free air gravity and the topography (Table 18) is also irregular. Part of this irregularity can be attributed to the fact that the predicted gravity values for about 30% of the data points used in the analysis may not be a true representation of the actual gravity of the area. However, there is really no way of testing this possibility until actual observational data are available.

It should also be pointed out that a part of the correlation between Bouguer anomaly and topography could also be due to the incorrect value of the crustal density used in the Bouguer reduction. The use of incorrect density will make the Bouguer anomaly topography-dependent. However, this factor is not likely to be important as the dependence of the Bouguer anomaly on crustal density is small (4 mgal for 0.1 gm/cm^3 per 1000 meters on land and about 0.5 mgal per 0.1 gm/cm^3 per 1000 meters depth at sea).

The degree of compensation can also be gauged, perhaps more clearly, by comparing the spectra of the Bouguer gravity anomalies and the anomalies that would result if the topography were supported as a surficial load by a rigid crust. The Bouguer anomalies reflect the effect of compensation plus the effect of other mass anomalies, if any, not related to the topography. Let A_T denote the gravity effect of the topography alone, then

$$A_T = \Delta g_f - \Delta g_B$$

If the gravity effect of the topographic masses is represented by Equation (14), the Fourier coefficients E^T_{nm} (a_{nm}, b_{nm}, c_{nm}, or d_{nm}) of this representation will be determined by

$$E^T_{nm} = \frac{1}{\ell k} \int_R \int A_T \, g_i(x,y) \, dx \, dy \qquad (48)$$

$$= E^f_{nm} - E^B_{nm}$$

where

E^{f}_{nm} = free air anomaly coefficients

E^{B}_{nm} = Bouguer anomaly coefficients

and

$g_i(x,y)$ = the set of orthogonal functions used in Equation (14)

For the case when the topographic masses are supported by the crust as a surficial load, the spectrum of their attraction can be obtained from E^{T}_{nm}, i.e.

$$D_n(A_T) = \sum_m (E^{T}_{nm})^2 \qquad (49)$$

This spectrum is given in Table 20, column 1.

Another method of finding the attraction of the topographic masses is to compute it from the Fourier coefficients of topography. The underlying idea is the same as discussed by Jeffreys (1962, p. 182) for a spherical surface and used by Kaula (1967a) for comparing the topography with the gravity field of the earth. However, Jeffreys' formula (1962), makes use of Green's theorem for a closed surface and cannot be applied here per se. The simplest way in the present problem seems to be to make a straightforward use of the infinite slab assumption. Denote the gravity effect of an infinite slab of rock material of thickness h by A^{c}_{T}. Then

$$A^{c}_{T} = 2\pi G\rho h$$

and

$$D_n(A_T^c) = (2\pi G\rho)^2 D_n(T) \qquad (50)$$

Table 20, column 2, lists the spectrum of the attraction of the topographic masses computed from Equation (50). It should be identical to that based on Equation (49) except for two factors. First, the Bouguer anomalies used in Equation (49) are corrected for the terrain effect. Consequently, one could expect the two spectra to differ by an amount which will be related to the terrain correction applied to the data. Second, the value of ρ used in computing column 2, Table 20, is the difference between the mean crustal and ocean-water densities. There is a small percentage of the land area included in the area of investigation and for this the density ρ, used in computing the gravity effect of topography, should be taken equal to the crustal density. However, since the area of investigation is predominantly oceanic, and since the adoption of two separate values of density would complicate the calculations considerably, the difference of the mean crustal and ocean water densities was considered to be an appropriate approximation for ρ. Again, it should be remembered that a part of the difference between the spectra of the attraction of the topographic masses listed in columns 1 and 2 of Table 20 could be due to the fact that about 30% of the data points used in this analysis were obtained from simple interpolation of the surrounding data. However, since the spectrum given in column 1, Table 20, makes allowance for the terrain effect, it is likely to approximate the attraction of the topographic masses more accurately. Hence, further discussion will be based on it.

Note that for $n = 0$, $D_n(A_T)$ is somewhat smaller than $D_n(\Delta g_B)$. This is suggestive of complete regional compensation of the topographic masses and the possible existence, in the upper mantle or crust, of an additional mass anomaly.

For the band of frequencies corresponding to $1 \leq n \leq 9$, the compensation seems to be only partial. The degree of compensation can be studied, though only roughly, by examining the spectral ratio function

of the gravity effect of the topographic and the compensating masses. This function is given in Table 19, column 2, and indicates roughly the percentage of the compensated topographic masses for a certain wavelength. Note that the percentage of compensated topography in a certain wavelength, as computed from $\rho_n(\Delta g_B, T)$ and $R_n(\Delta g_B, A_T)$, do not agree very closely, but what is important is they both point to the same general conclusion. For $n = 0$, $R_n \geq 1$ which supports the conclusion derived before that there is an anomalous mass distribution present which is not connected with topography. This conclusion is further supported by the fact that the degree correlation coefficient between free air anomalies and bathymetry for $n = 0$ is less than zero. However, the difference between the spectra of the topographic and the compensating masses for $n = 0$ is marginal and some additional evidence is desirable before this hypothesis can be accepted. For $1 \leq n \leq 9$, $R_n < 1$ which indicates, as concluded before following a slightly different line of reasoning, that the compensation for the topographic masses in this band of frequencies is only partial.

Along the north-south axis, the situation is essentially the same. The compensation seems to be complete on a regional scale with evidence for an additional anomalous mass distribution in the upper mantle or even deeper. Also for the higher frequencies ($m \geq 1$), the topographic masses seem to be compensated only partially.

The spectrum of the topography for the case when it is completely compensated on a local scale can also be estimated. If the compensating masses are assumed to have the form of a disc, the computation can be considerably simplified. Let the residual attraction of the compensated topographic mass be denoted by Δg_r, then

$$\Delta g_r = 2\pi G\rho h\left(\frac{z}{\sqrt{z^2 + r^2}}\right) \tag{39}$$

where

z = depth at which the compensating mass may be assumed to be concentrated

r = radius of the disc-shaped compensating mass

and

ρ = crustal density

It may be noted that in deriving Equation (51), we have calculated the attraction of the topographic masses on the basis of an infinite slab assumption and that of the compensating masses from the formula for the gravity attraction of a circular disc of finite radius. However, since 99% of the attraction of an infinite slab is realized within a radius of 1^{o} from any point on the earth's surface, this approximation is justified. The assumption of a vertical cylinder of finite dimensions would probably be more appropriate if actual density values for the crust were known, but without this knowledge no additional accuracy can be achieved by making such an assumption. None of the above-noted assumptions would take into account the effect of earth's curvature. If the effect of earth's curvature is to be considered, the formulas for the attraction of a spherical shell segment would be more appropriate.

Note that because of the way formula (51) is derived here, ρ is either the mean crustal density or the difference between the mean crustal and ocean-water densities, depending upon whether we are considering the land areas or the oceanic areas. It is not the difference between the densities of the mantle and the compensating mass in this case (unless, of course, h is taken to be the thickness of the compensating 'root').

The spectrum $D_n(\Delta g_r)$ for the case when the topographic masses are fully compensated, is then given by

$$D_n(\Delta g_r) = 2\pi G\rho \left(\frac{z}{\sqrt{z^2 + r^2}} \right)^2 D_n(T) \qquad (52)$$

This residual spectrum is given in Table 20, column 3.

It may be noted that although the lower frequencies of the spectrum $D_n(T)$ have much higher total energy concentration, the energy distribution in higher frequencies of the residual spectrum $D_n(\Delta g_r)$ is equal to or sometimes greater than that in the lower frequencies. In this particular case again, the 'spectral ratio function' can be used to elaborate this point further. This function is given in Table 19, column 3, for the spectra of the residual gravity field and the topography. It is readily seen that the function increases progressively as higher frequencies are approached. This shows that if Equation (51) simulates the actual physical situation to any reasonable degree, the smaller topographic features will give rise to significant gravity anomalies even when they are in perfect isostatic equilibrium. The same thing is shown by Woollard (1962) for a limited frequency range in regard to a hypothetical case.

The degree correlation function of the bathymetry and the satellite gravity is rather irregular again. However, if the negative correlation for the zero order harmonics is valid, it would indicate that the satellite gravity is not influenced to any great degree by the surficial features and that the concentration of energy in zero order harmonic in the satellite gravity only arises from sources in the mantle. The apparent correlation at higher frequencies is obviously fortuitous, for it is not realistic to expect that a satellite will be able to map such small wavelength features. Note the difference in the distribution of energy in $D_n(\Delta g_s, T)$ and $D_n(\Delta g_f, T)$.

It should be noted that the spectral ratio function is particularly suited for problems in which two representations of the same function, obtained by two different measurement techniques, are desired to be compared. It can also possibly be used as a useful measure for comparing two different functions if the aim of such a comparison is to make a comparative study of the relationship of two functions at different frequencies; but this ratio is not the same as the classical correlation coefficient. The comparison of two different functions with the help of this parameter, for the purposes of establishing correlation between them, could be misleading if the limitations of this parameter are not fully comprehended.

Conclusions on Frequency Analysis

The appropriate formulas for the frequency and spectral analysis of two-dimensional data on a rectangular area with defined boundaries are given in a form in which they can be readily applied to the analysis of the gravity and topographic data. Such analysis are useful for studying the correlation between the various harmonic components of two functions and hence are particularly suitable for studying the geophysical correlations.

As a specific example, the comparison of the satellite-determined gravity anomalies and the free air gravity anomalies over the Solomon Islands area shows that, when $1^{o} \times 1^{o}$ mean free-air anomalies are compared with the satellite-determined gravity anomalies at 1^{o} intervals obtained from an 8th degree spherical harmonic representation, the satellite 'sensing' for wavelengths of the order of 10^{o} or smaller is almost negligible. The zero order term indicating the mean value of anomalous surface gravity over the area appears to be well represented by the satellite results. The spectral ratio function between the satellite gravity and free air anomalies suggests that a part of the long-wavelength component of the satellite-determined field does originate from an integration of the higher frequency components which are not 'discernible' to the satellite because of the limited resolution imposed by the height of the satellite. Because of the near-zero energy in higher frequencies of the satellite gravity spectrum, the degree correlation function between the satellite gravity and the free air gravity becomes rather irregular and it is helpful to supplement the information supplied by it by studying a simple parameter called the 'spectral ratio function' which seems to be particularly suitable for comparing two versions of the same function obtained by different methods. The comparison of satellite gravity with the topography of the area, via the degree correlation function of the two, can only be interpreted to mean that the satellite gravity is related to deeper sources rather than the surficial features.

The analysis of the free air and the Bouguer gravity anomalies to obtain the spectra of the attraction of the topographic masses and the compensating masses over the area, in conjunction with the degree

correlation function between the free air anomalies and topography and the Bouguer anomalies and topography, indicate that the topographic features of the size of the area considered here are fully compensated. There is marginal evidence that on a regional scale, there may be some anomalous mass distribution in the upper mantle. This conclusion is supported by negative correlation between the free air anomalies and topography for the zero order term. As would be expected, topographic features of smaller extent seem to be only partially compensated and the degree of compensation is generally less for higher frequencies. This conclusion remains valid even when one takes into account the residual gravity effect which will show up as an anomaly even when a small-scale feature is fully compensated.

It is obvious that analysis of this nature, for areas of the size considered here, gives results of general character only. It is probable that 1^{o} interval chosen for this analysis may be too large for surface data and too small for satellite data. However, with the available amount and detail of surface and satellite gravity data, it seems to be the most suitable choice for this specific study.

REVIEW OF SEISMIC REFRACTION RESULTS IN THE SOLOMONS REGION AND THEIR RELATION TO FREQUENCY ANALYSIS RESULTS

If the results of the frequency analysis are examined in terms of the crustal parameters defined by the seismic refraction measurements in the Solomons area, it is found that there is general corroboration for most of the mass anomaly occurring near the surface rather than at a depth of around 12^{o} as suggested by the satellite gravity anomaly half-width value. Rose et al. (1968) have given one analytical solution that would account for all the mass anomaly being actually associated with the crust. There are reasons though for attributing part of the anomaly to the upper mantle. The pertinent seismic data are given in Table 21 and the site locations shown in Figure 23.

The gravity data included in Table 21 are mean values along the line of each seismic measurement.

As brought out earlier, the upper mantle velocity is usually related to both the thickness of the crust and also the development of the basal layer of the crust. Also as indicated earlier, continental data indicate there is a relation between free air and isostatic gravity anomalies and the velocity of the mantle and crustal thickness. On the basis of these observations the data of Table 21 were first plotted in terms of variations in mantle velocity values and departures in crustal thickness from "normal values" to be expected for the equivalent surface elevation as a function of the free air anomaly values. This plot is shown in Figure 24. The data fall into five groups. A group being defined by an apparent coherent systematic relation between abnormality in crustal thickness and mantle velocity as a function of free air anomaly values. If we eliminate Station M in the Bougainville Trench as representing a special case, and Station RB (Rabal) as being questionable because of incomplete data, there are three groups of values. Group II (Stations B, K, I and J) and Group III (Stations P, G, F, and E) show a normal relationship in that the crustal thickness is directly related to the free air anomaly. However, both groups show an abnormal inverse relationship of mantle velocity to free air anomaly and crustal thickness abnormality. It also is to be noted that both these groups of data are displaced from each other. This displacement is very similar

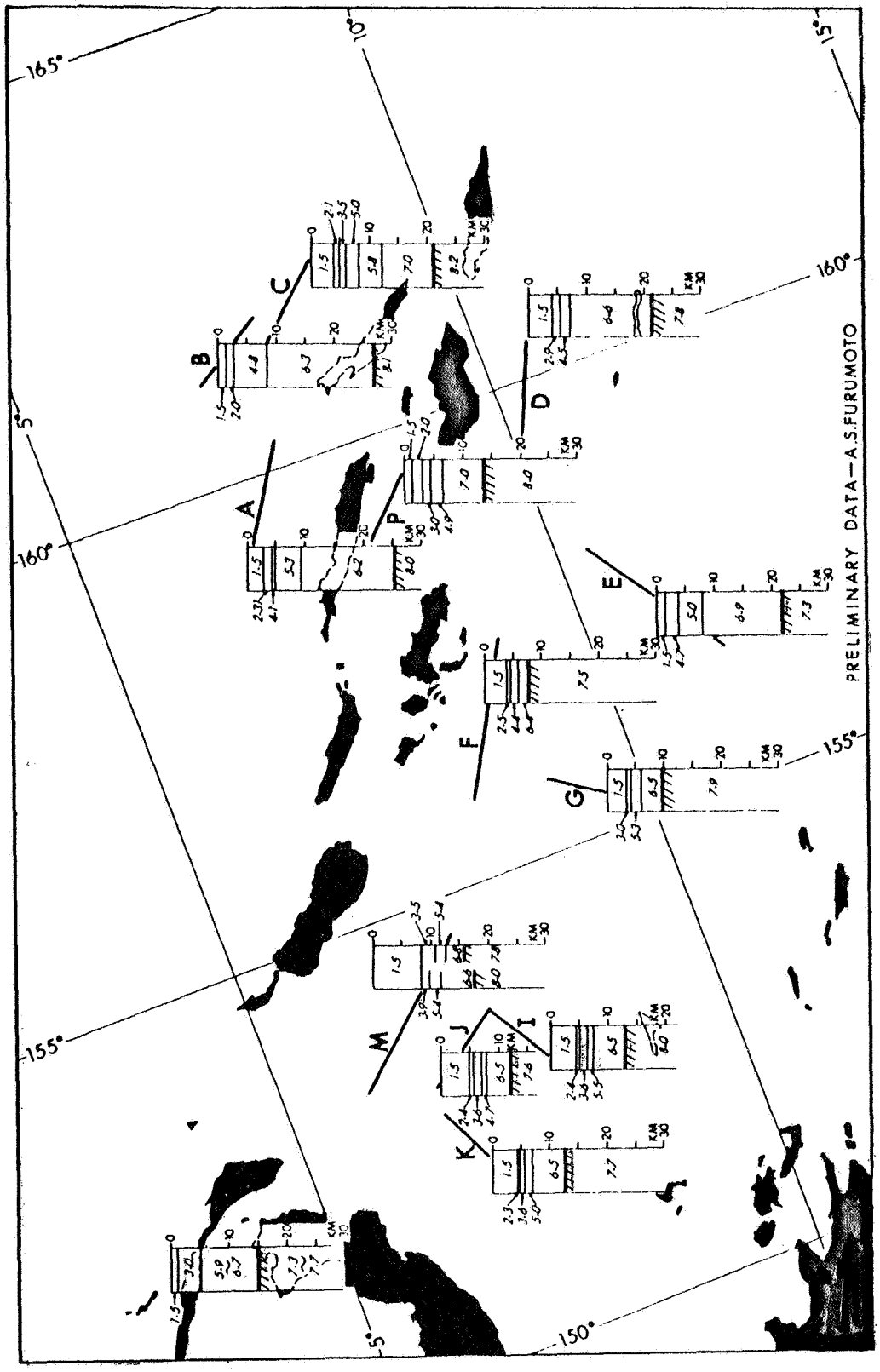

Fig. 23. Seismic refraction sites for the Solomon Islands area.

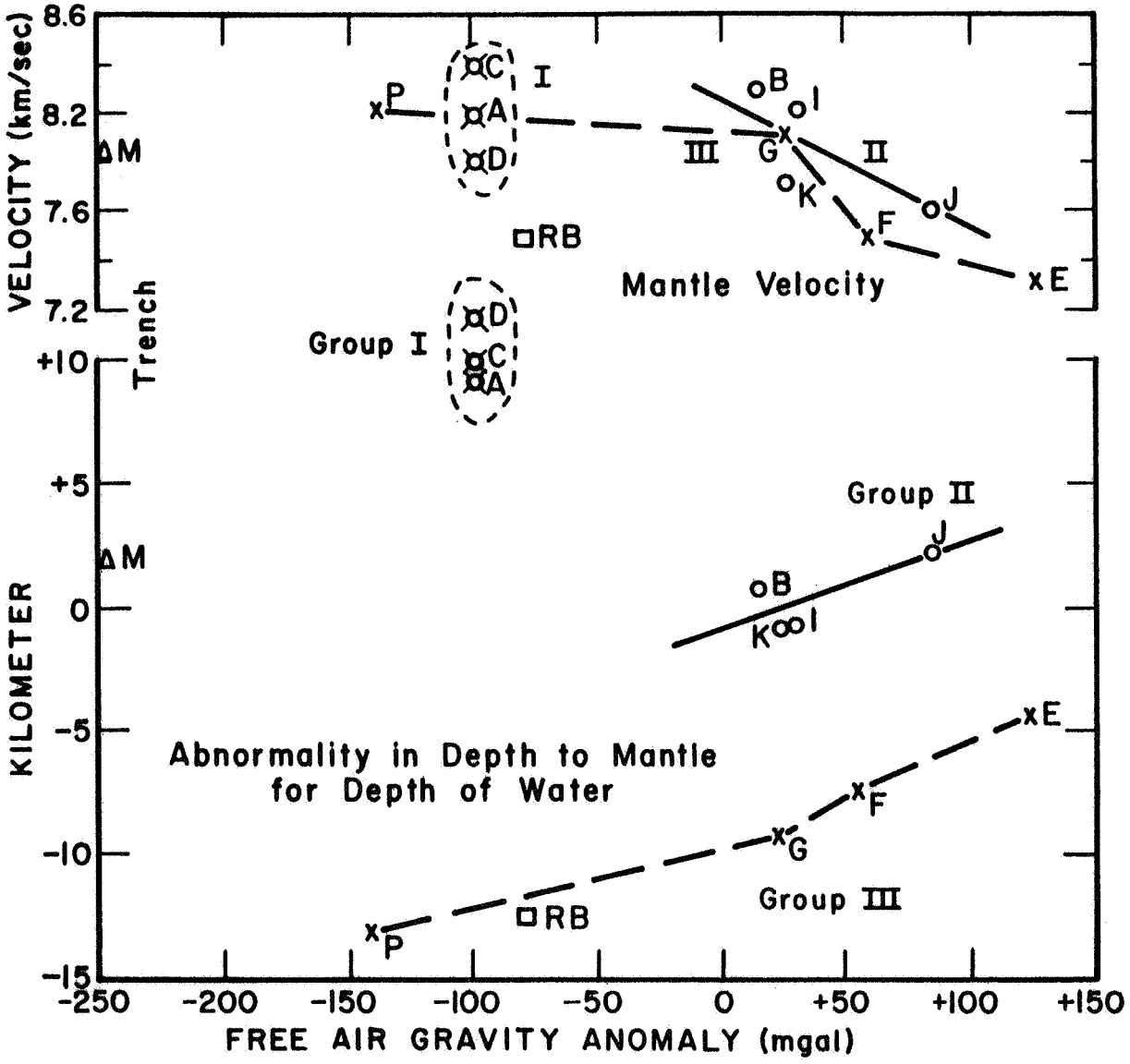

Fig. 24. Variations in the mantle velocity and crustal thickness values from their respective 'normal values' as a function of free air anomaly values.

to that noted for the data for the Basin and Range area in the United States which are displaced from the data for the rest of North America. Group I (Stations A, C and D) show a similar inverse dependence of the change in crustal abnormality and mantle velocity, but all have the same free air gravity anomaly (-100 mgal).

If the data for the two parameters, mantle velocity and abnormality in crustal thickness for surface elevation are plotted independently without regard to the free air anomaly, the values fall into the same identical three groups displaced from each other as shown in Figure 25. Each group as before shows that the crust thins as the mantle velocity increases. However, if we disregard the groups as such and consider only the overall plot, it is evident that there is an anomalous increase in crustal thickness as the velocity of the mantle increases. This general relation is substantiated if we plot the seismic data as a crustal cross section across the Solomon Islands region along with a companion plot of mantle velocity values as shown in Figure 26. This overall relation is the same as that observed on the continents in that variations in crustal thickness appear to be a mirror image of variations in mantle velocity. As shown in Figure 9, a similar relationship is found between crustal thickness and mantle velocity for the mid-Atlantic Ridge and the East Pacific Rise.

The only way of reconciling the conflicting relationships portrayed and in particular the inverse relationship from the normal one for the relation of free air anomalies to mantle velocity is to have the inter-relationship between the density of the crust and mantle with change in mantle velocity differ from that found on the continents. On the continents the higher the mantle velocity, the lower the apparent density contrast between the crust and mantle. High mantle velocity values characterize areas having a thick crust and occur where the geologic evidence (basins) defines subsidence. The positive gravity found in these areas can only be accounted for by an increase in crustal density since there is an obvious extra crustal root increment whose effect has to be cancelled.

In the Solomon Islands area although an increase in gravity is also associated with an increase in crustal thickness for two of the groups of data, there is no overall systematic pattern or generalization possible

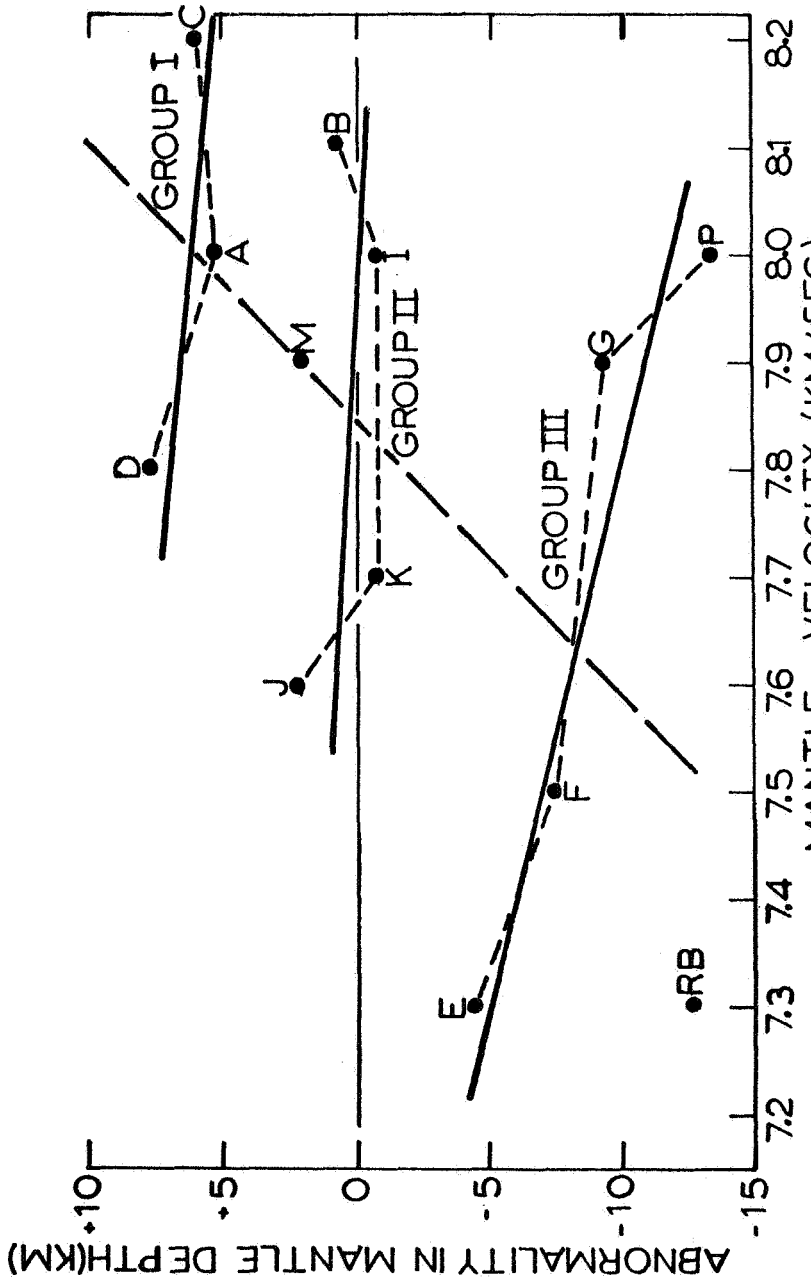

Fig. 25. Abnormality in depth to mantle, as a function of mantle velocity, Solomon Islands area.

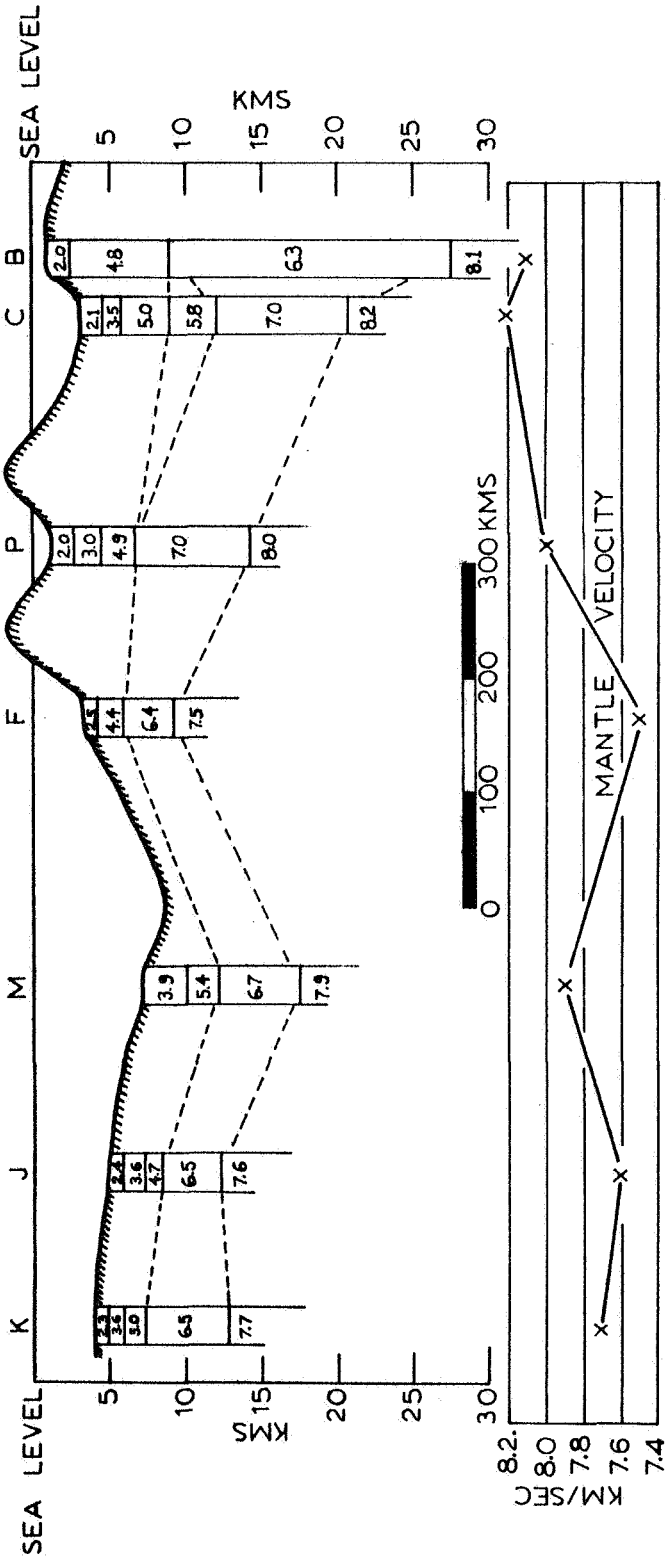

Fig. 26. Crustal cross section across the Solomon Islands region and the mantle velocities.

such as appears between mantle velocity and crustal thickness. The explanation does not appear to be in tectonic displacement and a lack of isostatic equilibrium as the sign of the departures are reversed; for example, a subnormal crustal thickness due to a horst should be an area of positive gravity rather than negative gravity as observed. The explanation therefore has to be in the physical properties of the crust and mantle either because of changes in composition or the physical environment. That three regimes are represented is obvious because of the offsets in values. That the trend in each is one of decreasing density contrast between the crust and mantle with decrease in mantle velocity attended by an increase in gravity characterizes two of the groups and also the third group, except that there is no change in gravity with change in crustal thickness and mantle velocity for this group (Group I).

As normally velocity and density are directly related, a decrease in mantle velocity would suggest a decrease in density which would explain the increase in crustal thickness within each group for a decrease in mantle velocity. The overall increase in crustal thickness with mantle velocity indicated for all the data treated as a single group indicate that there are three mantle regimes represented. The relations cannot be attributed to the crust in that the values of crustal thickness in each group are both large and variable. These regimes cannot be differentiated on the basis of mantle velocity values as the spread in values is quite large. They, however, with only two exceptions fall into geographic areas. Group I, which is characterized by negative gravity (-100 mgal free air anomaly) and which has the greatest excess values of crustal thickness (+6 km ave.) which implies the smallest density differential between the crust and mantle, lies on the eastern end of the Solomon Islands. Group II, which is characterized by positive free air anomalies (+20 to +80 mgal) and which has essentially normal values of crustal thickness, lies to the south of the western end of the Solomon Islands. Group III, which is characterized by a wide range of free air anomalies (-140 to +120 mgal) and subnormal values of crustal thickness (5 to 13 km) which implies a high density contrast between the crust and mantle, lies south of the central Solomon Island area. This geographic distribution cannot be related to tectonic activity, but the available heat flow data

suggests there may be a correlation with this factor. Group I coincides with an area of subnormal heat flow; Group II with an area of normal heat flow; and Group III with an area of high heat flow. On an overall basis this would explain the observed relations since velocity is sensitive to temperature. The highest mean mantle velocity is associated with Group I, the area of subnormal heat flow (0.71-0.73 μ cal/cm^2 sec), and the lowest mean mantle velocity is associated with Group III the area of abnormal heat flow (1.9-3.0 μ cal/cm^2 sec). There is no systematic gravity relationship involved, but as indicated the crust is abnormally thick where the heat flow is subnormal, and subnormal in thickness where the heat flow is abnormal. Where heat flow is normal (1.2 μ cal/cm^2 sec) the value of crustal thickness are normal. The implied density contrasts between the crust and mantle however are reversed from what might be expected in that a high temperature presumably would also lower the density of the mantle and hence decrease the density contrast between the crust and mantle and result in crustal subsidence (too thick a crust). Either there has been crustal uplift through thermal dilation or partial melting with an attendent change in mantle mineralogy which would raise its density and lower its velocity. If there were just thermal dilation, one would expect subnormal gravity values. In point of fact the free air gravity anomaly values for the seismic observation sites in the area of high heat flow are all positive (+20 to +125 mgal), and the mantle velocity values range from 7.3 to 7.9 km/sec. The relations therefore are quite similar to those observed in the northern part of the Basin and Range area of the United States and where Woollard (1968) has computed there would have to be an increase of about 0.6 gm/cm^3 in mantle density to maintain the surface elevation with the observed subnormal value of crustal thickness under isostatic conditions.

All the evidence therefore points to the excess mass in the area of the Group III observations being associated with the upper mantle rather than the crust, and that the top of this disturbing mass lies for the most part at depths less than 15 km. The same explanation probably applies to the area of the Group II observations even though there is no abnormality in crustal thickness, the mantle velocities are

subnormal and the free air anomalies significantly positive. Only the area of the Group I observations lying to the north of the Solomon Islands where there is an abnormally thick crust is characterized by negative free air anomalies. If we are dealing with a reversal process that is temperature controlled, this might explain the observed relations, but it is also possible that there is tectonic control in the area of the Group I observations and that the thick crust is due to underthrusting of the ocean plate beneath the Solomon Islands platform. This is suggested by the seismic crustal section (Fig. 26) and also the increase in depth of earthquake foci going to the north across the Solomon Islands. The gravity control for the Group I observations therefore appears to be of crustal origin whereas for Group II and Group II it appears to be of mantle origin. In all cases it is shallow-seated.

That the integrated pattern of relatively short-wavelength free air anomalies would give a pattern similar to that defined by the satellite derived anomalous gravity field is evident from Figure 21 which shows contoured 1^{o} x 1^{o} average values and 5^{o} x 5^{o} average values. It appears significant that although only a partial closure is defined by the 5^{o} x 5^{o} values, it agrees closely in position and in sign with that defined by the satellite data and would have a long wavelength if the data were available for fully defining it. The half-width value of the satellite-defined gravity high is 12^{o} which would place the maximum depth to the center of disturbing mass beneath the Earth's surface at about 8^{o}, and it is clear from Figure 27, which compares profiles across the Solomon Islands at about 10^{o}S latitude, that 10^{o} x 10^{o} average values might well give a comparable value.

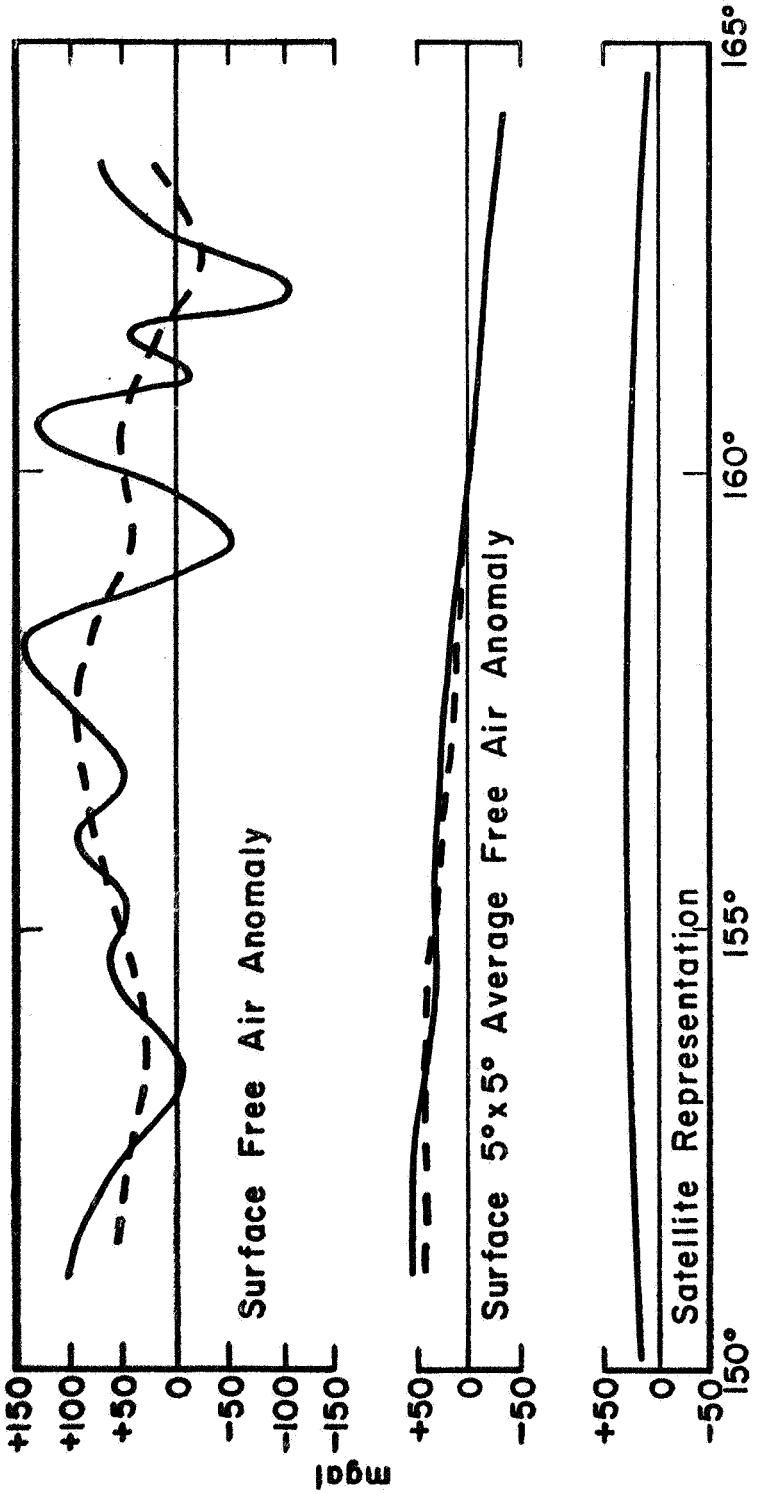

Fig. 27. Gravity profiles across the Solomon Islands.

RECAPITULATION ON FREQUENCY ANALYSIS AND GEOPHYSICAL RELATIONS

There is general agreement between the results of the frequency analysis and the geophysical analysis. The evidence from the frequency analysis indicates: (1) that neither the satellite defined or surface gravity anomaly over the Solomon Islands area is associated with the topographic and bathymetric features of the area. This is also borne out by the geophysical analysis. (2) Although the frequency analysis cannot resolve whether the anomaly originates from overcompensation in the crust, or from sources in the upper mantle, or from changes in the interrelationships of the geophysical parameters of the crust and the mantle, the fact that the correlation of bathymetric features with the satellite-determined gravity field is greater than that of the bathymetric features with the surface gravity field, and is in the same sense, indicates that the part of the gravity anomaly unrelated to topography is relatively of long-wavelength origin and hence should be relatively deep-seated as the surficial features of comparable wavelength are all isostatically compensated. (3) The geophysical analysis shows that there are adequate reasons to believe that the excess mass in question is associated with the upper mantle rather than the crust, over most of the area being considered here, and that the top of this excess mass lies for the most part at depths not exceeding 15 km, though the disturbing mass may extend to much greater depths and may be associated mostly with the upper mantle. (4) The geophysical analysis points out the existence of three regimes of geophysical interrelationships. The eastern part of the Solomon Islands (Group I) is characterized by negative free air gravity anomalies, abnormally thick crust and subnormal heat flow. The part lying to the south of the western end of the Solomon Islands (Group II) is characterized by positive free air gravity anomalies, normal values of crustal thickness and normal heat flow. The part lying to the south of the central Solomon Islands area (Group III) is marked by a wide range of free air gravity anomalies (-140 to +120 mgal), subnormal values of crustal thickness and high heat flow. Within each of these groups the relationship of the crustal thickness with the mantle velocity is anomalous, in comparison to that for the continental areas in the sense that within each of these groups, the mantle

velocity increases as the crustal thickness decreases. However the overall trend is normal and the same as that for the continental area; that is, the mantle velocity increases with the crustal thickness. There is no apparent systematic relationship of these groups to areas of tectonic activity with the possible exception of Group I in which case the abnormally thick crust may have been caused by the underthrusting of the ocean plate beneath the Solomon Islands platform. In that case, it would be possible to explain the gravity pattern in the area of Group I as due to crustal origin. The gravity anomaly field in the remaining part of the Solomons would have to be attributed to sources in the upper mantle. The spectral analysis was not used to differentiate between these three regimes of geophysical interrelationships. This would have required the frequency analysis of the geophysical data of each group independently, and such analyses would also require a much denser geophysical coverage of the area than is now available. It may be possible to make these studies when more geophysical data for the area become available, as probably on the successful conclusion of the present geophysical expedition which is now operating in that area.

(5) That the satellite-derived gravity field represents only the average gravity anomaly pattern over the area is obvious from the discussion of both the spectral as well as geophysical analyses. The fact that most of the energy of the satellite-derived gravity field over the area is concentrated in the zero order terms shows this fact clearly. The same is also borne out by the geophysical discussion given in the preceding section. In any case, this is what one would expect on a logical basis also. (6) That a part of the gravity anomaly sensed by the satellite and represented as long-wavelength component of a specific frequency may be a result of the integration of the short-wavelength features and hence not genuinely belonging to the frequency in question, is certainly suggested by the frequency analysis which shows that the energy in the zero order terms of the satellite-determined gravity fields is greater than that in the corresponding frequencies of the surface gravity field. As pointed out earlier, an alternate explanation of this may be the lack of complete surface gravimetric coverage of the area under consideration and consequent lack of information on the long-wavelength components which are not properly represented. To completely resolve this question, several global comparisons

of the surface and the satellite-determined gravity fields will be needed based on more extensive gravimetric coverage as well as more complete satellite solutions. The only other comparison now possible, that for the North Atlantic area, has only been examined in terms of the gross relations that exist between the satellite-defined anomalous gravity field and 5^{o} x 5^{o} and 10^{o} x 10^{o} averages of surface free air anomaly values. This comparison does show that the surface and the satellite-derived gravity fields show similar long-wavelength features. Since, however, a detailed analysis of the type reported here for the Solomon Islands region is not available for the North Atlantic area--or for any other area for that matter--it is difficult at this stage to draw any parallel based on such analysis for different areas.

ACKNOWLEDGMENTS

This research was supported by the National Aeronautics and Space Administration under Grant No. NGR 12-001-045.

BIBLIOGRAPHY

Anderle, R. J., Geodetic parameter set NWL-5E-6 based on Doppler satellite observations, NWL Report No. 1978, 1966.

Blake, D. H. and Y. Miezitis, Geology of Bougainville and Buka Islands, Territory of Papua and New Guinea, Australia Bur. Mineral Resources, Geol. Geophys. Records, 62, 76 pages, 1966.

Byerly, William E., An Elementary Treatise on Fourier's Series and Spherical, Cylindrical and Ellipsoidal Harmonics with Applications to Problems in Mathematical Physics, Dover Publications, Inc., New York, 1959.

Coleman, P. J., Stratigraphical and structural notes on the British Solomon Islands with reference to the First Geological Map, 1962, Report No. 29 in The British Solomon Islands Geological Record, 2, 1959-62, pp. 17-31, Geological Survey, Honiara, 1965.

Coleman, P. J. et al., A first geological map of the British Solomon Islands, 1962, Report No. 28, in The British Solomon Islands Geological Record, 2, 1959-62, pp. 16-17, Geological Survey, Honiara, 1965.

Darby, E. K. and E. B. Davies, The analysis and design of two-dimensional filters for two-dimensional data, Geophysical Prospecting, 15, 3, pp. 383-406, 1967.

Gaposhkin, E. M., A dynamical solution for the tesseral harmonics of the geopotentials for station coordinates, Trans. Am. Geophys. Union, 47, 47, 1966.

Hardy, G. H. and W. W. Rogosinski, Fourier Series, Cambridge University Press, London, 1962.

Heirtzler, J. R., Sea-floor spreading, Scientific American, vol. 219, no. 6, pp. 60-70.

Heiskanen, W. A. and Helmut Moritz, Physical Geodesy, W. H. Freeman and Company, San Francisco, 1967.

Jeffreys, H., The Earth, Cambridge University Press, Cambridge, 1952, 1962.

Jeffreys, H., On the hydrostatic theory of the figure of the earth, Geophys. J., 8, 196-202, 1963.

Jones, R. H., Stochastic processes on a sphere, Ann. Math. Stat., 34, 213-218, 1963.

Kaula, W. M., Tests and combination of satellite determinations of the gravity field and gravimetry, J. Geophys. Res., 71, 22, pp. 5303-5313, 1966.

Kaula, W. M., Geophysical implications of satellite determinations of the earth's gravitational field, Space Science Reviews, 7, pp. 769-794, 1967a.

Kaula, W. M., Theory of statistical analysis of data distributed over a sphere, Reviews of Geophysics, 5, 1, pp. 83-107, 1967b.

Kozai, Y., New determination of zonal harmonic coefficients of the earth's gravitational potential, Smith. Astrophys. Obsy. Sp. Rept. No. 165, 1964.

Kohnlein, W., The earth's gravitational field as derived from a combination of satellite data with gravity anomalies, Smith. Astrophys. Obsy. Special Report No. 264, 1967.

Khan, M. A., A general solution of the problem of hydrostatic equilibrium of the earth, (in prep.), 1968a.

Khan, M. A., On the equilibrium figure of the earth, Hawaii Institute of Geophysics scientific report No. HIG-68-10, 1968b.

Khan, M. A. and G. P. Woollard, A review of perturbation theory as applied to the determination of geopotential, Hawaii Institute of Geophysics scientific report No. HIG-68-1, 1968.

Lee, Y. M., Statistical Theory of Communication, John Wiley & Sons, Inc., Publishers, New York, 1964.

Laudon, T. S., Land gravity survey of the Solomon Islands, in Leon Knopoff, Charles L. Drake, and Pembroke J. Hart (eds.), The Crust and Upper Mantle of the Pacific Area, Am. Geophys. Union, Geophys. Mono. No. 12, American Geophysical Union, Washington, D. C., 1968.

Lighthill, M. J., Introduction to Fourier Analysis and Generalized Functions, Cambridge University Press, London, 1964.

Mesko, A., Some notes concerning the frequency analysis for gravity interpretation, Geophysical Prospecting, 13, 3, pp. 475-488, 1965.

Miller, K. S., Engineering Mathematics, Rinehart and Company, Inc., New York, 1956.

Moore, J. G., Petrology of deep-sea basalt near Hawaii, Am. J. Sci., 263, 40-52, 1965.

O'Keefe, J. A., Letter to the symposium on the determination of the figure of the earth, Studia Geophysica et Geodatica, 2, 9, 1965.

O'Keefe, J. A. and W. M. Kaula, Stree differences and the reference ellipsoid, Science, 142, 3590, 1963.

Rose, J. et al., Marine gravity and magnetic studies of the Solomon Islands, in The Crust and Upper Mantle of the Pacific Area, Geophys. Mono. 12, L. Knopoff, C. L. Drake and P. J. Hart (eds.), Am. Geophys. Union, Washington, D. C., 1968.

Runcorn, S. K., Wandering continents, in The Earth's Mantle, T. F. Gaskell (ed.), Academic Press, 1967.

Schoenberg, I. J., Positive definite functions on spheres, Duke Math. J., 9, 96-108, 1942.

Strange, W. M., Comparison with surface gravity, Smith. Astrophys. Obsy. Special Report No. 200, 1966.

Talwani, M., B. C. Heezen and J. L. Worzel, Gravity anomalies, physiography, and crustal structure of the mid-Atlantic Ridge, Trav. Sci. Bur. Centr. Seism., UGG 1, Int. Series A, FACS, 22, pp. 88-111, 1961.

Tolstov, G. P., Fourier Series, Prentice-Hall, Inc., New Jersey, 1962.

Uotila, U. A., Harmonic Analysis of world-wide gravity material, Publ. Isos., Inst. Intern. Assic. Geod., 39, 18 pp., 1962.

Wangsness, R. K., Introduction to Theoretical Physics, Classical Mechanics and Electrodynamics, John Wiley and Sons, New York, 1963.

Woollard, G. P., The interrelationship of the crust, the upper mantle, and the isostatic gravity anomalies in the United States, in The Crust and Upper Mantle of the Pacific Area, Geophys. Mono. No. 12, Leon Knopoff, C. L. Drake and P. J. Hart (eds.), pp. 312-341, American Geophysical Union, Washington, D. C., 1968.

Woollard, G. P., Regional isostatic relations in the United States, in The Earth Beneath the Continents, Geophys. Mono. No. 10, John S. Stienhart and T. Jefferson Smith (eds.), pp. 557-594, American Geophysical Union, Washington, D. C., 1966.

Woollard, G. P., The relation of gravity anomalies to surface elevation, crustal structure and geology, The University of Wisconsin Research Report Series Number 62-9, 1962.

Worzel, J. Lamar, Pendulum Gravity Measurements at Sea, 1939-1959, John Wiley and Sons, New York, 1965.

APPENDIX.

Tables 1 through 21

Table 1. Observed Crustal Thickness and Gravity Anomaly Values

(From Woollard, 1968)

Area	h Elv m	Iso Anom	Boug Anom	H (km)	Normal Value H for h*	Diff km
Va. Piedmont	120	+19	+ 18	37.2	34.1	+ 3.1
NE Georgia	305	+10	- 40	45.0	35.8	+ 9.2
C. Minnesota	390	+10	- 45	46.6	36.6	+10.0
C. Wisconsin	380	-15	- 45	37.4	37.5	- 0.1
N. Missouri	250	-25	- 35	36.1	35.4	+ 0.7
N. Missouri	290	-24	- 55	37.9	36.3	+ 1.6
C. Arkansas	150	+22	+ 5	41.2	34.5	+ 6.7
SE Texas	60	-19	- 25	33.0	33.8	- 0.8
W. N. Dakota	680	+38	- 50	58.0	39.0	+19.0
E. Montana	720	+30	- 70	58.0	39.3	+18.7
E. Montana	840	+25	- 95	58.0	40.7	+17.3
N. C. Montana	965	+35	-100	52.1	41.4	+10.7
N. C. Wyoming	1180	+38	-120	50.0	43.3	+ 6.7
N. C. Wyoming	1290	+30	-130	46.0	44.2	+ 1.8
E. Colorado	1220	+10	-120	50.0	43.4	+ 6.6
SE New Mexico	1295	+20	-117	50.8	44.2	+ 6.6
S. Alberta	850	+25	-100	47.5	40.5	+ 7.0
NW Montana	1450	+15	-160	47.8	45.6	+ 2.2
SE Montana	1450	+25	-180	50.6	45.6	+ 5.0
C. Colorado	2690	+20	-270	54.0	55.9	- 1.9
S. Colorado	2400	-15	-240	42.0	53.6	-11.6
C. Mexico	2200	-20	-210	43.4	51.9	- 8.5
S. Idaho	1140	+20	-105	50.8	42.9	+ 7.9
S. Idaho	1420	15	-115	47.3	45.4	+ 1.9
S. Idaho	1800	- 5	-190	47.0	48.5	- 1.5
N. Nevada	1830	- 8	-190	37.4	48.8	-11.4
N. Nevada	1650	+ 4	-200	34.1	47.3	-13.2

S. Nevada	1220	+10	-135	28.0	43.6	-15.6
S. Nevada	1550	-10	-190	25.5	46.4	-20.1
S. Nevada	1750	-15	-180	29.0	48.1	-19.1
S. Nevada	1140	0	-130	34.0	42.8	- 8.8
S. California	610	-25	-100	26.0	48.2	-22.2
S. California	760	-20	-100	30.0	39.7	- 9.7
S. California	470	-30	- 90	27.0	37.2	-10.2
S. California	1070	- 5	-160	40.0	42.3	- 2.3
N. Utah	1550	+20	-150	25.0	46.4	-21.4
SC Arizona	1070	+10	-150	32.0	42.3	-10.3
Sierra Nevada	2130	-60	-220	54.0	51.5	+ 2.5
Cascade Mts.	1070	-25	-115	30.0	42.3	-12.3
Great Valley	50	-30	- 30	20.0	33.7	-13.7
S. Mississippi	100	- 5	- 7	28.5	34.1	- 5.6
Gulf Mexico	- 50	+18	+ 30	31.3	33.1	- 1.8
E. New York	305	+ 4	- 37	36.0	35.8	+ 0.2
W. New York	200	+ 6	- 25	34.8	32.9	+ 1.9
C. Pennsylvania	450	- 6	- 48	32.7	37.1	- 4.4
E. Maryland	10	-20	- 18	34.1	34.2	- 0.1
E. Tennessee	760	-25	- 75	45.3	39.7	+ 5.6
E. Tennessee	760	-25	- 75	41.8	39.7	+ 2.1
C. Tennessee	360	+ 8	- 20	40.0	36.3	+ 3.7
L. Superior Minnesota	30	+20	- 30	35.0	33.5	+ 1.5
N. Michigan	230	-17	- 45	40.7	34.5	+ 6.2
NE Wisconsin	230	-25	- 60	37.5	35.1	+ 2.4
Iowa	240	+10	- 45	43.6	35.1	+ 8.5
NW Wisconsin	350	+ 4	- 40	42.4	36.2	+ 6.2
N. Michigan	230	+ 8	- 15	38.2	35.1	+ 3.1
W. Alberta	1650	- 8	-170	32.0	47.4	-15.4

*Normal value of H for $\bar{\Delta h}$

$H = 33.2 + 7.5\ \bar{\Delta h} + \Delta h$ (Woollard, 1962)

Table 2. 1° x 1° Mean Free Air Gravity Anomalies (with reference to the International Reference Ellipsoid)

Units: Milligals

Latitude	Longitude 148.5°E	150.5°	152.5°	154.5°	156.5°	158.5°	160.5°	162.5°	164.5°	166.5°	168.5°E
5.5°S	150.0 130.0	110.0 -15.0	-97.5 -99.0	74.0 64.0	36.0 25.0	-33.5 -50.2	-47.8 -27.8	-14.6 -11.7	-18.6 -29.2	-39.4 -45.7	
6.5°	36.1 -50.0	-40.0 -57.5	-19.0 -63.5	-90.0 85.5	48.5 10.8	-92.0 -67.0	-45.5 -7.8	-1.4 -8.8	-25.4 -39.9	-49.6 -52.0	
7.5°	26.5 -30.0	-22.5 -6.5	49.0 -13.3	-25.5 9.5	76.5 61.5	33.0 -1.0	-24.0 30.0	5.0 -16.2	-42.1 -54.4	-59.4 -54.4	
8.5°	103.2 49.4	34.0 75.0	17.5 33.8	66.5 41.1	77.5 58.9	11.0 28.0	44.0 -33.0	-20.0 -37.5	-68.1 -66.7	-64.5 -49.5	
9.5°	92.0 75.0	71.0 52.5	64.0 64.6	47.5 30.0	27.5 -6.0	-27.0 -18.0	57.7 14.5	-32.5 -61.2	-100.0 -60.0	-4.5 -11.5	
10.5°	95.4 98.8	122.5 50.0	55.5 50.0	47.5 45.0	35.0 79.5	31.0 10.0	-75.0 23.0	-42.5 -75.0	-51.7 -41.0	-23.5 19.5	
11.5°S	95.0 -94.5	90.1 57.6	65.2 75.0	100.0 -37.5	-8.3 20.8	33.9 50.0	22.0 -78.5	-106.5 -8.5	-7.5 -125.0	-25.0 25.0	

Table 3. 1° x 1° Mean Bouguer Gravity Anomalies (with reference to the International Reference Ellipsoid)

Units: Milligals

Latitude	Longitude 148.5°	150.5°	152.5°	154.5°	156.5°	158.5°	160.5°	162.5°	164.5°	166.5°	168.5°
5.5°S	281.4 286.7	253.4 176.7	228.3 216.0	150.0 172.5	200.0 186.8	188.0 189.7	176.1 156.2	144.3 153.8	174.6 197.0	219.8 236.3	
6.5°	276.1 320.0	330.0 365.5	400.0 386.5	252.5 143.5	147.5 173.6	189.3 191.4	162.5 136.2	132.4 163.4	195.3 219.4	242.6 252.8	
7.5°	232.2 310.0	333.5 356.5	396.5 391.0	316.0 195.0	132.5 127.0	120.5 140.5	147.1 110.0	128.6 194.3	227.2 243.6	266.0 263.0	
8.5°	154.4 298.8	287.6 241.7	272.5 292.5	259.5 285.0	195.0 118.5	88.5 81.0	87.5 113.0	200.5 260.0	260.0 260.0	288.3 260.0	
9.5°	10.0 273.0	247.2 206.7	215.0 221.0	254.5 292.0	305.5 313.0	274.0 152.5	90.0 96.0	275.0 284.3	294.8 231.2	221.4 208.8	
10.5°	118.8 227.5	182.0 116.7	178.5 265.5	287.5 305.5	314.0 311.0	278.0 251.0	244.5 216.0	254.2 317.8	329.5 255.5	178.0 196.1	
11.5°S	159.8 200.7	173.9 165.8	214.8 251.0	236.6 185.7	210.7 164.2	184.2 190.7	245.8 326.0	325.0 320.0	320.0 290.0	169.0 214.2	

Table 4. 1° x 1° Mean Bathymetry and Elevation

Units: Meters

Latitude	148.5°E	150.5°	152.5°	154.5°	156.5°	158.5°	160.5°	162.5°	164.5°	166.5°	168.5°E
5.5°S	- 700 - 650	- 550 -1750	-4411 -3835	-1800 -2325	-2371 -2314	-3000 -3000	-4500 -4500	-4500 -4500	-4500 -4500	-4500 -4500	
6.5°	-2950 -4250	-4125 -4960	-5225 -5750	-4025 - 770	-1412 -2255	-2605 -2635	-1930 -2270	-2990 -3500	-3500 -3600	-3750 -3750	
7.5°	-2805 -4600	-4335 -4540	-4375 -4560	-4675 -3025	- 828 - 662	-1215 -1938	-2525 -2015	-2515 -3450	-3500 -3750	-3750 -3800	
8.5°	- 210 - 800	- 845 -2950	-3025 -3445	-2750 -3500	-2625 -1475	-1125 - 650	-1275 -2595	-2660 -3130	-3405 -3930	-4365 -4005	
9.5°	0 - 50	- 100 -1437	-1505 -2295	-3090 -3565	-3600 -3500	-2995 -1725	- 720 -1462	-3120 -3600	-3075 -1890	-2505 -3225	
10.5°	-2000 -1781	- 600 -1125	-2000 -2600	-2650 -2935	-3090 -2240	-2860 -2955	-3615 -2015	-2805 -3440	-3680 -1975	-1685 -2765	
11.5°S	-2800 -2805	-2885 -2685	-2305 -1580	-2545 -2660	-2300 -2430	-3150 -2894	-2972 -4350	-4300 -4355	-4775 -4400	-1965 -2310	

Table 5A. Satellite-Determined Gravity Anomalies at 1° Interval (with reference to the International Reference Ellipsoid)

Units: Milligals

Latitude	Longitude																							
	148.5°E		150.5°		152.5°		154.5°		156.5°		158.5°		160.5°		162.5°		164.5°		166.5°		168.5°E	
5.5°S	19.1	19.4	19.7	20.0	20.1	20.1	20.0	19.8	19.4	18.9	18.3	17.6	16.8	15.9	14.8	13.7	12.5	11.2	9.9	8.5		
6.5°	19.3	19.7	20.1	20.4	20.5	20.6	20.5	20.3	20.0	19.6	19.0	18.3	17.5	16.6	15.6	14.5	13.3	12.1	10.8	9.4		
7.5°	19.5	19.9	20.3	20.6	20.8	20.9	20.9	20.8	20.5	20.1	19.6	19.0	18.2	17.3	16.3	15.3	14.1	12.9	11.6	10.3		
8.5°	19.5	20.0	20.4	20.8	21.0	21.2	21.2	21.1	20.9	20.5	20.1	19.5	18.7	17.9	17.0	15.9	14.8	13.6	12.3	11.0		
9.5°	19.4	19.9	20.4	20.8	21.1	21.3	21.4	21.3	21.2	20.8	20.4	19.9	19.2	18.4	17.5	16.5	15.4	14.2	13.0	11.8		
10.5°	19.1	19.8	20.3	20.7	21.1	21.3	21.4	21.4	21.3	21.1	20.7	20.2	19.5	18.8	17.9	17.0	15.9	14.8	13.6	12.4		
11.5°S	18.8	19.5	20.1	20.6	21.0	21.2	21.4	21.4	21.4	21.1	20.8	20.3	19.8	19.1	18.3	17.4	16.4	15.3	14.2	13.0		

Table 5B. Satellite-Determined Gravity Anomalies at 1° Interval (with reference to the Equilibrium Figure, Flattening = 1/299.75)

Units: Milligals

Latitude	Longitude																							
	148.5°E		150.5°		152.5°		154.5°		156.5°		158.5°		160.5°		162.5°		164.5°		166.5°		168.5°E	
5.5°S	29.1	29.5	29.8	30.0	30.1	30.1	30.0	29.8	29.4	29.0	28.4	27.6	26.8	25.9	24.8	23.7	22.5	21.2	19.9	18.5		
6.5°	29.2	29.6	30.0	30.3	30.4	30.5	30.4	30.2	29.9	29.5	28.9	28.2	27.4	26.5	25.5	24.4	23.2	22.0	20.7	19.3		
7.5°	29.2	29.7	30.1	30.4	30.6	30.7	30.7	30.5	30.3	29.9	29.4	28.7	28.0	27.1	26.1	25.0	23.9	22.6	21.3	20.0		
8.5°	29.1	29.6	30.0	30.4	30.7	30.8	30.8	30.7	30.5	30.2	29.7	29.1	28.4	27.5	26.6	25.5	24.4	23.2	22.0	20.7		
9.5°	28.8	29.4	29.9	30.3	30.6	30.8	30.8	30.8	30.6	30.3	29.9	29.3	28.6	27.8	26.9	25.9	24.9	23.7	22.5	21.2		
10.5°	28.4	29.0	29.6	30.0	30.4	30.6	30.7	30.7	30.6	30.3	29.9	29.4	28.8	28.0	27.2	26.2	25.2	24.1	22.9	21.7		
11.5°S	27.9	28.5	29.1	29.6	30.0	30.3	30.5	30.5	30.4	30.2	29.9	29.4	28.8	28.1	27.3	26.4	25.4	24.4	23.2	22.1		

Table 6A. Free Air Gravity Anomaly Coefficients (computed from anomalies referred to the International Reference Ellipsoid)

Units: Milligals

n	m	a_{nm}	b_{nm}	c_{nm}	d_{nm}
0	0	0.59621E 01	0.0	0.0	0.0
0	1	-0.14302E 01	0.0	0.19107E 02	0.0
0	2	0.80477E 01	0.0	0.44919E 01	0.0
0	3	0.41005E 00	0.0	-0.50975E 01	0.0
1	0	-0.26479E 01	0.38125E 02	0.0	0.0
1	1	0.19367E 02	0.21428E 00	0.11527E 02	0.30431E 02
1	2	0.11506E 01	0.95512E 01	-0.11412E 02	0.46658E 01
1	3	0.15474E 01	-0.23714E 01	-0.17535E 01	0.10097E 01
2	0	0.15082E 02	0.14633E 02	0.0	0.0
2	1	0.85642E 01	-0.34894E 01	0.38908E 01	0.19170E 02
2	2	0.52609E 01	0.97769E 01	-0.93673E 00	0.37939E 01
2	3	-0.35050E 01	0.55264E 01	-0.99577E 01	0.18545E 01
3	0	0.84163E 01	0.22086E 02	0.0	0.0
3	1	-0.19759E 01	0.10594E 02	0.35553E 01	-0.17678E 02
3	2	0.10522E 01	0.62982E 00	-0.13750E 02	-0.15304E 02
3	3	0.22828E 01	-0.65509E 01	0.22600E 01	-0.18308E 02
4	0	0.13389E 01	0.48524E 01	0.0	0.0
4	1	-0.38114E 01	0.16643E 02	0.16306E 01	0.97860E 01
4	2	-0.30538E 01	0.19774E 02	0.16398E 02	0.27990E 01
4	3	0.18806E 01	-0.84482E-01	0.57601E 01	0.33222E 00
5	0	0.37224E 01	0.80054E 01	0.0	0.0
5	1	-0.31918E 01	-0.71414E 01	-0.98689E 01	-0.32298E 01
5	2	0.19325E 01	-0.51633E 01	0.19833E 01	-0.61826E 00
5	3	-0.25943E 01	0.62145E 00	0.13888E 02	0.16031E 01

6	0	0.25016E 01	0.17988E 01	0.0	0.0
6	1	0.49594E 01	-0.60485E 01	0.21689E 01	-0.98048E 01
6	2	0.36129E 01	-0.89745E 01	0.16047E 01	-0.47514E 01
6	3	-0.17190E 01	-0.26802E 01	-0.61694E 01	-0.99050E 01
7	0	-0.45807E 00	0.72124E 01	0.0	0.0
7	1	-0.33475E 01	-0.38727E 01	-0.45557E 00	-0.11906E 01
7	2	-0.16446E 01	0.14450E 02	0.14739E 01	-0.68399E 01
7	3	-0.41971E 01	-0.18893E 01	-0.41907E 01	-0.88577E 00
8	0	-0.41256E 00	0.41209E 01	0.0	0.0
8	1	-0.32660E 01	-0.42188E 01	-0.50637E 01	-0.63549E 00
8	2	-0.61459E 01	0.18017E 01	-0.67306E 01	-0.24121E 01
8	3	-0.15784E 01	0.15110E 01	0.13804E 01	0.14583E 01
9	0	0.41278E 01	0.99338E 01	0.0	0.0
9	1	0.33981E 01	0.39932E 01	0.59240E 00	-0.33338E 01
9	2	-0.16828E 01	-0.69142E 01	0.30876E 01	-0.13984E 01
9	3	0.31232E 01	-0.38313E 01	-0.50827E 01	-0.17702E 01

Table 6B. Free Air Gravity Anomaly Coefficients (computed from anomalies referred to the equilibrium figure, flattening = 1/299.75)

Units: Milligals

n	m	a_{nm}	b_{nm}	c_{nm}	d_{nm}
0	0	0.40282E 01	0.0	0.0	0.0
0	1	-0.14688E 01	0.0	0.19698E 02	0.0
0	2	0.80395E 01	0.0	0.48195E 01	0.0
0	3	0.40816E 00	0.0	-0.48349E 01	0.0
1	0	-0.26479E 01	0.38125E 02	0.0	0.0
1	1	0.19367E 02	0.21429E 00	0.11527E 02	0.30431E 02
1	2	0.11506E 01	0.95512E 01	-0.11412E 02	0.46658E 01
1	3	0.15474E 01	-0.23714E 01	-0.17535E 01	0.10097E 01
2	0	0.15082E 02	0.14633E 02	0.0	0.0
2	1	0.85642E 01	-0.34894E 01	0.38908E 01	0.19170E 02
2	2	0.52609E 01	0.97769E 01	-0.93674E 00	0.37939E 01

2	3	-0.35050E 01	0.55264E 01	-0.99578E 01	0.18545E 01
3	0	0.84163E 01	0.22086E 02	0.0	0.0
3	1	-0.19759E 01	0.10594E 02	0.35553E 01	-0.17678E 02
3	2	0.10522E 01	0.62981E 00	-0.13750E 02	-0.15304E 02
3	3	0.22828E 01	-0.65509E 01	0.22600E 01	-0.18308E 02
4	0	0.13389E 01	0.48525E 01	0.0	0.0
4	1	-0.38114E 01	0.16643E 02	0.16306E 01	0.97860E 01
4	2	-0.30538E 01	0.19774E 02	0.16398E 02	0.27990E 01
4	3	0.18806E 01	-0.84478E-01	0.57601E 01	0.33223E 00
5	0	0.37224E 01	0.80054E 01	0.0	0.0
5	1	-0.31918E 01	-0.71414E 01	-0.98689E 01	-0.32298E 01
5	2	0.19325E 01	-0.51633E 01	0.19833E 01	-0.61826E 00
5	3	-0.25943E 01	0.62145E 00	0.13888E 02	0.16031E 01
6	0	0.25016E 01	0.17988E 01	0.0	0.0
6	1	0.49594E 01	-0.60485E 01	0.21689E 01	-0.98048E 01
6	2	0.36129E 01	-0.89745E 01	0.16048E 01	-0.47514E 01
6	3	-0.17190E 01	-0.26802E 01	-0.61694E 01	-0.99050E 01
7	0	-0.45807E 00	0.72124E 01	0.0	0.0
7	1	-0.33475E 01	-0.38727E 01	-0.45558E 00	-0.11906E 01
7	2	-0.16446E 01	0.14450E 02	0.14739E 01	-0.68399E 01
7	3	-0.41971E 01	-0.18893E 01	-0.41907E 01	-0.88576E 00
8	0	-0.41256E 00	0.41209E 01	0.0	0.0
8	1	-0.32660E 01	-0.42188E 01	-0.50637E 01	-0.63549E 00
8	2	-0.61459E 01	0.18017E 01	-0.67306E 01	-0.24121E 01
8	3	-0.15784E 01	0.15110E 01	0.13804E 01	0.14583E 01
9	0	0.41278E 01	0.99338E 01	0.0	0.0
9	1	0.33981E 01	0.39932E 01	0.59241E 00	-0.33338E 01
9	2	-0.16828E 01	-0.69143E 01	0.30876E 01	-0.13984E 01
9	3	0.31232E 01	-0.38313E 01	-0.50827E 01	-0.17702E 01

Table 7A. Bouguer Gravity Anomaly Coefficients (computed from anomalies referred to the International Reference Ellipsoid)

Units: Milligals

n	m	a_{nm}	b_{nm}	c_{nm}	d_{nm}
0	0	0.22461E 03	0.0	0.0	0.0
0	1	-0.24281E 01	0.0	0.36788E 01	0.0
0	2	-0.13779E 02	0.0	0.94714E 01	0.0
0	3	-0.19587E 01	0.0	0.51400E 01	0.0
1	0	0.23691E 02	0.25274E 02	0.0	0.0
1	1	-0.20452E 02	-0.33939E 02	-0.57708E 02	-0.53667E 02
1	2	0.18704E 02	-0.15174E 02	0.44120E 01	-0.94769E 01
1	3	-0.42222E 01	0.19078E 01	0.35562E 01	-0.57907E 01
2	0	-0.21562E 02	-0.16813E 02	0.0	0.0
2	1	0.12889E 02	0.21907E 02	0.30868E 00	-0.35517E 02
2	2	-0.41942E 01	-0.46996E 01	-0.25785E 02	0.36097E 00
2	3	0.43959E 00	0.19234E 01	-0.21280E 02	0.28543E 01
3	0	-0.12234E 02	0.14955E 01	0.0	0.0
3	1	0.13079E 02	-0.31291E 01	-0.77053E 01	0.33999E 02
3	2	0.12668E 02	0.94667E 01	0.14952E 02	-0.10890E 02
3	3	-0.90559E 01	0.62622E 00	-0.49547E 01	-0.19576E 01
4	0	0.18742E 01	0.98489E 01	0.0	0.0
4	1	0.54411E 01	0.27977E 01	-0.49724E 01	0.22438E 01
4	2	-0.62719E 01	-0.73948E 01	-0.37842E 01	0.58467E 01
4	3	0.26196E 01	-0.28762E 01	0.43191E 01	-0.57196E 01
5	0	-0.79544E 01	0.12186E 01	0.0	0.0
5	1	0.47580E 01	0.17679E 02	-0.52120E 01	-0.70278E 01
5	2	0.13720E 01	-0.14139E 01	0.43028E 01	0.67552E 01
5	3	-0.35548E 01	-0.37394E 01	-0.41882E 01	-0.23150E 01
6	0	-0.10750E 02	-0.83170E 01	0.0	0.0
6	1	0.76705E 01	0.52319E 01	-0.15864E 01	-0.31936E 01

6	2	-0.26957E 01	0.47242E 01	0.76512E 01	-0.17280E 01
6	3	0.15807E 01	-0.12218E 00	0.35054E 01	0.21271E 01
7	0	-0.28438E 01	-0.99543E 01	0.0	0.0
7	1	0.85070E 01	0.27345E 01	-0.15633E 01	-0.83137E 01
7	2	0.43479E 00	-0.34109E 01	0.27468E 01	0.33283E 01
7	3	-0.48785E 00	0.58282E 00	0.26681E 01	-0.42115E 00
8	0	0.16900E-01	-0.83137E 01	0.0	0.0
8	1	0.12280E 01	0.72232E 01	0.25160E 00	-0.99455E 01
8	2	0.18034E 01	0.17999E 01	0.31648E 00	0.37358E 01
8	3	-0.17593E 01	-0.47985E 01	-0.33074E 01	-0.16976E 01
9	0	-0.20630E 01	-0.84034E 01	0.0	0.0
9	1	0.63788E 01	0.28807E 01	-0.26840E 01	-0.96287E 01
9	2	0.16784E 01	0.65269E 00	0.46661E 01	-0.96109E-01
9	3	-0.65498E 00	-0.38028E 01	-0.16866E 00	-0.58038E 01

Table 7B. Bouguer Gravity Anomaly Coefficients (computed from anomalies referred to the equilibrium figure, flattening = 1/299.75)

Units: Milligals

n	m	a_{nm}	b_{nm}	c_{nm}	d_{nm}
0	0	0.22267E 03	0.0	0.0	0.0
0	1	-0.24667E 01	0.0	0.42697E 01	0.0
0	2	-0.13787E 02	0.0	0.97990E 01	0.0
0	3	-0.19606E 01	0.0	0.54027E 01	0.0
1	0	0.23691E 02	0.25274E 02	0.0	0.0
1	1	-0.20452E 02	-0.33939E 02	-0.57708E 02	-0.53667E 02
1	2	0.18704E 02	-0.15174E 02	0.44120E 01	-0.94770E 01
1	3	-0.42222E 01	0.19078E 01	0.35561E 01	-0.57906E 01

2	0	-0.21562E 02	-0.16813E 02	0.0	0.0
2	1	0.12889E 02	0.21907E 02	0.30865E 00	-0.35517E 02
2	2	-0.41942E 01	-0.46996E 01	-0.25785E 02	0.36093E 00
2	3	0.43960E 00	0.19233E 01	-0.21280E 02	0.28542E 01
3	0	-0.12234E 02	0.14955E 01	0.0	0.0
3	1	0.13079E 02	-0.31290E 01	-0.77053E 01	0.33999E 02
3	2	0.12668E 02	0.94667E 01	-0.14952E 02	-0.10890E 02
3	3	-0.90559E 01	0.62618E 00	-0.49547E 01	-0.19576E 01
4	0	0.18742E 01	0.98489E 01	0.0	0.0
4	1	0.54411E 01	0.27978E 01	-0.49724E 01	0.22438E 01
4	2	-0.62719E 01	-0.73948E 01	-0.37842E 01	0.58468E 01
4	3	0.26196E 01	-0.28762E 01	0.43191E 01	-0.57196E 01
5	0	-0.79544E 01	0.12186E 01	0.0	0.0
5	1	0.47580E 01	0.17679E 02	-0.52120E 01	-0.70278E 01
5	2	0.13721E 01	-0.14139E 01	0.43028E 01	0.67553E 01
5	3	-0.35548E 01	-0.37394E 01	-0.41882E 01	-0.23150E 01
6	0	-0.10750E 02	-0.83170E 01	0.0	0.0
6	1	0.76705E 01	0.52319E 01	-0.15864E 01	-0.31936E 01
6	2	-0.26957E 01	0.47242E 01	0.76512E 01	-0.17280E 01
6	3	0.15807E 01	-0.12218E 00	0.35054E 01	0.21272E 01
7	0	-0.28438E 01	-0.99542E 01	0.0	0.0
7	1	0.85070E 01	0.27345E 01	-0.15632E 01	-0.83137E 01
7	2	0.43480E 00	-0.34109E 01	0.27468E 01	0.33284E 01
7	3	-0.48784E 00	0.58283E 00	0.26681E 01	-0.42113E 00
8	0	0.16898E-01	-0.83137E 01	0.0	0.0
8	1	0.12281E 01	0.72231E 01	0.25162E 00	-0.99455E 01
8	2	0.18034E 01	0.17999E 01	0.31652E 00	0.37358E 01
8	3	-0.17593E 01	-0.47985E 01	-0.33074E 01	-0.16975E 01
9	0	-0.20630E 01	-0.84034E 01	0.0	0.0
9	1	0.63788E 01	0.28807E 01	-0.26840E 01	-0.96287E 01
9	2	0.16784E 01	0.65270E 00	0.46660E 01	-0.96101E-01
9	3	-0.65497E 00	-0.38028E 01	-0.16867E 00	-0.58038E 01

Table 8A. Satellite-Determined Gravity Anomaly Coefficients (with reference to the International Reference Ellipsoid)

Units: Milligals

n	m	a_{nm}	b_{nm}	c_{nm}	d_{nm}
0	0	0.18167E 02	0.0	0.0	0.0
0	1	-0.24056E 00	0.0	0.86955E 00	0.0
0	2	-0.45845E-01	0.0	0.48534E 00	0.0
0	3	-0.81508E-02	0.0	0.38797E 00	0.0
1	0	-0.22829E 01	0.29151E 01	0.0	0.0
1	1	0.27631E-01	-0.35818E-01	-0.44487E-01	-0.63169E 00
1	2	0.67426E-02	-0.93020E-02	-0.19106E-01	-0.35180E 00
1	3	0.48389E-02	-0.84958E-02	-0.98666-02	-0.27315E 00
2	0	-0.49526E 00	0.14221E 01	0.0	0.0
2	1	-0.89320E-02	-0.22976E-01	-0.10111E-01	-0.29767E 00
2	2	-0.93344E-02	-0.36541E-02	0.11220E-03	-0.16755E 00
2	3	0.23172E-02	-0.48047E-02	-0.10223E-01	-0.13623E 00
3	0	-0.20835E 00	0.96131E 00	0.0	0.0
3	1	-0.23774E-02	-0.15341E-01	-0.49519E-02	-0.20389E 00
3	2	0.71033E-02	0.43646E-03	-0.11206E-01	-0.11337E 00
3	3	0.12946E-01	-0.21743E-02	-0.53728E-02	-0.91710E-01
4	0	-0.11047E 00	0.74024E 00	0.0	0.0
4	1	-0.33498E-02	-0.25177E-01	0.19283E-02	-0.16006E 00
4	2	-0.30871E-02	-0.12343E-02	-0.31140E-02	-0.87500E-01
4	3	-0.31395E-02	-0.14031E-02	-0.25150E-02	-0.79747E-01
5	0	-0.62671E-01	0.61419E 00	0.0	0.0
5	1	-0.11770E-02	-0.56620E-02	-0.17551E-02	-0.13213E 00
5	2	0.59800E-02	-0.49817E-03	-0.31587E-02	-0.75512E-01
5	3	0.15239E-01	-0.29193E-02	-0.39418E-02	-0.61961E-01
6	0	-0.43241E-01	0.53927E 00	0.0	0.0
6	1	0.27540E-02	-0.13362E-01	-0.69750E-02	-0.12128E 00

6	2	0.31329E-02	0.75375E-02	-0.52229E-02	-0.65633E-01
6	3	0.20605E-02	-0.60880E-02	-0.17544E-02	-0.57982E-01
6	0	-0.24359E-01	0.48919E 00	0.0	0.0
7	1	-0.12632E-01	-0.85753E-02	-0.84728E-03	-0.11478E 00
7	2	0.26880E-02	-0.18940E-02	-0.65184E-02	-0.62339E-01
7	3	-0.14895E-02	-0.58685E-03	0.47305E-02	-0.44979E-01
8	0	-0.20485E-01	0.46254E 00	0.0	0.0
8	1	-0.98949E-04	-0.76206E-02	-0.58145E-02	-0.10783E 00
8	2	-0.53719E-02	0.29611E-02	0.37318E-02	-0.59032E-01
8	3	0.13228E-02	-0.43028E-04	-0.19838E-02	-0.44358E-01
9	0	-0.42154E-02	0.43923E 00	0.0	0.0
9	1	0.13418E-02	-0.67770E-02	0.66542E-02	-0.10396E 00
9	2	-0.59997E-02	-0.45625E-02	0.44426E-02	-0.57061E-01
9	3	0.53861E-02	-0.58330E-03	-0.26085E-02	-0.50331E-01

Table 8B: Satellite-Determined Gravity Anomaly Coefficients (with reference to the equilibrium figure, flattening = 1/299.75)

Units: Milligals

n	m	a_{nm}	b_{nm}	c_{nm}	d_{nm}
0	0	0.27750E 02	0.0	0.0	0.0
0	1	-0.28792E 00	0.0	-0.50395E 00	0.0
0	2	-0.56302E-01	0.0	-0.27581E 00	0.0
0	3	-0.13383E-01	0.0	-0.21870E 00	0.0
1	0	-0.22829E 01	0.29277E 01	0.0	0.0
1	1	0.24529E-01	-0.35625E-01	0.31612E-01	0.62437E 00
1	2	-0.10287E-02	-0.12942E-01	0.28701E-01	0.35108E 00
1	3	-0.32049E-02	0.20886E-02	0.13674E-01	0.27564E 00
2	0	-0.49067E 00	0.14201E 01	0.0	0.0
2	1	0.32368E-02	-0.27604E-01	0.91966E-02	0.31606E 00
2	2	0.99002E-02	-0.26525E-03	0.69069E-02	0.17015E 00

2	3	-0.14146E-02	0.23581E-02	0.31374E-02	0.14708E 00
3	0	-0.21532E 00	0.95565E 00	0.0	0.0
3	1	0.43108E-02	-0.95129E-02	0.32993E-02	0.21626E 00
3	2	0.66777E-02	-0.48672E-02	-0.62893E-02	0.11698E 00
3	3	-0.52225E-02	0.68867E-02	0.15865E-02	0.10243E 00
4	0	-0.10969E 00	0.73824E 00	0.0	0.0
4	1	-0.15899E-02	-0.84921E-02	0.35234E-02	0.16112E 00
4	2	0.75792E-02	0.14730E-02	-0.84512E-03	0.87604E-01
4	3	-0.46449E-02	0.97715E-02	-0.24728E-02	0.71294E-01
5	0	-0.70777E-01	0.61824E 00	0.0	0.0
5	1	-0.38386E-02	-0.14542E-01	-0.48166E-02	0.13617E 00
5	2	0.76438E-03	-0.15334E-02	-0.33367E-02	0.73152E-01
5	3	-0.24685E-02	0.18927E-02	0.11901E-02	0.65682E-01
6	0	-0.38537E-01	0.53652E 00	0.0	0.0
6	1	0.67965E-02	-0.57566E-02	0.69929E-02	0.11438E 00
6	2	0.38672E-02	0.28013E-02	-0.23257E-02	0.67675E-01
6	3	0.70990E-02	-0.14632E-05	-0.91393E-04	0.49759E-01
7	0	-0.27184E-01	0.48689E 00	0.0	0.0
7	1	0.72346E-03	-0.56071E-02	-0.40802E-02	0.11327E 00
7	2	-0.75911E-02	-0.89253E-03	-0.75485E-02	0.55844E-01
7	3	-0.20838E-02	-0.89452E-02	-0.61818E-02	0.42895E-01
8	0	-0.13283E-01	0.45627E 00	0.0	0.0
8	1	0.52546E-02	-0.17753E-02	-0.49069E-02	0.10627E 00
8	2	-0.97451E-03	-0.34206E-02	-0.16532E-02	0.61321E-01
8	3	-0.35971E-02	0.41136E-02	-0.63912E-03	0.41357E-01
9	0	-0.11420E-01	0.43899E 00	0.0	0.0
9	1	0.80157E-02	-0.58056E-02	-0.58804E-03	0.97912E-01
9	2	0.35232E-03	-0.17131E-02	-0.62061E-02	0.63062E-01
9	3	-0.39750E-03	-0.23229E-02	-0.81404E-03	0.44219E-01

Table 9. Topography (mainly bathymetry) Coefficients

Units: Kilometers

n	m	a_{nm}	b_{nm}	c_{nm}	d_{nm}
0	0	-0.28095E 01	0.0	0.0	0.0
0	1	-0.30748E 00	0.0	0.47345E 00	0.0
0	2	0.25285E-01	0.0	-0.13716E 00	0.0
0	3	-0.38463E-01	0.0	-0.43272E-01	0.0
1	0	-0.17481E 00	0.26130E 00	0.0	0.0
1	1	0.18393E 00	0.58473E 00	0.83413E 00	0.48410E 00
1	2	0.53396E-01	0.49606E 00	-0.40494E 00	-0.19758E 00
1	3	0.69198E-01	0.26179E-01	-0.15945E 00	-0.22465E 00
2	0	0.52615E 00	0.43628E 00	0.0	0.0
2	1	-0.16391E-01	-0.42539E 00	-0.36709E 00	0.37458E 00
2	2	0.14484E 00	0.31162E 00	0.37816E-01	-0.38725E 00
2	3	-0.22086E-01	-0.10839E-01	-0.33878E-01	-0.13889E 00
3	0	0.33450E-01	0.25729E 00	0.0	0.0
3	1	0.73837E-01	0.26710E-01	-0.36182E-01	-0.44142E 00
3	2	-0.28267E-01	0.48584E-01	-0.77259E-01	-0.22724E 00
3	3	0.27771E-02	-0.15098E 00	0.25617E 00	-0.28666E 00
4	0	-0.14530E 00	0.36978E-01	0.0	0.0
4	1	-0.59623E-01	-0.11896E 00	-0.22099E-01	0.13105E-01
4	2	0.15946E 00	0.40665E 00	0.36190E 00	-0.35087E 00
4	3	0.39624E-01	-0.97597E-01	-0.19219E-01	-0.90484E-01

5	0	-0.44430E-01	0.10153E 00	0.0	0.0
5	1	-0.25908E-01	-0.25853E 00	-0.24319E 00	0.42779E-01
5	2	-0.15448E-01	0.20154E-02	-0.22571E-02	-0.67736E-01
5	3	0.21533E-01	0.13616E 00	0.21020E 00	0.67485E-01
6	0	0.32682E-02	0.81988E-01	0.0	0.0
6	1	-0.14868E-01	-0.93934E-01	-0.93370E-01	-0.71249E-01
6	2	-0.52894E-01	-0.13147E 00	-0.90150E-01	-0.12460E 00
6	3	-0.44765E-01	-0.21936E-01	-0.14853E 00	-0.92389E-01
7	0	0.51222E-01	0.13299E 00	0.0	0.0
7	1	-0.48119E-01	0.12916E-01	-0.37493E-01	0.47818E-01
7	2	0.41162E-01	0.14575E 00	0.16341E-01	-0.10966E 00
7	3	0.38492E-01	-0.15948E-01	-0.11834E 00	-0.10632E 00
8	0	0.28397E-01	0.99416E-01	0.0	0.0
8	1	-0.89530E-01	0.21476E-02	-0.26291E-01	-0.33773E-02
8	2	-0.77486E-01	-0.13561E-01	-0.31371E-01	-0.30453E-01
8	3	-0.44469E-01	0.63917E-01	0.10699E 00	-0.32987E-01
9	0	0.53611E-01	0.18878E 00	0.0	0.0
9	1	-0.85270E-01	-0.24960E-01	0.41544E-01	0.17507E-02
9	2	-0.29632E-01	-0.58963E-02	-0.42859E-01	-0.32734E-01
9	3	-0.36348E-01	-0.27298E-01	-0.92535E-01	-0.61639E-01

Table 10. Free Air Gravity Anomaly Residuals*

Units: Milligals

Latitude	Longitude																							
	148.5°E		150.5°		152.5°		154.5°		156.5°		158.5°		160.5°		162.5°		164.5°		166.5°		168.5°E	
5.5°S	8.9	-8.9	8.9	-8.9	8.9	-8.9	8.9	-8.9	8.9	-8.9	8.9	-8.9	8.9	-8.9	8.9	-8.9	8.9	-8.9	8.9	-8.9		
6.5°	-1.4	1.4	-1.4	1.4	-1.4	1.4	-1.4	1.4	-1.4	1.4	-1.4	1.4	-1.4	1.4	-1.4	1.4	-1.4	1.4	-1.4	1.4		
7.5°	4.6	-4.6	4.6	-4.6	4.6	-4.6	4.6	-4.6	4.6	-4.6	4.6	-4.6	4.6	-4.6	4.6	-4.6	4.6	-4.6	4.6	-4.6		
8.5°	5.1	-5.1	5.1	-5.1	5.1	-5.1	5.1	-5.1	5.1	-5.1	5.1	-5.1	5.1	-5.1	5.1	-5.1	5.1	-5.1	5.1	-5.1		
9.5°	5.8	-5.8	5.8	-5.8	5.8	-5.8	5.8	-5.8	5.8	-5.8	5.8	-5.8	5.8	-5.8	5.8	-5.8	5.8	-5.8	5.8	-5.8		
10.5°	-3.3	3.3	-3.3	3.3	-3.3	3.3	-3.3	3.3	-3.3	3.3	-3.3	3.3	-3.3	3.3	-3.3	3.3	-3.3	3.3	-3.3	3.3		
11.5°S	9.3	-9.3	9.3	-9.3	9.3	-9.3	9.3	-9.3	9.3	-9.3	9.3	-9.3	9.3	-9.3	9.3	-9.3	9.3	-9.3	9.3	-9.3		

*See text for explanation.

Table 11. Bouguer Gravity Anomaly Residuals*

Units: Milligals

Latitude	Longitude																							
	148.5°E		150.5°		152.5°		154.5°		156.5°		158.5°		160.5°		162.5°		164.5°		166.5°		168.5°E	
5.5°S	2.2	-2.2	2.2	-2.2	2.2	-2.2	2.2	-2.2	2.2	-2.2	2.2	-2.2	2.2	-2.2	2.2	-2.2	2.2	-2.2	2.2	-2.3		
6.5°	-1.2	1.2	-1.2	1.2	-1.2	1.2	-1.2	1.2	-1.2	1.2	-1.2	1.2	-1.2	1.2	-1.2	1.2	-1.3	1.2	-1.2	1.2		
7.5°	-1.5	1.5	-1.6	1.6	-1.6	1.5	-1.5	1.5	-1.5	1.6	-1.6	1.5	-1.5	1.5	-1.5	1.6	-1.6	1.6	-1.5	1.5		
8.5°	-5.8	5.8	-5.9	5.9	-5.9	5.8	-5.8	5.8	-5.8	5.9	-5.9	5.8	-5.8	5.8	-5.8	5.8	-5.9	5.9	-5.8	5.8		
9.5°	-4.5	4.5	-4.6	4.6	-4.6	4.5	-4.5	4.5	-4.6	4.6	-4.6	4.6	-4.5	4.6	-4.5	4.6	-4.6	4.6	-4.6	4.5		
10.5°	-4.8	4.9	-4.9	4.9	-4.9	4.9	-4.8	4.9	-4.9	4.9	-4.9	4.9	-4.9	4.8	-4.9	4.9	-4.8	4.9	-4.9	4.8		
11.5°S	-3.4	3.4	-3.4	3.5	-3.4	3.4	-3.4	3.4	-3.4	3.5	-3.5	3.4	-3.4	3.4	-3.4	3.4	-3.5	3.4	-3.4	3.4		

*See text for explanation.

Table 12A. Satellite-Determined Gravity Anomaly Residuals (with reference to the International Reference Ellipsoid)*

Units: Milligals

Latitude	Longitude																							
	148.5°E		150.5°		152.5°		154.5°		156.5°		158.5°		160.5°		162.5°		164.5°		166.5°		168.5°E	
5.5°S	0.3	-0.3	0.3	-0.3	0.3	-0.3	0.3	-0.3	0.3	-0.3	0.3	-0.3	0.3	-0.3	0.3	-0.3	0.3	-0.3	0.3	-0.3		
6.5°	0.3	-0.3	0.3	-0.2	0.3	-0.2	0.3	-0.3	0.3	-0.2	0.3	-0.3	0.3	-0.2	0.3	-0.3	0.3	-0.3	0.3	-0.2		
7.5°	0.2	-0.2	0.2	-0.2	0.2	-0.2	0.2	-0.2	0.2	-0.2	0.2	-0.2	0.2	-0.2	0.2	-0.2	0.2	-0.2	0.2	-0.2		
8.5°	0.2	-0.2	0.2	-0.2	0.2	-0.2	0.2	-0.2	0.2	-0.2	0.2	-0.2	0.2	-0.2	0.2	-0.2	0.2	-0.2	0.2	-0.2		
9.5°	0.2	-0.2	0.2	-0.2	0.2	-0.2	0.2	-0.2	0.2	-0.2	0.2	-0.2	0.2	-0.2	0.2	-0.2	0.2	-0.2	0.2	-0.2		
10.5°	0.2	-0.2	0.2	-0.2	0.2	-0.2	0.2	-0.2	0.2	-0.2	0.2	-0.2	0.2	-0.2	0.2	-0.2	0.2	-0.2	0.2	-0.2		
11.5°S	0.2	-0.2	0.2	-0.2	0.2	-0.2	0.2	-0.2	0.2	-0.2	0.2	-0.2	0.2	-0.2	0.2	-0.2	0.2	-0.2	0.2	-0.2		

*See text for explanation.

Table 12B. Satellite-Determined Gravity Anomaly Residuals (with reference to the Equilibrium Figure, Flattening = 1/299.75)*

Units: Milligals

Latitude	Longitude																							
	148.5°E		150.5°		152.5°		154.5°		156.5°		158.5°		160.5°		162.5°		164.5°		166.5°		168.5°E	
5.5°S	1.3	0.9	0.8	0.2	0.2	-0.3	-0.4	-0.8	-0.8	-1.3	-1.4	-2.0	-1.8	-2.3	-2.4	-2.9	-2.7	-3.4	-3.1	-3.7		
6.5°	1.0	0.4	0.6	0.2	0.2	-0.3	-0.1	-0.7	-0.5	-1.0	-0.8	-1.3	-1.2	-1.7	-1.5	-2.0	-1.8	-2.3	-2.0	-2.6		
7.5°	0.6	0.1	0.4	-0.1	0.2	-0.3	0.1	-0.5	-0.1	-0.6	-0.3	-0.8	-0.4	-0.9	-0.6	-1.1	-0.8	-1.3	-1.0	-1.4		
8.5°	0.2	-0.2	0.2	-0.2	0.2	-0.2	0.2	-0.2	0.2	-0.2	0.2	-0.2	0.2	-0.2	0.2	-0.2	0.2	-0.2	0.2	-0.2		
9.5°	-0.2	-0.6	0.1	-0.3	+0.2	-0.2	0.4	0	0.6	0.1	0.7	0.3	0.8	0.4	1.1	0.7	1.3	0.9	1.5	1.0		
10.5°	-0.5	-0.9	-0.1	-0.6	0.3	-0.2	0.6	0.3	1.0	0.5	1.3	1.0	1.7	1.2	2.0	1.6	2.3	1.8	2.5	2.1		
11.5°S	-0.9	-1.3	-0.4	-0.7	0.2	-0.1	0.8	0.4	1.3	0.9	1.8	1.5	2.3	1.9	2.8	2.4	3.2	2.9	3.6	3.3		

*See text for explanation.

Table 13. Bathymetry and Elevation Residuals*

Units: Meters

Latitude	Longitude																							
	148.5°E		150.5°		152.5°		154.5°		156.5°		158.5°		160.5°		162.5°		164.5°		166.5°		168.5°E			
5.5°S	50	- 50	50	- 50	50	- 50	50	- 50	50	- 50	50	- 50	50	- 50	50	- 50	50	- 50	50	- 50				
6.5°	60	- 60	70	- 60	70	- 60	70	- 60	60	- 70	70	- 70	60	- 60	60	- 60	60	- 60	60	- 60				
7.5°	100	- 90	90	- 90	90	- 90	90	- 90	90	- 90	90	- 90	100	-100	90	- 90	90	- 90	90	- 90				
8.5°	210	-210	210	-210	210	-200	210	-210	210	-210	210	-210	200	-210	210	-210	210	-210	210	-200				
9.5°	100	-100	100	-100	110	-110	100	-100	100	-100	100	-100	100	-100	100	-100	100	-100	110	-100				
10.5°	-60	60	-60	60	-60	60	-60	50	-60	60	-60	60	-60	50	-50	60	-60	50	-50	60				
11.5°S	20	- 20	30	- 20	30	- 20	30	- 20	20	- 20	20	- 20	30	-20	20	- 30	20	- 20	30	- 20				

*See text for explanation.

Table 14. Variance* of the Satellite-Determined, Free Air, and Bouguer Gravity Anomalies, Topographic (mainly bathymetric) Data and their Residuals

Satellite-Determined Gravity Anomalies

$VAR(\Delta g_s)$	(with reference to the International Reference Ellipsoid) (milligals^2) $VAR(\Delta g_s^i - \Delta g_s^o)$	$\sum_n D_n(\Delta g_s)$	$VAR(\Delta g_g)$	(with reference to the equilibrium figure, flattening = 1/299.75) (milligals^2) $VAR(\Delta g_s^i - \Delta g_s^o)$	$\sum_n D_n(\Delta g_s)$
336.3	0.05	340.3	771.1	1.7	780.0

$VAR(\Delta g_f)$	Free Air Gravity Anomalies (milligals^2) $VAR(\Delta g_f^i - \Delta g_f^o)$	$\sum_n D_n(\Delta g_f)$	$VAR(\Delta g_B)$	Bouguer Gravity Anomalies (milligals^2) $VAR(\Delta g_B^i - \Delta g_B^o)$	$\sum_n D_n(\Delta g_B)$
3219.7	36.6	3222.0	55157.6	14.0	55803.5

VAR(T)	Topography (mainly bathymetry) (kilometers^2) $VAR(T^i - T^o)$	$\sum_n D_n(T)$
9.329	0.010	9.420

*The columns for which the symbol VAR(Δg) is used, are calculated from Equation (32) directly.

Table 15. Spectrum of Topography (mainly bathymetry) Over the Solomon Islands Area

Units: Kilometers

n	D_n (T)	m	D_m (T)
0	8.06404	0	8.26545
1	0.50921	1	0.69902
2	0.42029	2	0.34042
3	0.14208	3	0.11506
4	0.13196		
5	0.05641		
6	0.02828		
7	0.02727		
8	0.01420		
9	0.02622		

Table 16A. Spectra of the Gravity Field Over the Solomon Islands Area

(computed from gravity anomalies referred to the International Reference Ellipsoid)

Units: Milligals^2

n	$D_n(\Delta g_s)$	$D_n(\Delta g_f)$	$D_n(\Delta g_B)$	m	$D_m(\Delta g_s)$	$D_m(\Delta g_f)$	$D_m(\Delta g_B)$
0	330.64	274.65	50614.26	0	339.45	1414.85	51800.39
1	7.00	1152.94	2734.39	1	0.56	978.00	3038.48
2	1.17	408.82	1143.08	2	0.17	555.75	730.78
3	0.50	592.93	600.75	3	0.11	271.42	233.90
4	0.29	288.63	119.31				
5	0.20	140.54	164.70				
6	0.15	111.51	144.71				
7	0.12	108.07	101.43				
8	0.11	47.44	87.85				
9	0.10	96.48	93.07				

Table 16B. Spectra of the Gravity Field Over the Solomon Islands Area

(computed from gravity anomalies referred to the equilibrium figure, flattening = 1/299.75)

Units: Milligals^2

n	$D_n(\Delta g_s)$	$D_n(\Delta g_f)$	$D_n(\Delta g_B)$	m	$D_m(\Delta g_s)$	$D_m(\Delta g_f)$	$D_m(\Delta g_B)$
0	770.29	267.01	49753.64	0	779.50	1395.53	50932.26
1	7.04	1152.94	2734.39	1	0.33	991.52	3040.92
2	1.17	408.82	1143.08	2	0.09	557.21	734.04
3	0.50	592.93	600.75	3	0.06	270.12	235.28
4	0.29	288.63	119.31				
5	0.20	140.54	164.70				
6	0.15	111.51	144.71				
7	0.12	108.07	101.02				
8	0.11	47.44	87.85				
9	0.10	96.48	93.07				

Table 17A. A Cross-Spectra of the Gravity Field and Topography (mainly bathymetry) Over the Solomon Islands Area

(computed from gravity anomalies referred to the International Reference Ellipsoid)

n	$D_n(\Delta g_s, \Delta g_f)$	$D_n(\Delta g_f, T)$	$D_n(\Delta g_s, T)$	$D_n(\Delta g_B, T)$	m	$D_m(\Delta g_s, \Delta g_f)$	$D_m(\Delta g_f, T)$	$D_m(\Delta g_s, T)$	$D_m(\Delta g_B, T)$
0	116.71	-12.11	-50.84	-630.69	0	192.71	0.71	-49.99	-641.23
1	53.36	14.37	0.52	- 24.69	1	3.21	16.39	0.15	- 33.88
2	5.01	9.53	0.18	- 15.80	2	0.99	8.00	0.02	- 5.43
3	11.50	7.78	0.16	- 3.33	3	- 0.56	3.42	0.02	- 0.56
4	1.14	2.69	0.03	- 1.74					
5	2.43	2.13	0.03	- 1.22					
6	0.96	1.18	0.03	- 0.85					
7	1.93	1.30	0.03	- 1.19					
8	1.01	0.55	0.02	- 0.63					
9	2.32	1.10	0.04	- 0.97					

Table 17B. Cross-Spectra of the Gravity Field and Topography (mainly bathymetry) Over the Solomon Islands Area

(computed from gravity anomalies referred to the equilibrium figure, flattening = 1/299.75)

n	$D_n(\Delta g_s, \Delta g_f)$	$D_n(\Delta g_f, T)$	$D_n(\Delta g_s, T)$	$D_n(\Delta g_B, T)$	m	$D_m(\Delta g_s, \Delta g_f)$	$D_m(\Delta g_f, T)$	$D_m(\Delta g_s, T)$	$D_m(\Delta g_B, T)$
0	106.67	- 6.56	-78.01	-625.13	0	196.31	6.15	-76.91	-635.78
1	64.15	14.37	0.62	- 24.69	1	0.69	16.53	0.01	- 33.74
2	8.48	9.53	0.19	- 15.80	2	- 1.04	7.98	- 0.04	- 5.45
3	7.76	7.78	0.08	- 3.33	3	0.08	3.42	- 0.03	- 0.57
4	2.14	2.69	0.01	- 1.74					
5	2.30	2.13	0.04	- 1.22					
6	- 0.03	1.18	0.02	- 0.85					
7	1.64	1.30	0.03	- 1.19					
8	0.91	0.55	0.02	- 0.63					
9	2.04	1.10	0.04	- 0.97					

Table 18. Degree Correlation Functions for Free Air Gravity Anomalies, Bouguer Gravity Anomalies, Satellite-Determined Gravity Anomalies and Topography (mainly bathymetry) (computed from gravity anomalies referred to the International Reference Ellipsoid)

n	$\rho_n(\Delta g_s, \Delta g_f)$	$\rho_n(\Delta g_f, T)$	$\rho_n(\Delta g_s, T)$	$\rho_n(\Delta g_B, T)$
0	0.39	-0.26	-0.98	-0.99
1	0.59	0.59	0.28	-0.66
2	0.23	0.73	0.25	-0.72
3	0.67	0.85	0.58	-0.36
4	0.12	0.44	0.16	-0.44
5	0.46	0.76	0.30	-0.40
6	0.23	0.66	0.43	-0.42
7	0.52	0.76	0.57	-0.72
8	0.44	0.67	0.59	-0.57
9	0.74	0.69	0.83	-0.62

m	$\rho_m(\Delta g_s, \Delta g_f)$	$\rho_m(\Delta g_f, T)$	$\rho_m(\Delta g_s, T)$	$\rho_m(\Delta g_B, T)$
0	0.28	0.01	-0.94	-0.98
1	0.14	0.63	0.24	-0.73
2	0.10	0.58	0.08	-0.34
3	-0.10	0.61	0.21	-0.11

Table 19. Spectral Ratio Functions of the Satellite-Determined Gravity Anomalies and the Free Air Gravity Anomalies, the Attraction of the Compensating Masses and the Topographic Masses[1], the Residual Gravity Field and the Topography (mainly bathymetry) and the Satellite-Determined Gravity and the Topography (mainly bathymetry) Over the Solomon Islands Area

n	Satellite-Determined Gravity vs Free Air Gravity Anomalies $R_n(\Delta gs, \Delta gf)$ (in units of 10^{-3})	The Attraction of the Compensating Masses vs Topographic Masses $R_n(\Delta g_B, A_T)$	The Residual Gravity Field vs Topography $R_n(\Delta g_r, T)$
0	1203.84	1.05	0.28
1	6.08	0.61	1.11
2	2.86	0.49	4.42
3	0.84	0.37	9.93
4	1.00	0.29	17.64
5	1.40	0.43	27.51
6	1.36	0.45	39.55
7	1.15	0.30	53.72
8	2.35	0.44	69.73
9	1.04	0.40	88.26

m	Satellite-Determined Gravity vs Free Air Gravity Anomalies $R_m(\Delta gs, \Delta gT)$ (in units of 10^{-3})	The Attraction of the Compensating Masses vs Topographic Masses $R_m(\Delta g_B, A_T)$	The Residual Gravity Field vs Topography $R_m(\Delta g_r, T)$
0	239.92	1.03	2.26
1	0.58	0.51	9.01
2	0.30	0.45	35.89
3	0.39	0.50	80.18

[1]Computed from Free Air and Bouguer Gravity Anomaly Coefficients

Table 20. Spectra of the Attraction of Topographic Masses Computed from Free Air and Bouguer Anomaly Coefficients, the Attraction of Topographic Masses Computed from Equation (50) and the Residual Gravity Field Computed from Equation (51) Over the Solomon Islands Area

Units: Milligals^2

n	The Attraction of Topographic Masses Computed from Free Air and Bouguer Gravity Anomaly Coefficients $D_n(A_T)$	The Attraction of Topographic Masses Computed from Equation (36) $D_n(A_T^C)$	The Residual Gravity Field Computed from Equation (37) $D_n(\Delta g_r)$
0	48233.13	47951.14	2.23
1	4457.89	3027.91	0.56
2	2354.08	2499.17	1.86
3	1617.20	844.85	1.41
4	410.11	784.67	2.33
5	379.08	335.43	1.55
6	319.31	168.16	1.12
7	333.81	162.15	1.46
8	199.52	84.44	0.99
9	234.26	155.91	2.31

m	The Attraction of Topographic Masses Computed from Free Air and Bouguer Gravity Anomaly Coefficients $D_m(A_T)$	The Attraction of Topographic Masses Computed from Equation (36) $D_m(A_T^C)$	The Residual Gravity Field Computed from Equation (37) $D_m(\Delta g_r)$
0	50486.65	49148.78	18.64
1	5955.88	4156.57	6.30
2	1630.22	2024.24	12.22
3	465.63	684.18	9.23

Table 21. Seismic Refraction Results of Solomon Island Region

Sa	Location Lat	Long	Depth H_2O (km)	Equiv Elv (km)	Depth of Mantle (km)	Mantle Vel k/s	FA	BA	Norm* Mantle Depth	Anom Mantle Depth
A	7°-8°S	159°-160°E	2.8	1.7	25.6	8.0	-100	+170	20.4	+ 5.2
B	7°-8°S	161°-162°E	1.4	0.9	27.2	8.1	+ 15	+153	26.4	+ 0.8
C	8°-9°S	161°-162°E	3.8	2.4	21.2	8.2	-100	+193	15.2	+ 6.0
D	10°-11°S	159°-160°E	4.2	2.6	21.5	7.8	-100	+277	13.7	+ 7.8
E	10°-11°S	157°-158°E	1.5	0.9	22.1	7.3	+125	+233	26.4	- 4.3
F	8°-9°S	156°-158°E	3.8	2.4	7.9	7.5	+ 55	+371	15.2	- 7.3
G	9°-10°S	155°-156°E	3.1	1.9	9.8	7.9	+ 25	+264	19.0	- 9.2
I	7°-8°S	153°-154°E	4.2	2.6	12.8	8.0	+ 30	+354	13.7	- 0.9
J	7°-8°S	153°-154°E	4.9	3.1	12.2	7.6	+ 75	+422	10.0	+ 2.2
K	6°-7°S	152°-153°E	4.2	2.6	12.8	7.7	+ 25	+349	13.7	- 0.9
M	6°-7°S	153°-154°E	7.2	4.5	17.0	7.9	-250	+290	15.0**	+ 2.0
P	8°-9°S	159°-160°E	1.3	0.8	14.0	8.0	- 40	+ 52	27.2	-13.2
RB	3°-4°S	152°-153°E	1.2	0.7	15.2	7.3	+ 20	+112	27.9	-12.7

*Based on equivalent elevation = Depth H_2O x 1.03/2.75
and expression Hm = $-[33.2 - 7.5\ \Delta h^1]$ where
h^1 = equivalent elevation

**Based on normal trench relationship Hm = $-(3.13\ \Delta h^1 + 0.9)$